UNIVERSITY
OF MICHIGAN
JUN 20 1952
ENGINEERING
LIBRARY

JOURNAL OF THE AERONAUTICAL SCIENCES

VOLUME 19 JUNE, 1952 NUMBER 6

CONTENTS

General Reverse Flow and Variational Theorems in Lifting-Surface Theory ..... A. H. FLAX 361

Diffuser Efficiency of Free-Jet Supersonic Wind Tunnels at Variable Test Chamber Pressure ..... RUDOLF HERMANN 375

Free-Flight Air-Drag Measurement Techniques (with Appendix by R. E. ROBERSON) ..... A. B. J. CLARK AND F. T. HARRIS 385

Impingement of Spherical Water Droplets on a Wedge at Supersonic Speeds in Air.. ..... MYRON TRIBUS AND ARMAND GUIBERT 391

Dynamic Stability of a Missile in Rolling Flight ..... RAY E. BOLZ 395

Two-Dimensional Losses in Turbine Blades ..... CHARLES A. MACGREGOR 404

Ripple-Type Buckling of Sandwich Columns ..... A. CEMAL ERINGEN 409

A High-Speed Schlieren Technique for Investigation of Aerodynamic Transients .... WALTER S. BRADFIELD AND WALTER Y. FISH 418

Readers' Forum: "On the General Solution for Unsteady Motion of a Rectangular Wing in Supersonic Flow," by John W. Miles; "A Nyquist Approach to Flutter," by John Dugundji; "Comments 'On the Deflection of Swept Cantilevered Surfaces,'" by David B. Hall; "On an Extension of Slender-Wing Theory," by Mac C. Adams and W. R. Sears; "Diffraction of Blasts by Axisymmetric Bodies," by H. F. Ludloff and M. B. Friedman; "Effect of Wind-Tunnel Nozzle on Steady-Flow Nonuniformities," by H. S. Ribner and M. Tucker; "Comments on 'Supersonic Flow of a Two-Dimensional Jet,'" by E. B. Klunker and Keith C. Harder, with "Author's Reply," by S. I. Pai; "An Approximate Method for the Calculation of the Laminar and Turbulent Boundary Layer by Simple Quadrature for Two-Dimensional and Axially Symmetric Flow," by E. Truckenbrodt; "Suggested Way of Comparing Overall Efficiency of Helicopters," by W. Z. Stepniewski; "On the Stability of Plane Parallel Laminar Flows to Two- and Three-Dimensional Disturbances," by Martin Lessen 421–432

Published by the

INSTITUTE OF THE AERONAUTICAL SCIENCES, INC.

JOURNAL OF THE AERONAUTICAL SCIENCES

Editor: HUGH L. DRYDEN, *Director, N.A.C.A.*

Associate Editor: ROBERT R. DEXTER *Managing Editor:* BERNEICE H. JARCK

Editorial Committee

Aerodynamics

Francis Clauser
Howard Emmons
Alexander Flax
R. Paul Harrington
R. T. Jones
Carl Kaplan
H. W. Liepmann
C. C. Lin
H. F. Ludloff
Harold Luskin
John R. Markham
Clark B. Millikan
Shatswell Ober
W. Bailey Oswald
Allen E. Puckett
Elliott G. Reid
H. J. F. Reid
Russell Robinson
G. B. Schubauer
W. R. Sears
John Stack
Theodore von Kármán
Richard von Mises

Flight Testing

W. K. Ebel
R. R. Gilruth
Melvin N. Gough
E. G. Stout

Meteorology

C. F. Brooks
D. M. Little
E. J. Minser
F. W. Reichelderfer
H. C. Willett

Structures and Materials

W. B. Bleakney
E. W. Conlon
L. H. Donnell
E. C. Hartmann
N. J. Hoff
Samuel Levy
E. E. Lundquist
Alfred S. Niles
W. Ramberg
E. Reissner
F. R. Shanley
H. W. Sibert
C. R. Strang
S. Timoshenko
H. S. Tsien
Chi-Teh Wang

Rotating Wing Aircraft

F. B. Gustafson
K. H. Hohenemser
Bartram Kelley
R. B. Maloy
Ralph McClarren
R. H. Miller
R. H. Prewitt
Igor I. Sikorsky

Physiologic Problems

H. G. Armstrong
Louis H. Bauer
Robert J. Benford
Eugene Du Bois
W. Randolph Lovelace, II
Ross A. MacFarland

Flight Propulsion

George W. Brady
Frank W. Caldwell
L. S. Hobbs
E. E. Johnson
Joseph Keenan
R. P. Kroon
Hans Reissner
Abe Silverstein
C. Fayette Taylor
E. S. Taylor
P. Taylor
E. S. Thompson
H. S. Tsien

Aircraft Design

W. E. Beall
W. K. Ebel
Hall L. Hibbard
Richard Hutton
C. L. Johnson
A. A. Kartveli
C. J. McCarthy
Fred E. Weick
Robert J. Woods

Air Transport

Charles Froesch
J. A. Herlihy
R. D. Kelly
Otto E. Kirchner
Jerome Lederer
John C. Leslie
R. Dixon Speas

Instruments

Allan G. Binnie
J. R. Bradburn
Charles H. Colvin
C. S. Draper
S. G. Eskin
O. E. Esval
H. W. Holzapfel
W. L. Howland
George H. Purcell
C. F. Savage
O. Hugo Schuck
C. L. Seward, Jr.
L. D. Statham
R. C. Sylvander
D. K. Warner

Vibration and Flutter

Lee Arnold
M. A. Biot
R. L. Bisplinghoff
William Bollay
Chieh-Chien Chang
I. E. Garrick
Martin Goland
J. P. Den Hartog

Fuels and Oils

D. P. Barnard
J. H. Doolittle
Graham Edgar
R. T. Goodwin
S. D. Heron
A. M. Rothrock

SUBSCRIPTION RATES

JOURNAL OF THE AERONAUTICAL SCIENCES, Published Monthly.—United States and Possessions: 1 Year, $12.00; Single Copies, $1.50. Foreign Countries Including Canada (American Currency Rates): 1 Year, $13.00; Single Copies, $1.50.

AERONAUTICAL ENGINEERING REVIEW, Published Monthly.—United States and Possessions: 1 Year, $3.00; Single Copies, $0.50. Foreign Countries Including Canada (American Currency Rates): 1 Year, $3.50; Single Copies, $0.50.

Notices of change of address should be sent to the Institute at least 30 days prior to actual change of address.

Manuscripts for publication, proofs, and all correspondence should be addressed to the Editorial Office of the JOURNAL.

Correspondence regarding subscriptions may be addressed to Publication Office, 20th and Northampton Sts., Easton, Pa., or to the Editorial Office of the JOURNAL OF THE AERONAUTICAL SCIENCES, 2 East 64th Street, New York 21, New York.

Copyright, 1952, by the Institute of the Aeronautical Sciences, Inc.

Entered as Second Class Matter at the Post Office, Easton, Pa., May 1, 1937. Acceptance for mailing at a special rate of Postage provided for in the Act of August 24, 1912. Authorized April 29, 1937.

VO

By i
adjoint
surface
are deri
of a lifti
reverse
joint, th
of the ec
tionship
lead to
tics of v
superson
moment,
may be e
distributi
tions cor
stant ang
with unif
eralizatio
to which
joint vari
tained.
method, t
mate solu
variationa
steps in th
ner, and
ame meth

U

$u(x, y)$

$\bar{u}(x, y)$

x, ξ

y, η

Receive

* Head

JOURNAL OF THE AERONAUTICAL SCIENCES

VOLUME 19 JUNE, 1952 NUMBER 6

General Reverse Flow and Variational Theorems in Lifting-Surface Theory

A. H. FLAX*

Cornell Aeronautical Laboratory, Inc.

SUMMARY

By introducing the integral equation and auxiliary conditions adjoint to the integral equation and Kutta condition of lifting-surface theory, certain general theorems in lifting-surface theory are derived. It is shown that the adjoint to the integral equation of a lifting surface is the integral equation for the same surface in reverse flow and that to satisfy the requirements on such an adjoint, the Kutta condition must also be imposed on the solutions of the equation for the surface in reverse flow. The adjoint relationship between wings in direct and reverse flow is shown to lead to a general class of relationships between the characteristics of wings in direct and reverse flow for either subsonic or supersonic speeds. Also, it is shown that the total lift, pitching moment, and rolling moment on a wing of any camber and twist may be expressed as a closed-form integral over certain pressure distributions of the same wing in reverse flow. These distributions correspond to the case of the wing in reverse flow at constant angle of attack, pitching with uniform velocity, and rolling with uniform velocity. The formulas may be regarded as generalizations of the Munk two-dimensional airfoil integral relations to which they reduce for infinite aspect ratio. Finally, an adjoint variational principle for lifting surfaces in subsonic flow is obtained. In combination with the form of the Rayleigh-Ritz method, this is shown to lead to suitable methods for approximate solution of lifting-surface problems. On the basis of the variational principle, certain apparently arbitrary or intuitive steps in the approximate theories of Prandtl, Weissinger, Reissner, and Lawrence are shown to be logical applications of the same method.

SYMBOLS

U	= free-stream velocity
$u(x, y)$	= local perturbation velocity in the free-stream direction divided by U
$\bar{u}(x, y)$	= local perturbation velocity in the free-stream direction divided by U for wing in reverse flow
x, ξ	= Cartesian coordinates in free-stream direction
y, η	= Cartesian coordinates perpendicular to x and lying in the base plane of the wing
z	= Cartesian coordinate perpendicular to x and y and measuring distance from the base plane of the wing
M	= free-stream Mach Number
$p(x, y)$	= lift per unit area $= 2\rho U^2 u$
$\bar{p}(x, y)$	= lift per unit area $= 2\rho U^2 u$ for wing in reverse flow
$w(x, y)$	= local slope of lifting surface in stream direction
$\bar{w}(x, y)$	= local slope of lifting surface in stream direction for wing in reverse flow
ρ	= free-stream mass density
$s(x)$	= wing semispan
c	= wing chord
d	= distance from wing leading edge
A	= denotes integration over area of wing
$K(x, y; \xi, \eta)$	= kernel of lifting surface integral equation
$\bar{K}(x, y; \xi, \eta)$	= kernel adjoint to K
β	$= \sqrt{M^2 - 1}$
α	= wing angle of attack
q	= wing pitching velocity (rad. per sec.)
q	= dynamic pressure $= (1/2)\rho U^2$
p	= wing rolling velocity (rad. per sec.)
δ	= variation of
A, B, C / $\bar{A}, \bar{B}, \bar{C}$	= constants
$\phi(y)$	= spanwise lift distribution function
$g'(x)$	= chordwise lift distribution function

(1) INTRODUCTION

RECENTLY, ATTENTION HAS BEEN FOCUSED on the existence in linearized wing theory of some rather unexpected relationships between the characteristics of wings in reversed flows, or reverse flow theorems as these relationships are sometimes called. von Kármán[1] appears to have been the first to point out such a relationship. He showed that the supersonic wave drag due to thickness of a body would be unaltered by a reversal of direction of flight. Hayes[2] then showed, by other methods, that not only would the drag be unaltered but also that, for a restricted class of plan forms, the slope of the

Received June 8, 1951.

* Head, Aerodynamic Research Department.

lift curve would remain the same for such a reversal of flow direction. Munk,[3] using still another line of reasoning, proved both the drag theorem and the lift theorem, the latter for a somewhat less restricted class of plan forms than Hayes, although he was not explicit in defining all the restrictions. The present author[4] showed, for wings with supersonic leading and trailing edges, that not only were there relations between lift and drag in reversed flows but also that were was a more general class of relationships between the stability derivatives in reversed flows. Such relationships were extended to a somewhat less restricted class of plan forms in supersonic flow by Harmon.[5] Brown,[6] using an extension of Munk's approach, demonstrated that the drag due to thickness, the slope of the lift curve, the damping in pitch, and the damping in roll were all unchanged by a reversal of flow direction for any plan form and either subsonic or supersonic flow velocities, as long as linearized wing theory could be employed.

The present paper presents a general form of the relationships between the characteristics of wings in direct and reverse flows, which includes all of those previously known, as well as an infinity of others, and is applicable, within the limits of linearized lifting surface theory, to wings of any plan form in either subsonic or supersonic flow. The basis for the present result is the observation that the reversal of flow direction has the effect that the kernel of the integral equation of linearized lifting surface theory is the mathematical adjoint of the kernel appropriate to the original direction of flow. In order further to satisfy the mathematical requirements on adjoint solutions to these equations, it is shown that it is necessary that the Kutta condition be satisfied on the trailing edges in the reverse flow. Thus, an adjoint solution is completely specified as any solution of a lifting-surface problem for the same plan form with flow direction reversed. Among the interesting results of the generalized relationships obtained in this paper which are likely to be of practical value are generalizations of Munk's two-dimensional theorems for lift and moment to three-dimensional wings. The first of these gives the lift on a wing with any camber and twist distribution (or specified normal boundary velocity resulting from pitching, rolling, structural deformation, etc.) in terms of the lifting pressure distribution on a flat plate of the same plan form with the flow direction reversed. The second theorem of this type gives the pitching moment on a wing with any camber and twist distribution in terms of the lifting pressure distribution on a pitching flat plate of the same plan form with the flow direction reversed. In the special case of two-dimensional flow, these theorems reduce to precisely the Munk result. For high aspect ratio wings, for which lifting-line theory is applicable, the adjoint solutions are simply any solutions of the lifting-line equation itself, and the generalized Munk lift theorem gives the total lift on a wing with any twist distribution (due to geometrical twist, structural deformation, flap deflection, etc.) in terms of an integral over the lift distribution on an untwisted wing at constant angle of attack. A similar result is obtained for rolling moment on a lifting surface in terms of an integral over the lift distribution of a rolling wing in reverse flow.

As a direct consequence of the adjoint relationship between the solutions to the lifting-surface problem and the solutions of the lifting-surface problem for the same plan form with the flow direction reversed, it is found possible to formulate a variational principle of the adjoint type for lifting-surface theory. This variational principle is of interest because it offers a systematic means of obtaining approximate solutions for lifting-surface problems. Since exact solutions to the integral equation of lifting-surface theory in subsonic flow are rarely obtainable, good approximations are of great importance. In particular, the variational method may be used to obtain approximate one-dimensional integral equations to replace the two-dimensional integral equation of lifting-surface theory, for very high or very low aspect ratio wings. The theories of Prandtl,[7] Weissinger,[8] Lawrence,[9] and Reissner[10] are shown to be formulable on the same basis from the variational principle. These theories all involve multiplication of the two-dimensional integral equation by some weighting factor in one variable and integration over that variable, after a suitable approximation to the kernel has been made. In the Prandtl, Weissinger, Lawrence, and Reissner theories, the choice of weighting function appears to have been made intuitively or by recourse to analogy with the limiting cases of two-dimensional theory or with very low aspect ratio theory (Jones). The variational method not only gives the form the weighting function must have but indicates how any particular approximation may be further improved. The two-dimensional integral equation of lifting-surface theory may be approximated in this way by any finite number of one-dimensional integral equations or by any finite number of algebraic

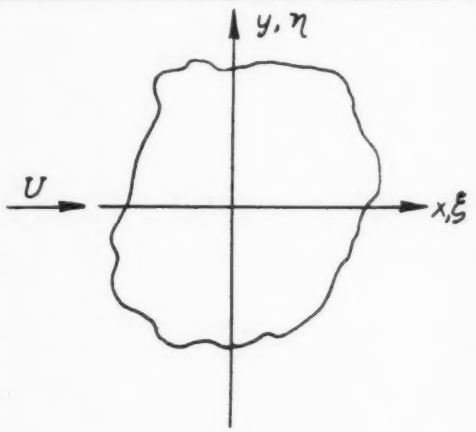

FIG. 1.

equations. Because of the stationary property of the integrals in the variational method, the accuracy of results for any given number of either one-dimensional integral equations or algebraic equations is considerably better than if the same number of equations had been obtained by simple point collocations, such as were carried out by Blenk[11] in lifting-surface theory or by Glauert[12] in lifting-line theory. In the limiting case of lifting-line theory, the adjoint variational principle reduces to an ordinary variational principle, which has been discussed by Ziller[23] and the author.[24]

A recent paper by Ursell and Ward[13] presents the same general reverse flow relationship as developed in this paper but not the variational principle. Their line of attack is through the general equations for linearized flow potential and involves the use of momentum and energy integrals over properly selected bounding surfaces in the fluid. The present method is somewhat simpler, starting from the established integral equation of lifting-surface theory and retaining a direct connection with lifting-surface theory throughout. The variational principle then results almost as a direct consequence of the reverse flow relationship.

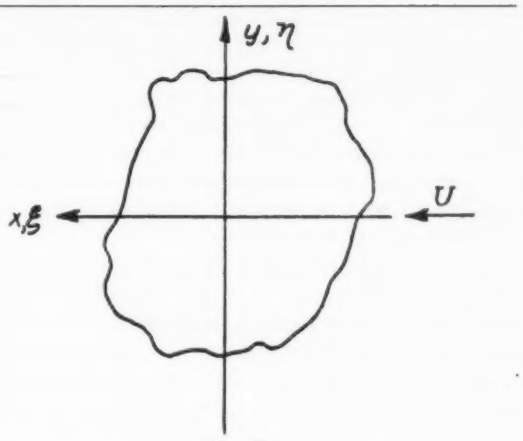

FIG. 2.

(2) THE INTEGRAL EQUATION OF LIFTING-SURFACE THEORY AND ITS ADJOINT IN INCOMPRESSIBLE FLOW

The linearized theory of the lifting surface has been formulated in a variety of ways, but for the present purpose, the integral equation formulation is most direct. For concreteness, the particular case of incompressible flow will be considered first. It will then be shown that the same considerations apply to compressible subsonic and supersonic linearized wing theory. For incompressible flow, the form of the lifting-surface integral equation derived by Lawrence[9] from a result of Reissner's[14] is most suitable. This is

$$w(x, y) = \frac{1}{2\pi}\frac{\partial}{\partial y}\int\int_A d\xi\, d\eta\, \frac{u(\xi, \eta)}{y - \eta}\left[1 + \frac{\sqrt{(x - \xi)^2 + (y - \eta)^2}}{(x - \xi)}\right] \tag{1}$$

where principal values are to be taken when necessary. The subscript A beneath the integrals denotes integration over the wing, and $w(x, y)$ is the local angle of attack, which is assumed to be small enough everywhere so that the assumptions of linearized theory are valid. By the same token, the lifting surface is assumed to lie in a plane insofar as calculation of distances between elements or of integrals over the surface are concerned. $u(\xi, \eta)$ is the jump in the streamwise component of the perturbation velocity across the wing surface made dimensionless with respect to the free-stream velocity U. The lift per unit area is given as

$$p(x, y) = 2\rho U^2 u \tag{2}$$

The coordinate system is shown in Fig. 1 and is one in which the direction of positive x and ξ is in the direction of U, the free-stream velocity.

Now, if an integral equation adjoint[15] to Eq. (1) is desired, it is necessary to interchange x and ξ and y and η, respectively in the kernel. Thus, an adjoint might be

$$\bar{w}(x, y) = \frac{1}{2\pi}\frac{\partial}{\partial y}\int\int_A d\xi\, d\eta\, \frac{\bar{u}(\xi, \eta)}{y - \eta}\left[1 + \frac{\sqrt{(x - \xi)^2 + (y - \eta)^2}}{\xi - x}\right] \tag{3}$$

where $\bar{w}(x, y)$ is any distribution of local angle of attack† and $\bar{u}(x, y)$ is the corresponding distribution of lift. Here it is to be noted that the y and η under the integral signs have not been interchanged, nor has the differentiation with respect to y outside the integral sign been changed to differentiation with respect to η in seeming violation of the definition of the adjoint equation. The reason for this is connected with the singular nature of the integral, which does not permit the differentiation to be done under the sign. If this were possible, the kernel of the integral equation would actually be

† To keep some of the expressions obtained positive in the sign of direct and reverse flow lifts, $\bar{w}$ is defined as the negative of the usual definition here and in all that follows. This amounts to reversing the usual direction of positive slope for the reverse flow.

$$\frac{\partial}{\partial y}\left\{\frac{1}{y-\eta}\left[1+\frac{\sqrt{(x-\xi)^2+(y-\eta)^2}}{(x-\xi)}\right]\right\} \tag{4}$$

Since the term in braces is an antisymmetrical function of $(y-\eta)$, its derivative with respect to y is a symmetrical function of $(y-\eta)$ and therefore is unaffected by interchange of y and η. This basic symmetry property of the operator (actually the sequence of operations: double integration followed by differentiation) is not affected by the singular nature of the integral as long as the functions $u(x, y)$ and $\bar{u}(x, y)$ are not themselves singular. As is well known from the theory of lifting surfaces, these functions may become singular on edges, and this problem will be considered subsequently.

Before proceeding with any further discussion, it will be useful to consider a physical interpretation of Eq. (3). This can readily be done by considering the lifting-surface integral equation appropriate to a reversal of flow direction. Eq. (1) would still be applicable if, as shown in Fig. 2, the direction of positive x and ξ were redefined so as to coincide with the new direction of the free-stream flow. If it is, instead, desired to retain the definitions of positive x and ξ as shown in Fig. 1, it is only necessary to replace x by $-x$ and ξ by $-\xi$. This procedure leads directly to Eq. (3). Thus, Eq. (3) may be regarded as the integral equation of the lifting surface in a reverse flow when the definition of positive x and ξ is retained as in the original flow direction.

It is well known that integral equations of types (1) and (3) do not have unique solutions without the specification of additional conditions on the solutions, $u(x, y)$. In the case of Eq. (1), which is the lifting-surface equation, the specification of the Kutta condition at the trailing edge of the wing—namely, that $u(x, y)$ be zero at such an edge—is sufficient to make the solution unique. But nothing up to this point has imposed any such condition on the solutions of Eq. (3). Therefore, it is not possible to state what solutions for $\bar{u}(x, y)$ are admissible as solutions of the adjoint equation. If the admissible solutions of the adjoint integral are actually to be those corresponding to the lifting surface in reverse flow, it is necessary to show that an admissible solution of the adjoint equation must satisfy the Kutta condition on the trailing edges in the reverse flow—i.e., on the edges that were leading edges in the original problem. This will be done next.

To simplify the following discussion, Eqs. (1) and (3) will be written, respectively, as

$$w(x, y) = \overset{*}{\int_A} u(\xi, \eta)K(x, y: \xi, \eta)\, d\xi\, d\eta \tag{5}$$

$$\bar{w}(x, y) = \overset{*}{\int_A} \bar{u}(\xi, \eta)\bar{K}(x, y: \xi, \eta)\, d\xi\, d\eta \tag{6}$$

where the symbol $\overset{*}{\int}$ stands for the operations of double integration over the area, followed by partial differentiation with respect to y. Now, in order that the solutions of the adjoint equation satisfy the usual mathematical requirements,[15] it is necessary that

$$\int_A \bar{u}(x, y) \overset{*}{\int_A} u(\xi, \eta)K(x, y: \xi, \eta)\, d\xi\, d\eta\, dx\, dy = \int_A u(x, y) \overset{*}{\int_A} \bar{u}(\xi, \eta)\bar{K}(x, y: \xi, \eta)\, d\xi\, d\eta\, dx\, dy \tag{7}$$

where the integral symbol, $\int$, denotes double integration over the area of the wing for any admissible functions $u(x, y)$ and $\bar{u}(x, y)$. It can be seen that the expression on the right-hand side is essentially that on the left, with the orders of integration over ξ, η and x, y interchanged. The operation of differentiation with respect to y, which is interposed between the integrations, causes no difficulties because of the symmetry of the entire operation in y and η, as discussed previously. In essence, $\overset{*}{\int} K$ and $\overset{*}{\int} \bar{K}$ are identical with regard to y and η. This is brought out more clearly in Appendix (II), where, as a result of some manipulation, the symmetrical form in y and η of the expressions in Eq. (7) is made more apparent. Thus, if the interchanges in order of integration are carried out on the right-hand side of Eq. (7), the expression becomes

$$\int_A \bar{u}(\xi,\eta) \overset{*}{\int_A} u(x,y)\bar{K}(x, y: \xi,\eta)\, dx\, dy\, d\xi\, d\eta \tag{8}$$

$\overset{*}{\int_A}$ now denoting integration with respect to x and y followed by differentiation with respect to η. Then it may be seen that expression (8) is identical to the expression on the left-hand side of Eq. (7), since x, y, ξ, and η are merely integration variables and do not appear in the results.

It remains to consider under what conditions an interchange of orders of integration is permissible. If the function $f(x,y,\xi,\eta) = \bar{u}(x,y)u(\xi,\eta)$ is everywhere bounded, continuous, and differentiable, including the vicinity of points where $x = \xi$ and $y = \eta$, then such an interchange is justifiable, even in spite of the fact that the integrals are only definable in terms of their Cauchy principal value (see, for instance, Schwartz[16]). Now, the function $u(x, y)$, representing the local lift distribution over a lifting surface, will satisfy this condition everywhere except

possibly near the edges. Near an edge, u must either go to zero or become infinite as $1/\sqrt{d}$, where d is the distance from the edge, if finite values of the local angle of attack are to be obtained from Eq. (1).[17] The Kutta condition specifies that $u(x, y)$ go to zero on trailing edges; on leading edges, it goes to infinity as $1/\sqrt{d}$, where d is the distance from the leading edge. Therefore, the conditions for interchange of order of integration as in Eq. (8) above will be satisfied if it is required that $\bar{u}(x, y)$ go to zero on the leading edges of the original wing—i.e., the trailing edges of the wing in reverse flow. But this is exactly the requirement of a Kutta condition on the adjoint solutions for the wing in reverse flow. Thus, a sufficient condition for the specification of an adjoint solution $\bar{u}(x, y)$ is that it satisfy the integral Eq. (3) for a lifting surface in reverse flow and that it satisfy the Kutta condition at the trailing edges in reverse flow.

In order that the adjoint solution $\bar{u}(x, y)$ corresponding to a given $\bar{w}(x, y)$ be unique, it is further required that it be shown that the satisfaction of the Kutta condition is not only sufficient to specify the adjoint but also is necessary. This is done in Appendix (I), where it is shown that the interchange of orders of integration required in order to prove Eq. (7) is not permissible if both $u(x, y)$ and $\bar{u}(x, y)$ become infinite as $1/\sqrt{d}$ at any edge. The difficulty arises from the singular behavior of the integrals (7) near such an edge. If $u \approx C/\sqrt{d}$ and $\bar{u} \approx \bar{C}/\sqrt{d}$ in the vicinity of the edge, then the leading-edge singularity contributes a term proportional to $\pi C\bar{C}$ to the integral for one order of integration and proportional to $-\pi C\bar{C}$ for the reverse order. The form of these expressions and the fact that they arise from edge singularities suggest that the difficulty arises from the same source as requires the insertion of the leading-edge suction into calculations of drag from lifting-surface theory. This is indeed the case; in fact, if $\bar{u}$ is taken to be u, the expressions (7) become the drag integrals of lifting-surface theory, and the term under consideration becomes πC^2, which is exactly the term annulled by leading-edge suction.[17]

(3) The Integral Equation and Its Adjoint for Compressible Flows

For subsonic compressible flows, it is apparent that the application of the three-dimensional Prandtl-Glauert transformation[18] to both the integral equation and its adjoint changes both in exactly the same way, so that all the results previously derived for incompressible flow are applicable without further discussion.

For supersonic flows, some further investigation is necessary, since all points on a lifting surface do not mutually interact because of the propagation of disturbances from a point only inside the downstream Mach cone from the point. In turn, a given point is influenced only by disturbances emanating from points within its upstream Mach cone. Using the system of axes shown in Fig. 1, with the addition of a z axis at right angles to the wing surface, which forms the plane $z = 0$, the expression for w is[18]

$$w = \lim_{z \to 0} \frac{1}{\pi} \frac{\partial}{\partial z} \int\int_c u(\xi, \eta)\, d\xi\, d\eta \, \frac{z(x - \xi)}{[(y - \eta)^2 + z^2]\,\{(x - \xi)^2 - \beta^2[(y - \eta)^2 + z^2]\}^{1/2}} \tag{9}$$

where $\beta = \sqrt{M^2 - 1}$, and the area of integration c consists of points on the wing in the Mach forecone of the point $\xi,\eta(x < \xi)$. This is the region in which the radical in the denominator of the integrand remains real. It may be seen that the kernel of this integral equation has the same basic symmetry properties as the subsonic kernel of Eq. (1)—namely, that it is symmetrical in y and η, and antisymmetrical in x and ξ—since the operation of partial differentiation with respect to z has no effect on these properties.

The adjoint integral equation is again obtained by interchanging x and ξ and y and η, respectively. This gives

$$\bar{w} = \frac{1}{\pi} \lim_{z \to 0} \frac{\partial}{\partial z} \int\int_{c'} \frac{\bar{u}(\xi, \eta)\, d\xi,\, d\eta(\xi - x)z}{[(y - \eta)^2 + z^2]\,\{(x - \xi)^2 - \beta^2[(y - \eta)^2 + z^2]\}^{1/2}} \tag{10}$$

The integral is now to be evaluated over the area $c'(\xi > x)$ in accordance with the rule that the roles of x and ξ are to be interchanged. It is seen that, as in the subsonic case, the adjoint integral Eq. (10) is simply the lifting-surface equation corresponding to a reversal of flow direction (Fig. 3).

Before proceeding, it will again be convenient to abbreviate the notation by writing

$$w = {}^{**}\!\int_c u(\xi, \eta) K(x, y; \xi, \eta)\, d\xi\, d\eta \tag{11}$$

$$\bar{w} = {}^{**}\!\int_{c'} \bar{u}(\xi, \eta) \bar{K}(x, y; \xi, \eta)\, d\xi\, d\eta \tag{12}$$

where now $**\int$ denotes double integration, followed by partial differentiation with respect to z and then by a limiting process as z goes to zero. Then, again, to meet the requirements on the adjoint solutions $\bar{u}(x, y)$,

$$\int_A \bar{u}(x, y)\, {}^{**}\!\int_c u(\xi, \eta) K(x, y; \xi, \eta)\, d\xi\, d\eta\, dx\, dy = \int_A u(x, y)\, {}^{**}\!\int_{c'} \bar{u}(\xi, \eta) \bar{K}(x, y; \xi, \eta)\, d\xi\, d\eta\, dx\, dy \tag{13}$$

This will again be true if an interchange of orders of integration in the repeated integral on the right-hand side is permissible, since then the expressions on the two sides will be identical, x and ξ being integration indices only. At first glance, the possibility of such an interchange may seem surprising, since the integral Eqs. (11) and (12) involve integrations over different areas (c and c'). Referring to Eq. (13), however, it may be seen that the interchange of order of integration corresponds physically merely to calculating the product of $\bar{u}(\xi, \eta)$ and the downwash produced at each point (ξ, η) on the area c' by the doublets of strength u at a given point (x, y), integrating over ξ and η, and then integrating over all x and y, rather than calculating the downwash produced at point (x, y) by all doublets of strength $u(\xi, \eta)$ in area c and then multiplying by $\bar{u}(x, y)$ and integrating over all x and y. Clearly, these two methods of integration should be equivalent as long as the function $f(x, y, \xi, \eta) = u(x, y)\bar{u}(\xi, \eta)$ is bounded, continuous, and differentiable. If there are subsonic leading edges, u becomes infinite as $1/\sqrt{d}$ as in the purely subsonic case and again $\bar{u}$ must go to zero at such points for the interchange of order of integration to be permissible. Thus, at the subsonic trailing edges of the reversed flow (i.e., subsonic leading edges of the original flow), the Kutta condition must be satisfied. This condition is again just sufficient to completely specify the adjoint or reverse flow solutions $\bar{u}$.

(4) The General Relationship Between Reverse Flows

The adjoint relationship between reverse flows leads immediately to a general relationship between certain significant integrals in such flows. If Eq. (5) is first multiplied by $\bar{u}(x, y)$ and integrated over the wing area, it becomes

$$\int_A w(x, y)\bar{u}(x, y)\, dx\, dy = \int_A \bar{u}(x, y) \int_A^* u(\xi, \eta)K(x, y; \xi, \eta)\, d\xi\, d\eta\, dx\, dy \tag{14}$$

Similarly, multiplying Eq. (6) by $u(x, y)$ and integrating over the wing area gives

$$\int_A \bar{w}(x, y)u(x, y)\, dx\, dy = \int_A u(x, y) \int_A^* \bar{u}(\xi, \eta)\bar{K}(x, y; \xi, \eta)\, d\xi\, d\eta\, dx\, dy \tag{15}$$

By relationship (7), the right-hand sides of these two equations are equal, so that

$$\int_A w(x, y)\bar{u}(x, y)\, dx\, dy = \int_A \bar{w}(x, y)u(x, y)\, dx\, dy \tag{16}$$

By using Eqs. (11) and (12) in place of Eqs. (5) and (6), Eq. (16) may be seen to be true for supersonic flow as well. Eq. (16) is the general reverse flow relationship that has been obtained by different means and in a slightly different form by Ursell and Ward.[13]

(5) Specific Relationships Between Characteristics of Wings in Reverse Flow

(A) *Lifts*

Let $w = \alpha$ and $\bar{w} = \alpha$. Then,

$$\alpha \int_A u\, dx\, dy = \alpha \int_A \bar{u}\, dx\, dy \tag{17}$$

or the lifts of a wing in direct and reverse flow are equal at equal α.

(B) *Pitching Moment and Lift Due to Pitch*

Let $w = \alpha$ and $\bar{w} = qx/U$ (wing pitching about $x = 0$). Then,

$$\alpha \int_A \bar{u}\, dx\, dy = \frac{q}{U} \int_A ux\, dx\, dy \tag{18}$$

Thus, for unit α and q/U, the integral of the lift, $\bar{u}$, on a wing pitching about $x = 0$ is equal to the integral of the moment of the lift, ux, on a wing at constant angle of attack.

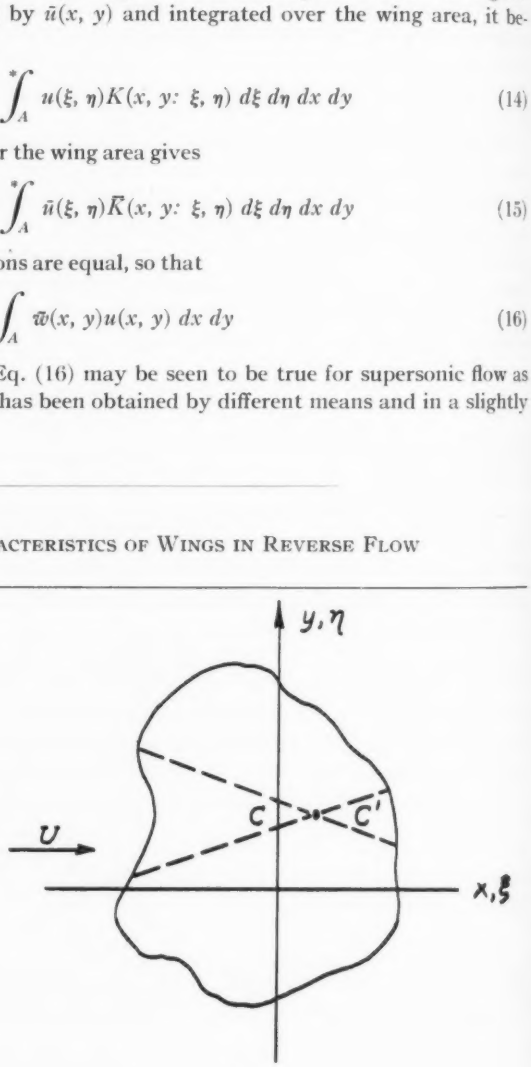

Fig. 3.

(C) *Damping in Pitch*

Let $w = qx/U$ and $\bar{w} = qx/U$. Then,

$$\frac{q}{U}\int_A \bar{u}x\,dx\,dy = \frac{q}{U}\int_A ux\,dx\,dy \qquad (19)$$

Thus, the damping moments on a pitching wing are the same for a wing in direct or reverse flow. A similar relationship for damping in roll obviously results if w and $\bar{w}$ are taken as py/U.

(D) *Drag Due to Lift*

If a lifting surface at constant angle of attack, α, has only supersonic leading and trailing edges so that there is no leading edge suction in either direct or reverse flow, then $D = L\alpha$, and the equality of lifts already demonstrated is sufficient to demonstrate the equality of drag due to lift in direct and reverse flow. It should be noted that side edges parallel to the free-stream flow are permitted, and any number of interacting regions from the tips will not alter the result. If subsonic leading edges are present in either the direct or reverse flow or in both, the drags due to lift will differ by the difference of the leading-edge suctions in the two cases.

(E) *Yawing Moment Due to Rolling*

Again, if the wing has no subsonic leading edges in either direct or reverse flow, the yawing moments due to rolling will be equal, since at any point the yawing moment contributed will be α times the rolling moment, and the equality of the damping in roll for direct and reverse flow has already been shown.

(F) *Rolling Moment Due to Sideslip or Differential Wing Deflection*

In subsonic flow, the effect of sideslip on a wing with dihedral and small sweep or of differential wing deflection is to produce an increment of angle of attack which is positive on one wing and negative on the other. This may be represented by $w = \Delta\alpha \operatorname{sgn} y$, where α is the differential angle of attack and sgn y denotes the sign of y.

Let $w = py$ and $\bar{w} = \Delta\alpha \operatorname{sgn} y$. Then

$$p\int_A \bar{u}y\,dx\,dy = \Delta\alpha\int_A u \operatorname{sgn} y\,dx\,dy \qquad (20)$$

For a spanwise symmetrical wing, the integral on the right-hand side is simply the sum of the absolute values of the lift on the two sides of a rolling wing. Thus, for unit p and $\Delta\alpha$, the rolling moment due to $\Delta\alpha$ is simply equal to the sum of the absolute values of the lift on a rolling wing. For supersonic flow, the $\Delta\alpha$ must be considered as arising from differential wing deflection only, since sideslip produces, in general, changes in regions bounded by the Mach cones from the tips, as well as changes in effective leading-edge Mach Number which may be important.

(6) Generalizations of the Munk Two-Dimensional Airfoil Theorems

The general reverse flow relationship (16) may be applied to a more general class of problems to give formulas for total lift, pitching moment, and rolling moment on a wing with any specified boundary conditions, $w = f(x, y)$, which reduce, for the two-dimensional case, to the well-known Munk formulas for lift and pitching moment.

(A) *Lift Formula*

Let $\bar{w} = \alpha$ and $w = f(x, y)$. Then,

$$\alpha\int_A u\,dx\,dy = \int_A \bar{u}f(x, y)\,dx\,dy$$

or

$$\int_A u\,dx\,dy = \int_A \frac{\bar{u}}{\alpha}f(x, y)\,dx\,dy \qquad (21)$$

Now the lift, L, is given by

$$L = 2\rho U^2\int_A u\,dx\,dy$$

so that

$$L = 2\rho U^2\int\frac{\bar{u}}{\alpha}f(x, y)\,dx\,dy$$

or

$$L = \int_A \frac{\bar{p}}{\alpha}f(x, y)\,dx\,dy \qquad (22)$$

where $\bar{p}$ is the local lift per unit area on the wing in reverse flow at angle of attack α. Thus, the lift distribution on the wing in reverse flow at constant unit angle of attack is the influence function for the total lift on the wing in direct flow. This formula is particularly useful for wings symmetrical chordwise about a spanwise axis, since then $\bar{u}(x)$ is simply $u(-x)$, and no actual calculation with the wing in reverse flow need be done. Also, in lifting-line theory, every wing is the same in direct and reverse flow, leading to a simple application of Eq. (22) to flapped and twisted wings.

In the limiting case of two-dimensional thin airfoils,[21]

$$u/\alpha = \sqrt{[1 - (2x/c)]/[1 + (2x/c)]}$$

Thus, substituting $-x$ for x,

$$\bar{u}/\alpha = -\sqrt{[1 + (2x/c)]/[1 - (2x/c)]}$$

and

$$L = -2\rho U^2\int_{-c/2}^{c/2} f(x)\sqrt{\frac{1 + (2x/c)}{1 - (2x/c)}}\,dx$$

where c is the chord and $f(x)$ is the local slope of the airfoil. This is exactly Munk's formula for lift.

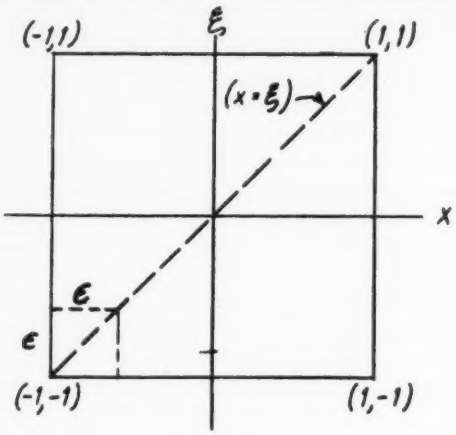

FIG. 4.

(B) *Pitching Moment Formula*

Let $\bar{w} = q(x/U)$ and $w = f(x, y)$. Then,

$$\frac{q}{U}\int_A ux\,dx\,dy = \int_A \bar{u}_1 f(x, y)\,dx\,dy \qquad (23)$$

or

$$\int_A ux\,dx\,dy = \int_A U\frac{\bar{u}_1}{q} f(x, y)\,dx\,dy$$

The moment about $x = 0$, M is given by

$$M_1 = 2\rho U^2 \int_A ux\,dx\,dy$$

so that

$$M_1 = 2\rho U^3 \int_A \frac{\bar{u}_1}{q} f(x, y)\,dx\,dy$$

or

$$M_1 = \int_A \frac{\bar{p}_1}{q} Uf(x, y)\,dx\,dy \qquad (24)$$

Thus, $\bar{p}_1 U/q$, where $\bar{p}_1$ is the lifting pressure distribution on the wing in reverse flow pitching with angular velocity q about the axis $x = 0$, is the influence function for total moment about $x = 0$ of the wing in direct flow. Again, this reduces to Munk's formula in two-dimensional flow as follows:[20]

$$\bar{p}_1/q = \rho c U\sqrt{1 - (2x/c)^2}$$

so that

$$M_1 = \rho c U^2 \int_{-c/2}^{c/2} f(x)\sqrt{1 - \left(\frac{2x}{c}\right)^2}\,dx$$

which is one form for the moment about the airfoil center according to Munk.[20]

(C) *Rolling Moment Formula*

Let $\bar{w} = py/U$ and $w = f(x, y)$. Then,

$$\frac{p}{U}\int_A uy\,dx\,dy = \int_A \bar{u}f(x, y)\,dx\,dy \qquad (25)$$

or

$$\int_A uy\,dx\,dy = \int_A \frac{U}{p}\,\bar{u}\cdot f(x, y)\,dx\,dy$$

The rolling moment is given by

$$M_2 = 2\rho U^2 \int_A uy\,dx\,dy$$

or

$$M_2 = \int_A \frac{\bar{p}_2 U}{p} f(x, y)\,dx\,dy \qquad (26)$$

Here it is seen that $\bar{p}_2 U/p$ plays the role of influence coefficient for total rolling moment, where $\bar{p}_2$ is the lifting pressure distribution on the wing in reverse flow rolling with angular velocity p.

(7) THE ADJOINT VARIATIONAL PRINCIPLE

The results that have been obtained establishing the adjoint relationship between direct and reverse flows over a lifting surface [Eq. (7)] may be used to formulate a variational principle for such flows. Consider, for subsonic flows,

$$\delta I = \delta\left[\int_A (\bar{w}u + w\bar{u})\,dx\,dy - \int_A \bar{u}\,{}^{*}\!\int_A Ku\,d\xi\,d\eta\,dx\,dy\right] \qquad (27)$$

where δ denotes the first variation in the usual sense of the calculus of variations and u and $\bar{u}$ are restricted to admissible functions satisfying the Kutta conditions in the direct and reverse flow, respectively. Subject to this limitation, the functions u and $\bar{u}$ are to be varied arbitrarily and independently of each other. Then,

$$\delta I = \int_A (\bar{w}\delta u + w\delta\bar{u})\,dx\,dy - \int_A \delta\bar{u}\,{}^{*}\!\int_A Ku\,d\xi\,d\eta\,dx\,dy - \int_A \bar{u}\,{}^{*}\!\int_A K\delta u\,d\xi\,d\eta\,dx\,dy \qquad (28)$$

But, by Eq. (7),

$$\int_A \bar{u} \int_A^* K \delta u \, d\xi \, d\eta \, dx \, dy = \int_A \delta u \int_A^* \bar{K} \bar{u} \, d\xi \, d\eta \, dx \, dy \tag{29}$$

Substituting Eq. (29) into Eq. (28),

$$\delta I = \int_A \left[\bar{w} - \int_A^* \bar{K} \bar{u} \, d\xi \, d\eta \right] \delta u \, dx \, dy + \int_A \left[w - \int_A^* K u \, d\xi \, d\eta \right] \delta \bar{u} \, dx \, dy \tag{30}$$

If u and $\bar{u}$ are the correct solutions corresponding to w and $\bar{w}$ in direct and reverse flow, respectively, then

$$\bar{w} - \int_A^* \bar{K} \bar{u} \, d\xi \, d\eta = 0; \quad w - \int_A^* K u \, d\xi \, d\eta = 0; \quad \delta I = 0$$

Thus the expression

$$\delta \left[\int_A (\bar{w} u + w \bar{u}) \, dx \, dy - \int_A \bar{u} \int_A^* K u \, d\xi \, d\eta \, dx \, dy \right] = 0 \tag{31}$$

is equivalent to the integral equations of lifting-surface theory for the direct and reverse flow over a given plan form with local slopes w and $\bar{w}$, respectively. The value of such a formulation as opposed to the integral equations themselves is that it lends itself most readily to approximate solutions by methods analogous to the Rayleigh-Ritz method for self-adjoint problems.[21] An important feature of solutions by the variational method is that the expression in brackets in Eq. (31) is stationary for first-order variations of u and $\bar{u}$ from the correct values. Thus, the errors in the expression itself tend to be minimized even with approximate u and $\bar{u}$. The integrals in the expression are closely related to lift, moment, and other qualities of physical interest. This matter will be pursued in greater detail in the following section.

(8) Approximate Methods for Subsonic Lifting-Surface Problems

On the basis of the adjoint variational principle, Eq. (31), various approximate methods for the solution of lifting-surface problems may be formulated. These methods are essentially similar to the Rayleigh-Ritz method, which is commonly used for self-adjoint problems. For most practical purposes, it is usually desirable to simplify the two-dimensional integral Eq. (7) of lifting-surface theory in at least two ways: first, by reducing the equation to a one-dimensional integral equation or a finite set of these; second, by introducing more readily integrable approximations to the kernel, K, appropriate to the wing shapes and aspect ratios being studied. The variational principle provides a direct systematic way of accomplishing the first of these simplifications; the second simplification is, of course, still necessary. The Prandtl,[7] Weissinger,[8] and Reissner[10] lifting-line theories for relatively high aspect ratio wings will be shown to follow from the variational principle plus the high aspect ratio kernel approximations, the nature of which have already been clearly brought out by Reissner.[10] For low aspect ratio wings, the Lawrence theory will be seen to follow from the variational principle plus the low aspect ratio approximation to the kernel presented by Lawrence.[9] In all of this work, the two-dimensional integral equation was multiplied by some weighting function in one variable and integrated over that variable after a suitable approximation to the kernel had been made, thus reducing the problem to that of solution of a one-dimensional integral equation or, in the case of Reissner's work, to two one-dimensional integral equations. For the theories of this type currently available, the choice of the weighting function appears to have been made intuitively or by recourse to analogy with the limiting cases of two-dimensional theory or of very low aspect ratio theory.[22] The variational principle leads to all of these weighting functions on a unified basis and indicates, as well, further approximations to lifting-surface theory.

It should be remarked here that, in principle, the two-dimensional integral equation of lifting-surface theory can be solved by collocation at a sufficient number of points spanwise and chordwise over the wing. This, however, usually turns out to be extremely cumbersome, and in few cases is such a procedure used in practice. Further, if a small number of points are to be used in collocation, it is usually to be expected that the variational technique involving a number of free parameters equal to the number of collocation points would be considerably more accurate. This follows from the fact that the variational method involves averaging of the satisfaction of the boundary conditions over the wing surface with a weighting function such as to make certain integrals closely related to the total lift and moments on the airfoil stationary with respect to first-order errors in the free parameters. The proper weighting functions are, of course, according to Eq. (31), the adjoint lift distributions. Some of these ideas will become clearer in specific applications.

(*A*) *High Aspect Ratio Theory*

For relatively high aspect ratios, the spanwise distribution is of principal interest, so that a suitable approximation for the lift distribution is of the form[11, 12]

$$u(\xi, \eta) = A\phi_1(\eta)\sqrt{\frac{(c/2) - \xi}{(c/2) + \xi}} + B\phi_2(\eta)\sqrt{1 - \left(\frac{2\xi}{c}\right)^2} + C\phi_3(\eta)\left(\frac{2\xi}{c}\right)\sqrt{1 - \left(\frac{2\xi}{c}\right)^2} + \ldots \tag{32}$$

If the wing is symmetrical about a spanwise axis, reversal of flow direction involves only a replacement of ξ by $-\xi$, so that

$$\bar{u}(\xi, \eta) = \bar{A}\phi_1(\eta)\cdot\sqrt{\frac{(c/2) + \xi}{(c/2) - \xi}} + \bar{B}\phi_2(\eta)\cdot\sqrt{1 - \left(\frac{2\xi}{c}\right)^2} - \bar{C}\phi_3(\eta)\cdot\left(\frac{2\xi}{c}\right)\sqrt{1 - \left(\frac{2\xi}{c}\right)^2} + \ldots \tag{33}$$

Here, c, the wing chord, may be a function of η, and the axis $\xi = 0$ is the axis of symmetry. The constants A, B, C, etc., multiplying each term are the free parameters to be established on the basis of the variational principle, while the ϕ's are unknown functions to be determined on the basis of the one-dimensional spanwise integral equations obtained. The chordwise functions are those originally introduced by Birnbaum[11] in two-dimensional wing theory; the first, $\sqrt{[(c/2) - \xi]/[(c/2) + \xi]}$, gives the chordwise distribution for constant angle of attack, w = constant; the second, $\sqrt{1 - (2\xi/c)^2}$, gives the chordwise distribution for $w\alpha\xi$; the third, $2\xi/c\sqrt{1 - (2\xi/c)^2}$, gives the chordwise distribution for $w\alpha[(2\xi/c)^2 - 1/2]$ (the s-shaped airfoil). As in the Rayleigh-Ritz method,

$$\delta\bar{u} = (\partial\bar{u}/\partial A)\delta A + (\partial\bar{u}/\partial B)\delta B \tag{34}$$

and since δA, δB, δC, etc., are arbitrary, each variation may be treated as independent.

To obtain a single one-dimensional integral equation corresponding to lifting-line theory, only the first terms of the series Eqs. (32) and (33) are used in conjunction with Eq. (31). Thus, in this case,

$$\left.\begin{aligned}\delta\bar{u} &= (\partial\bar{u}/\partial\bar{A})\ \delta\bar{A}\\ \delta u &= (\partial u/\partial A)\ \delta A\end{aligned}\right\} \tag{35}$$

Eq. (31) then leads to

$$\delta\bar{A}\int_A \phi_1(y)\sqrt{\frac{(c/2) + x}{(c/2) - x}}\left[w - \overset{*}{\int_A} KA\phi_1(\eta)\sqrt{\frac{(c/2) - \xi}{(c/2) + \xi}}\,d\xi\,d\eta\right]dx\,dy + \delta A\int_A \phi_1(y)\sqrt{\frac{(c/2) - x}{(c/2) + x}}\times$$
$$\left[\bar{w} - \overset{*}{\int_A} \bar{K}\bar{A}\phi_1(\eta)\sqrt{\frac{(c/2) + \xi}{(c/2) - \xi}}\,d\xi\,d\eta\right]dx\,dy = 0 \tag{36}$$

Since $\delta\bar{A}$ and δA are independent and since in this case only the wing in direct flow is of interest, the final result desired is obtained by setting the term multiplied by $\delta\bar{A}$ equal to zero,

$$\int_A \phi_1(y)\sqrt{\frac{(c/2) + x}{(c/2) - x}}\left[w(x, y) - \overset{*}{\int_A} KA\varphi_1(\eta)\sqrt{\frac{(c/2) - \xi}{(c/2) + \xi}}\,d\xi\,dn\right]dx\,dy = 0 \tag{37}$$

The integration over y may be dropped, since for arbitrary function, ϕ_1, the entire integral will be zero if the condition

$$\int\sqrt{\frac{(c/2) + x}{(c/2) - x}}\left[w(x, y) - \overset{*}{\int_A} KA\phi_1(\eta)\sqrt{\frac{(c/2) - \xi}{(c/2) + \xi}}\,d\xi\,d\eta\right]dx = 0 \tag{37a}$$

is satisfied. The problem now resolves itself into finding a suitable approximation to the kernel, so that the integration with respect to ξ and x may be readily carried out. Reissner[10] has discussed the nature of such approximations for the Prandtl and Weissinger lifting-line theories. When the integrations on ξ and x have been carried out, a one-dimensional integral equation for the spanwise lift remains.

By retaining the first and second terms of the series Eqs. (32) and (33), two simultaneous one-dimensional integral equations for the spanwise lift, as originally given by Reissner, are obtained. In this case,

$$\delta\bar{u} = (\partial\bar{u}/\partial\bar{A})\ \delta\bar{A} + (\partial\bar{u}/\partial\bar{B})\ \delta\bar{B} \tag{38}$$

$$u(\xi, \eta) = A\phi_1(\eta)\sqrt{\frac{(c/2) - \xi}{(c/2) + \xi}} + B\phi_2(\eta)\sqrt{1 - \left(\frac{2\xi}{c}\right)^2} \tag{39}$$

Further,

$$\left.\begin{aligned} \partial\bar{u}/\partial A &= \sqrt{[(c/2) + \xi]/[(c/2) - \xi]}\,\phi_1(\eta) \\ \partial u/\partial \bar{B} &= \sqrt{1 - (2\xi/c)^2}\,\phi_2(\eta) \end{aligned}\right\} \tag{40}$$

Then, using Eq. (31) and retaining only the equations applying to the wing in direct flow,

$$\int_A \phi_1(y)\sqrt{\frac{(c/2) + x}{(c/2) - x}}\left\{ w(x, y) - \int_A^* K\left[A\phi_1(\eta)\sqrt{\frac{(c/2) - \xi}{(c/2) + \xi}} + B\phi_2(\eta)\sqrt{1 - \left(\frac{2\xi}{c}\right)^2}\right] d\xi\, d\eta \right\} dx\, dy = 0 \tag{41}$$

$$\int_A \phi_2(y)\sqrt{1 - \left(\frac{2x}{c}\right)^2}\left\{ w(x, y) - \int_A^* K\left[A\phi_1(\eta)\sqrt{\frac{(c/2) - \xi}{(c/2) + \xi}} + B\phi_2(\eta)\sqrt{1 - \left(\frac{2\xi}{c}\right)^2}\right] d\xi\, d\eta \right\} dx\, dy = 0 \tag{42}$$

Once again, with an approximation for K which permits the integrations on x and ξ to be carried out, two one-dimensional integral equations result. These may be solved simultaneously for $A\phi_1(y)$ and $B\phi_2(y)$. Using the variational principle, the procedure for generalization to n simultaneous equations is obvious.

In lifting-line theory, the restriction of the above procedure to wings with a spanwise axis of symmetry is not essential, since the chordwise lift distribution is treated very approximately. Therefore, the above procedure may be carried over to any high aspect ratio wing of small sweep.

Once a one-dimensional integral equation has been obtained, it in turn may be solved by collocation or by a variational technique. The application of the variational technique to lifting-line theory has been carried out by Ziller[23] and by the author[24] and has been shown to be identical to the Lotz method if the chord and twist distributions are represented as Fourier series of the type used by Lotz. Thus, the Lotz method in Prandtl lifting-line theory may be viewed from the standpoint of the variational method as the application of Eq. (31) along with the Prandtl kernel approximation, and with the functions u and $\bar{u}$ given by

$$\left.\begin{aligned} u(x, y) &= \sqrt{\frac{(c/2) - x}{(c/2) + x}}\sum A_n y^n \sqrt{s^2 - y^2} \\ \bar{u}(x, y) &= \sqrt{\frac{(c/2) + x}{(c/2) - x}}\sum \bar{A}_n y^n \sqrt{s^2 - y^2} \end{aligned}\right\} \tag{43}$$

where s is the semispan. The success of the Lotz method may then be regarded as an indication of the power of the variational technique as well.

(B) *Low Aspect Ratio Wings*

Low aspect ratio wings have been treated by Lawrence.[9] His methods may be shown to fit into the framework of the variational method and may be generalized accordingly. Lawrence deals only with straight trailing edges; then, for sweptback leading edges, functions u and $\bar{u}$ having the proper edge conditions are, as used by Lawrence,

$$\left.\begin{aligned} u(x, y) &= A\,\frac{1}{\sqrt{s^2 - y^2}}\,g'(x) \\ \bar{u}(x, y) &= \bar{A}\sqrt{s^2 - y^2}\,\bar{g}'(x) \end{aligned}\right\} \tag{44}$$

where s is the span, which may be a function of x. It should be noted that for the wing in direct flow (u) there is a $1/\sqrt{d}$ singularity at the leading edge, while for the wing in reverse flow, (u), the lift goes to zero at that same edge as required by the Kutta condition. Application of Eq. (31) leads to

$$\int_A \sqrt{s^2 - y^2}\,\bar{g}'(x)\left[w(x, y) - \int_A^* K \times \frac{A}{\sqrt{s^2 - \eta^2}}\,g'(x)\, d\xi\, d\eta \right] dx\, dy = 0 \tag{45}$$

By a kernel approximation suitable for low aspect ratios, the integrations on y and η can be carried out leaving a one-dimensional integral equation in the chordwise direction. In this case, the integration on x may be dropped.

The foregoing procedure may be generalized to obtain any number of simultaneous one-dimensional integral equations by using the functions

$$\left.\begin{aligned} u(x, y) &= \sum_{n=0}^{\infty} \frac{A_n y^n}{\sqrt{s^2 - y^2}}\,g_n'(x) \\ \bar{u}(x, y) &= \sum_{n=0}^{\infty} \bar{A}_n y^n \sqrt{s^2 - y^2}\,\bar{g}_n'(x) \end{aligned}\right\} \tag{46}$$

Terms with n even correspond to symmetrical spanwise loading, while those with n odd correspond to antisymmetrical loading. Proceeding by analogy to the extremely low aspect ratio case (Jones[22]), Lawrence[9] has utilized the term $n = 1$ to investigate damping in roll of a low aspect ratio wing. It is perhaps worth remarking, for the sake of completeness, that the variational procedure may also be applied to the Jones theory, although in this case the integral equation is so simplified that exact solution by inversion of the equation is possible.[25]

In exactly the same manner as illustrated for the several cases discussed above, the variational method may be employed to construct solutions in subsonic lifting-surface theory to any desired degree of accuracy. In particular, sets of simultaneous one-dimensional equations may be obtained, or alternatively, the two-dimensional integral equation may be reduced to any number of linear algebraic equations for series representations of the solutions involving any number of spanwise and chordwise free parameters. The feasibility of this procedure is limited, however, by the practical difficulties involved in performing some of the required integrations. For this reason, approximations to the kernel of lifting-surface integral equations are of the greatest importance.

(9) Conclusions

Through the introduction of the concept of the integral equation and auxiliary conditions adjoint to the integral equation and Kutta condition of lifting-surface theory, a unified approach to many of the problems of the theory has been effected. It has been shown that the adjoint to the integral equation of a lifting surface is the integral equation for the same surface in reverse flow, and that to satisfy the requirements on an adjoint, the Kutta condition must also be imposed on the solutions of the equation for the surface in reverse flow. The adjoint relationship between wings in direct and reverse flow has been shown to lead directly to a general class of relationships between the characteristics of wings in direct and reverse flow for either subsonic or supersonic speeds. In addition, generalizations of the Munk formulas for lift and moment in two-dimensional flow to three-dimensional flow have been obtained. Finally, an adjoint variational principle for lifting surfaces in subsonic flow has been obtained. On the basis of this variational principle, certain apparently arbitrary or intuitive steps in the approximate theories of Prandtl, Weissinger, Reissner, and Lawrence are shown to be logical applications of the same method.

Further generalizations of this method have been indicated.

Appendix (I)

Conditions for Interchangeability of Order of Integration in Eq. (7)

Since the function $f(x, y, \xi, \eta) = \bar{u}(x, y)u(\xi, \eta)$ is bounded, continuous, and differentiable except near leading edges, only the contribution to the integral of points near such edges need be considered. Near an edge, the flow is essentially two-dimensional, so that the integrals corresponding to Eq. (7) for two-dimensional wings will suffice for this investigation. This integral is of the form

$$I = \frac{1}{2\pi}\int_{-1}^{1} \bar{u}(x) \int_{-1}^{1} \frac{u(\xi)}{x-\xi}\, d\xi\, dx \qquad \text{(I-1)}$$

The lift distribution in the direct flow, $u(\xi)$, will have a $1/\sqrt{d}$ singularity with distance d from the leading edge, $\xi = -1$, and will go to zero at the trailing edge, $\xi = +1$.[17] Thus, the function $f(x, \xi) = \bar{u}(x)\cdot u(\xi)$ will be regular at all points except possibly at the leading edge, where $\bar{u}(\xi)$ may also behave as $1/\sqrt{d}$. The repeated integration, Eq. (I-1), may then be considered to be a double integral in the x, ξ plane if the region $x = -1$ to $-1 + \epsilon$, $\xi = -1$ to $-1 + \epsilon$ is excluded, as shown in Fig. 3, since the function $f(x, \xi)$ is then regular over the region of integration. In this case, the interchangeability of order for the integral (I-1) has been shown by Schwartz.[16] It remains then to consider the excluded region, or

$$I_1 = \frac{1}{2\pi}\int_{-1}^{-1+\epsilon} \bar{u}(x) \int_{-1}^{-1+\epsilon} \frac{u(\xi)}{x-\xi}\, d\xi\, dx \qquad \text{(I-2)}$$

Let $x = -1 + \lambda$ and $\xi = -1 + \mu$. Then,

$$I_1 = \frac{1}{2\pi}\int_{0}^{\epsilon} \bar{u}(\lambda) \int_{0}^{\epsilon} \frac{u(\mu)}{\lambda-\mu}\, d\mu\, d\lambda \qquad \text{(I-3)}$$

Now, suppose near the leading edge ($\mu = \lambda = 0$)

$$\left.\begin{aligned} u(\mu) &\approx 2C/\sqrt{\mu} \\ \bar{u} &\approx 2\bar{C}/\sqrt{\lambda} \end{aligned}\right\} \qquad \text{(I-4)}$$

so that

$$I_1 = 4\,\frac{C\bar{C}}{2\pi}\int_{0}^{\epsilon} \frac{1}{\sqrt{\lambda}} \int_{0}^{\epsilon} \frac{1}{\sqrt{\mu}} \frac{1}{\lambda-\mu}\, d\mu\, d\lambda \qquad \text{(I-5)}$$

Integrating with respect to μ,

$$I_1 = 2\,\frac{C\bar{C}}{\pi}\int_{0}^{\epsilon} \frac{1}{\sqrt{\lambda}} \left[\frac{1}{\sqrt{\lambda}} \log\left|\frac{\sqrt{\lambda}+\sqrt{\epsilon}}{\sqrt{\lambda}-\sqrt{\epsilon}}\right|\right] d\lambda$$

or

$$I_1 = 2\,\frac{C\bar{C}}{\pi}\int_{0}^{\epsilon} \frac{1}{\sqrt{\lambda}} \left[\frac{1}{\sqrt{\lambda}} \log\frac{1+\sqrt{\lambda/\epsilon}}{1-\sqrt{\lambda/\epsilon}}\right] d\lambda$$

Expanding the logarithmic term in series,

$$I_1 = 4\,\frac{C\bar{C}}{\pi}\int_{0}^{\epsilon} \frac{1}{\sqrt{\lambda}} \cdot \frac{1}{\sqrt{\lambda}} \times \left[\sqrt{\frac{\lambda}{\epsilon}} + \frac{(\lambda/\epsilon)^{3/2}}{3} + \frac{(\lambda/\epsilon)^{5/2}}{5} + \cdots\right] d\lambda$$

$$I_1 = 4\,\frac{C\bar{C}}{\pi}\int_{0}^{\epsilon} \frac{1}{\sqrt{\lambda}} \left[\frac{1}{\sqrt{\epsilon}} + \frac{\lambda}{3\epsilon^{3/2}} + \frac{\lambda^2}{5\epsilon^{5/2}} + \cdots\right] d\lambda$$

Integrating with respect to λ,

$$I_1 = 4\,\frac{C\bar{C}}{\pi}\left[2\,\frac{\sqrt{\epsilon}}{\sqrt{\epsilon}} + \frac{1}{3\epsilon^{3/2}}\,\frac{\epsilon^{3/2}}{3/2} + \frac{1}{5\epsilon^{5/2}}\,\frac{\epsilon^{5/2}}{5/2} + \cdots\right]$$

$$I_1 = 8\frac{C\bar{C}}{\pi}\left[1 + \frac{1}{9} + \frac{1}{25} + \cdots\right]$$

$$I_1 = 8\frac{C\bar{C}}{\pi}\cdot\sum_0^\infty \frac{1}{(2n+1)^2} = 8\frac{C\bar{C}}{\pi}\frac{\pi^2}{8}$$

Finally,

$$I_1 = \pi C\bar{C} \tag{I-6}$$

If the order of integration in Eq. (I-5) is interchanged, the integral becomes

$$I_1' = 2\frac{C\bar{C}}{\pi}\int_0^\epsilon \frac{1}{\sqrt{\mu}}\int_0^\epsilon \frac{1}{\sqrt{\lambda}}\frac{1}{\lambda-\mu}\,d\lambda\,d\mu$$

Clearly, this only has the effect of changing the sign of the integral, since the remainder of the steps go through as above, so that

$$I_1' = -\pi C\bar{C} \tag{I-7}$$

Thus, the order of integration may not be interchanged unless either C or $\bar{C}$ is zero at the edge. At a subsonic leading edge of the wing in direct flow, C is obviously not zero, so that $\bar{C}$ must be, if the interchange of order of integration is to be permissible. Therefore, the requirement on the solution of the adjoint integral equation is that the lift go to zero at edges that are subsonic leading edges in the direct flow. But these are the subsonic trailing edges in the reverse flow, so that this requirement is exactly the Kutta condition for the reverse flow.

The singular behavior of these integrals near the leading edge is easily seen to be related to the effect of the leading-edge singularity on drag in lifting-surface theory, which must be removed by the introduction of leading-edge suction calculations into the theory. The drag integral for a two-dimensional lifting surface is

$$D = \frac{\rho}{2\pi}\int_{-1}^{1} u(x)\int_{-1}^{1}\frac{u(\xi)}{x-\xi}\,d\xi\,dx \tag{I-8}$$

with $u(x) \approx 2C/\sqrt{1+x}$ near $x = -1$. Except for the region near the leading edge $u(x)\cdot u(\xi)$ is regular, and the double integral for the remainder of the region of integration must be zero because of the antisymmetric character of the integral. For the region near the leading edge, the previous integration gives, according to Eq. (I-6) with $C = \bar{C}$,

$$D = \rho\pi C^2 \tag{I-9}$$

This is exactly the amount of drag annulled by the leading edge suction,[17] so that the drag of a two-dimensional wing is zero, which is required by perfect fluid theory.

Appendix (II)

Symmetric Form of Integrals over Adjoint Functions

The symmetry in y and η of the integrals in Eq. (7) is not immediately apparent from the forms used in the main body of this paper. It was pointed out that the restrictions on differentiation of an infinite integral under the sign caused the apparent lack of symmetry. The symmetry can readily be brought out by a careful application of the rules for differentiation under the sign. The integrals in Eq. (7) are of the form

$$I_4 = \int\int_A \bar{u}(x,y)\frac{\partial}{\partial y}\int\int_A u(\xi,\eta)\left[\frac{1}{y-\eta} + \frac{1}{y-\eta}\frac{\sqrt{(x-\xi)^2+(y-\eta)^2}}{(x-\xi)}\right]d\xi\,d\eta\,dx\,dy \tag{II-1}$$

where on all edges either u or $\bar{u}$ is zero or both are zero [Appendix (I)]. Now consider

$$I_5 = \frac{\partial}{\partial y}\int\int_A u(\xi,\eta)\left[\frac{1}{y-\eta} + \frac{1}{y-\eta}\frac{\sqrt{(x-\xi)^2+(y-\eta)^2}}{(x-\xi)}\right]d\xi\,d\eta \tag{II-2}$$

Denote the local semispan as $b(\xi)$; this will be the limit of integration on y. If a small region $\eta = y \pm \epsilon$ is excluded from the integration, the differentiation under the integral sign may be performed, provided due attention is given to the variable limits of integration. This corresponds, of course, to recognizing the definition of the integral according to its Cauchy principal value. Thus,

$$I_5 = \lim_{\epsilon\to 0}\int d\xi\frac{\partial}{\partial y}\left\{\int_{-b}^{y-\epsilon} d\eta\,u(\xi,\eta)\left[\frac{1}{y-\eta} + \frac{1}{y-\eta}\frac{\sqrt{(x-\xi)^2+(y-\eta)^2}}{(x-\xi)}\right] + \int_{y+\epsilon}^{b} d\eta\,u(\xi,\eta)\left[\frac{1}{y-\eta} + \frac{1}{y-\eta}\frac{\sqrt{(x-\xi)^2+(y-\eta)^2}}{(x-\xi)}\right]\right\} \tag{II-3}$$

Performing the differentiation under the sign,

$$I_5 = \lim_{\epsilon \to 0} \int d\xi \left\{ \frac{2u(\xi, y)}{\epsilon} \left[1 + \frac{\sqrt{(x-\xi)^2 + \epsilon^2}}{(x-\xi)} \right] - \int_{-b}^{y-\epsilon} d\eta \, \frac{1}{(y-\eta)^2} \left[1 + \frac{(x-\xi)}{\sqrt{(x-\xi)^2 + (y-\eta)^2}} \right] - \int_{y+\epsilon}^{b} d\eta \, \frac{1}{(y-\eta)^2} \left[1 + \frac{(x-\xi)}{\sqrt{(x-\xi)^2 + (y-\eta)^2}} \right] \right\} \quad \text{(II-4)}$$

Substituting this back into Eq. (II-1),

$$I_4 = \lim_{\epsilon \to 0} \int\int_A dx \, dy \, \bar{u}(x, y) \int d\xi \left\{ \frac{2u(\xi, y)}{\epsilon} \left[1 + \frac{\sqrt{(x-\xi)^2 + \epsilon^2}}{(x-\xi)} \right] - \int_{-b}^{y-\epsilon} d\eta \, \frac{1}{(y-\eta)^2} \left[1 + \frac{(x-\xi)}{\sqrt{(x-\xi)^2 + (y-\eta)^2}} \right] - \int_{y+\epsilon}^{b} d\eta \, \frac{1}{(y-\eta)^2} \left[1 + \frac{(x-\xi)}{\sqrt{(x-\xi)^2 + (y-\eta)^2}} \right] \right\} \quad \text{(II-5)}$$

This last equation is clearly symmetrical in y and η, since they only appear in the form $(y-\eta)^2$; the application of the limiting process can have no effect upon this symmetry.

References

[1] von Kármán, Th., *Supersonic Aerodynamics—Principles and Applications*, Journal of the Aeronautical Sciences, Vol. 14, No. 7, pp. 373–409, July, 1947.

[2] Hayes, W. D., *Linearized Supersonic Flow*, North American Aviation, Inc., Report AL No. 222, June 18, 1947.

[3] Munk, M. M., *The Reversal Theorem of Linearized Supersonic Airfoil Theory*, Journal of Applied Physics, Vol. 21, No. 2, pp. 159–161, February, 1950.

[4] Flax, A. H., *Relations Between the Characteristics of a Wing and Its Reverse in Supersonic Flow*, Journal of the Aeronautical Sciences, Vol. 16, No. 8, pp. 496–504, August, 1949.

[5] Harmon, S., *Theoretical Relations Between the Stability Derivatives of a Wing in Direct and in Reverse Supersonic Flow*, N.A.C.A. T.N. No. 1943, September, 1949.

[6] Brown, C. E., *The Reversibility Theorem for Thin Airfoils in Subsonic and Supersonic Flow*, N.A.C.A. T.N. No. 1944, September, 1949.

[7] Prandtl, L., *Tragflächentheorie. I. Mitteilung, Nachrichten der K. Gesellschaft der Wissenschaften zu Göttingen*, Math.-Phys. Klasse, pp. 451–477, 1918.

[8] Weissinger, J., *The Lift Distribution of Sweptback Wings*, N.A.C.A. T.M. No. 1120, March, 1947.

[9] Lawrence, H. R., *The Lift Distribution on Low-Aspect-Ratio Wings at Subsonic Speeds*, Cornell Aeronautical Laboratory Report No. AF-673-A-1, August, 1950.

[10] Reissner, E., *Note on the Theory of Lifting Surfaces*, Proc. Natl. Acad. Sci., Vol. 35, No. 4, pp. 208–215, April, 1949.

[11] von Kármán, Th., and Burgess, J. M., *General Aerodynamic Theory—Perfect Fluids; Aerodynamic Theory*, W. F. Durand, Ed., Vol. II, p. 194; Durand Reprinting Committee, 1943.

[12] Glauert, H., *The Elements of Aerofoil and Airscrew Theory*; Cambridge University Press, 1926.

[13] Ursell, F., and Ward, G. N., *On Some General Theorems in the Linearized Theory of Compressible Flow*, Quarterly Journal of Mechanics and Applied Mathematics, Vol. III, Part 3, pp. 326–348, September, 1950.

[14] Reissner, E., *On the General Theory of Thin Airfoils for Non-Uniform Motion*, N.A.C.A. T.N. No. 946, August, 1944.

[15] Lovett, W. V., *Linear Integral Equations;* McGraw-Hill Book Company, Inc., New York, 1944.

[16] Schwartz, L., *Berechnung der Druckverteilung einer harmonisch sich verformenden Tragfläche in ebener Strömung*, Luftfahrtforschung, Vol. 17, pp. 379–386, 1940.

[17] von Kármán, Th., and Burgess, J. M., *General Aerodynamic Theory—Perfect Fluids; Aerodynamic Theory*, W. F. Durand, Ed., Vol. II, p. 515, Durand Reprinting Committee, 1943.

[18] Göthert, B., *Plane and Three-Dimensional Flow at High Subsonic Speeds*, N.A.C.A. T.M. No. 1105, 1946.

[19] Ward, G. N., *Calculation of Downwash Behind a Supersonic Wing*, The Aeronautical Quarterly, Vol. 1, Part I, May, 1949.

[20] Betz, A., *Applied Airfoil Theory; Aerodynamic Theory*, W. F. Durand, Ed., Vol. IV, pp. 26–35, Durand Reprinting Committee, 1943.

[21] Flax, A. H., *Aeroelastic Problems at Supersonic Speeds, Appendix;* Proceedings of Second International Aeronautical Conference, I.A.S.-R.Ae.S., 1949, pp. 322–359, 1949.

[22] Jones, R. T., *Properties of Low-Aspect-Ratio Pointed Wings at Speeds Below and Above the Speed of Sound*, N.A.C.A. T.R. No. 835, 1946.

[23] Ziller, F., *Beitrag zur Theorie des Tragflugels von endlicher Spannweite*, Ingenieur-Archiv, Vol. 11, pp. 239–259, 1940.

[24] Flax, A. H., *On a Variational Principle in Lifting-Line Theory*, Readers' Forum, Journal of the Aeronautical Sciences, Vol. 17, No. 9, p. 596, September, 1950.

[25] Lomax, Harvard, and Heaslet, Max, *Linearized Lifting-Surface Theory for Sweptback Wings with Slender Planforms*, N.A.C.A T.N. No. 1992, December, 1949.

Diffuser Efficiency of Free-Jet Supersonic Wind Tunnels at Variable Test Chamber Pressure*

RUDOLF HERMANN†
University of Minnesota

SUMMARY

The flow process occurring in the diffuser of a supersonic wind tunnel with free jet and its efficiency have been previously investigated by the author (see *Air Force Technical Report No. 6334*, December, 1950) for the special case, where the pressure in the test chamber surrounding the jet is equal to the pressure in the exit cross section of the Laval nozzle.

The present analysis deals with the general case, where the test chamber pressure is different from the nozzle exit pressure. By using the basic equations of continuity, energy, and momentum flow through a control surface, an exact solution for one-dimensional, nonviscous, steady flow is obtained.

One of the basic results is that the flow—after the transformation process in the diffuser is completed—is subsonic if the test chamber pressure is above, equal to, or below the nozzle exit pressure. A supersonic flow is possible, too, if the test chamber pressure is smaller than a certain finite limit below the equilibrium.

The results are presented in eight graphs over a Mach Number range from 1 to 10, showing velocity and pressure after the transformation, diffuser efficiency, total pressure ratio, and diffuser throat area at variable chamber pressure. The analysis also shows, for the first time, the exact mechanism of test chamber pressure control for the subsonic solution by means of an adjustable diffuser throat and the quantitative description of a "slow starting" process of the tunnel.

NOMENCLATURE

a	=	velocity of sound
f	=	ratio of nozzle exit cross-section area to diffuser intake area [Eq. (03)]
f'	=	combination of f and ν [see Eq. (24)]
F	=	cross-section area
K	=	total pressure ratio
l	=	length of free jet
M^*	=	w/a^* = dimensionless velocity
M	=	w/a = Mach Number
p	=	static pressure
p_c	=	pressure in test chamber
p_0	=	total pressure
p_0'	=	total pressure after losses
P	=	p/p_0 = dimensionless pressure
R	=	gas constant
s	=	entropy
T	=	absolute temperature
w	=	velocity
γ	=	ratio of specific heats (1.405 for numerical calculations)
ϵ	=	half of expansion angle from nozzle exit to diffuser intake (see Fig. 1)
η	=	efficiency of pressure recovery [see Eq. (34)]
ϑ	=	function of M^* or M [see Eq. (37)]
Θ	=	dimensionless mass flux [see Eq. (13)]
ρ	=	density
ν	=	dimensionless test chamber pressure difference [see Eq. (07)]

Subscripts and Superscripts

L	=	limit at which $K_{P\alpha} = 1$
$max.$	=	maximum
α	=	supersonic solution
β	=	subsonic solution
NS	=	normal shock
P	=	transformation process
0	=	stagnation
1	=	nozzle exit
2	=	diffuser intake
*	=	first throat
*′	=	second throat

(1) INTRODUCTION

CONSIDERING SUPERSONIC WIND TUNNELS with regard to their type of test section, we can distinguish between those with closed wall test section and those with free-jet test section. The flow through the diffuser, the deceleration or transformation process, and, consequently, the pressure recovery are quite different in the case of the two tunnel types, as outlined before.[1, 2] When talking of pressure recovery or diffuser efficiency of a supersonic wind tunnel we must, therefore, differentiate clearly between the diffuser efficiency of a wind tunnel with closed test section and with a free jet. The term "diffuser efficiency" is used in the former[1, 2] and in the present investigation as an abbreviation for "total pressure ratio of the diffuser divided by that of a normal shock at test section Mach Number." A detailed reasoning for this definition was given previously (reference 2, pages 3–6), and its advantage will be evident again during the following analysis.

One of the basic features of a supersonic free jet is the fact that the static pressure surrounding the jet is, in

Received May 25, 1951. Presented at the Aerodynamics Session, Twentieth Annual Meeting, I.A.S., January 28–31, February 1, 1952.

* This report is based on work done previously at Air Engineering Development Division, Wright-Patterson Air Force Base, Dayton, Ohio. The author wishes to acknowledge the valuable assistance of E. Walk, long-time associate, for carefully performing the extended numerical computations and laborious preparation of all graphs; of K. Anderson for critical study of the draft; and of S. J. Guzik for his help in editing.

† Professor, Institute of Technology, Department of Aeronautical Engineering.

general, not equal to the static pressure in the Laval nozzle exit from which the jet emerges. In the case of a subsonic free jet, both of these pressures are necessarily equal. Hence, the supersonic problem has one variable more than the subsonic problem. The former papers[1, 2] calculated flow process and diffuser efficiency for the special case of pressure equilibrium. Then the pressure surrounding the free jet—i.e., the test chamber pressure—is equal to the nozzle exit pressure. For practical model testing this case is often preferred. The present paper deals with the general case of pressure nonequilibrium when the test chamber pressure is larger or smaller than the nozzle exit pressure.

Even though pressure nonequilibrium may not be used for model testing, the results of this analysis are of importance in the design and operation of such tunnels. They clarify the flow mechanism of pressure control in the test section by means of the adjustable diffuser throat, necessary to obtain a desired test chamber pressure—for instance, pressure equilibrium. They furnish numerical data for the needed accuracy of such control device. Also from these results, the "slow-starting" process of this tunnel type, so important for all supersonic wind tunnels, is now quantitatively understood.

This analysis can also be applied directly to the design of turbojet or ram-jet altitude test chambers if the engine jet is supersonic. In this case, pressure nonequilibrium must be used for testing in order to simulate various flight conditions with respect to flight Mach Number, altitude, and fuel consumption.

(2) Establishment of the Fundamental Equations

(A) *The Transformation Process*

In establishing the fundamental equations, we refer to the procedure given previously[1, 2] in detail. The air (Fig. 1) comes from the atmosphere or a stilling chamber with stagnation pressure p_0 and stagnation temperature T_0; passes the first throat F^* of the Laval nozzle; and attains supersonic velocity w_1, pressure p_1, and density ρ_1 in the exit cross section F_1. The air stream emerges from the nozzle exit as a free jet, which is surrounded by air at rest in the test chamber with the test chamber pressure p_c. A certain length l of the free jet is required by the model length, its suspension to the balance, or for the installation of other test devices. One of the main principles of the free jet is that it spreads out and increases its cross-section area in flow direction because of a turbulent mixing process at its surface.

To obtain any pressure recovery, the free jet has to be brought into the diffuser. This requires a "recapture" of the jet by means of a diffuser pickup in the intake area $F_2(F_2 > F_1)$ of the diffuser and a transformation into a flow between rigid walls. We assume that this "transformation process" takes place in the intake portion of the diffuser with constant cross-section area F_2, which corresponds to a relatively long diffuser design with small slope of the walls. Furthermore, we assume that in this "transformation zone" a complete transfer of all values of state occurs, which results in constant velocity w_2, constant pressure p_2, and constant density ρ_2 all over the cross section F_2. After the transformation process is completed, the air flows through a convergent-divergent diffuser with adjustable minimum section, through a fixed diffuser, and finally into the compressors.

(B) *Assumptions and Fundamental Equations*

We consider the flow as one-dimensional, steady, and frictionless, and we use the three theorems of conservation of mass, axial momentum, and energy for a rectangular-shaped bounding surface, which extends from the nozzle exit to the end of the transformation zone and has a constant cross section F_2 (Fig. 1). The advantage of such application of the momentum theorem is that the internal processes, such as recapturing and transformation, need not be known in detail. Evidently, they are irreversible and connected with entropy increase or total pressure loss ($p_0' < p_0$), which will eventually be determined by the calculation.

The continuity equation states the equality of mass entering and leaving the control volume†

$$F_1\rho_1 w_1 = F_2\rho_2 w_2 \tag{01}$$

The assumption of an airtight test chamber which has been made here is of greater importance than might be realized. Calculations show that a relatively small inleakage of air into the test section can produce quite a different flow process.

The momentum equation states that the increase in momentum flow through the control surface equals the net force acting on the surface in the same direction,

$$F_2\rho_2 w_2^2 - F_1\rho_2 w_1^2 = F_1 p_1 + (F_2 - F_1)p_c - F_2 p_2 \tag{05}$$

An analysis shows that a neglect of the turbulent shearing stresses as forces at the control surface in this equation introduces only minor errors. Their main effect is the spreading of the jet, which requires that the diffuser intake area F_2 be larger than the nozzle exit area F_1. This fact, however, is included in Eq. (05).

The energy equation for a closed system states that the total energy entering the control volume must equal the outgoing total energy. With the aid of the equation of state, this can be written

$$\frac{w_1^2}{2} + \frac{\gamma}{\gamma - 1}\cdot\frac{p_1}{\rho_1} = \frac{w_2^2}{2} + \frac{\gamma}{\gamma - 1}\cdot\frac{p_2}{\rho_2} = \frac{\gamma}{\gamma - 1}\cdot\frac{p_0}{\rho_0} \tag{11}$$

† The equations are numbered in agreement with the author's manuscript containing the complete calculations.

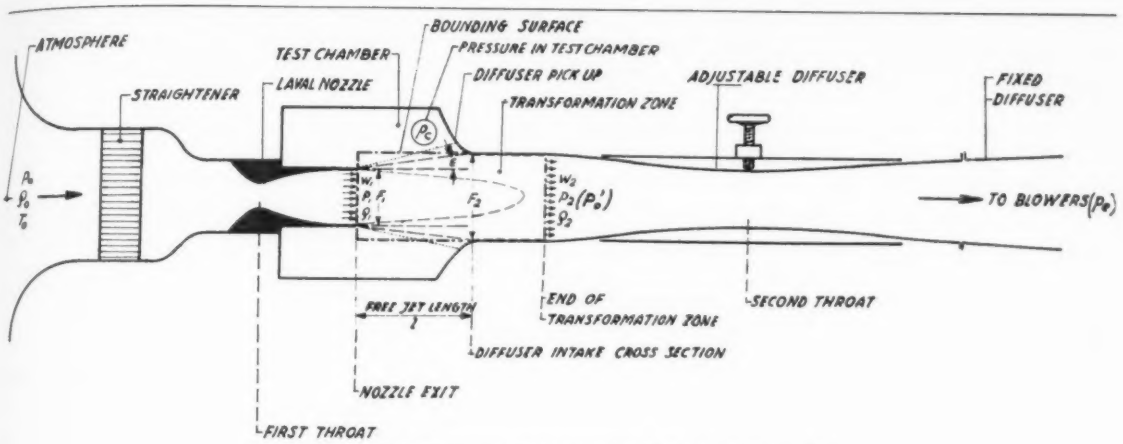

FIG. 1. Scheme of supersonic wind tunnel with free-jet test section.

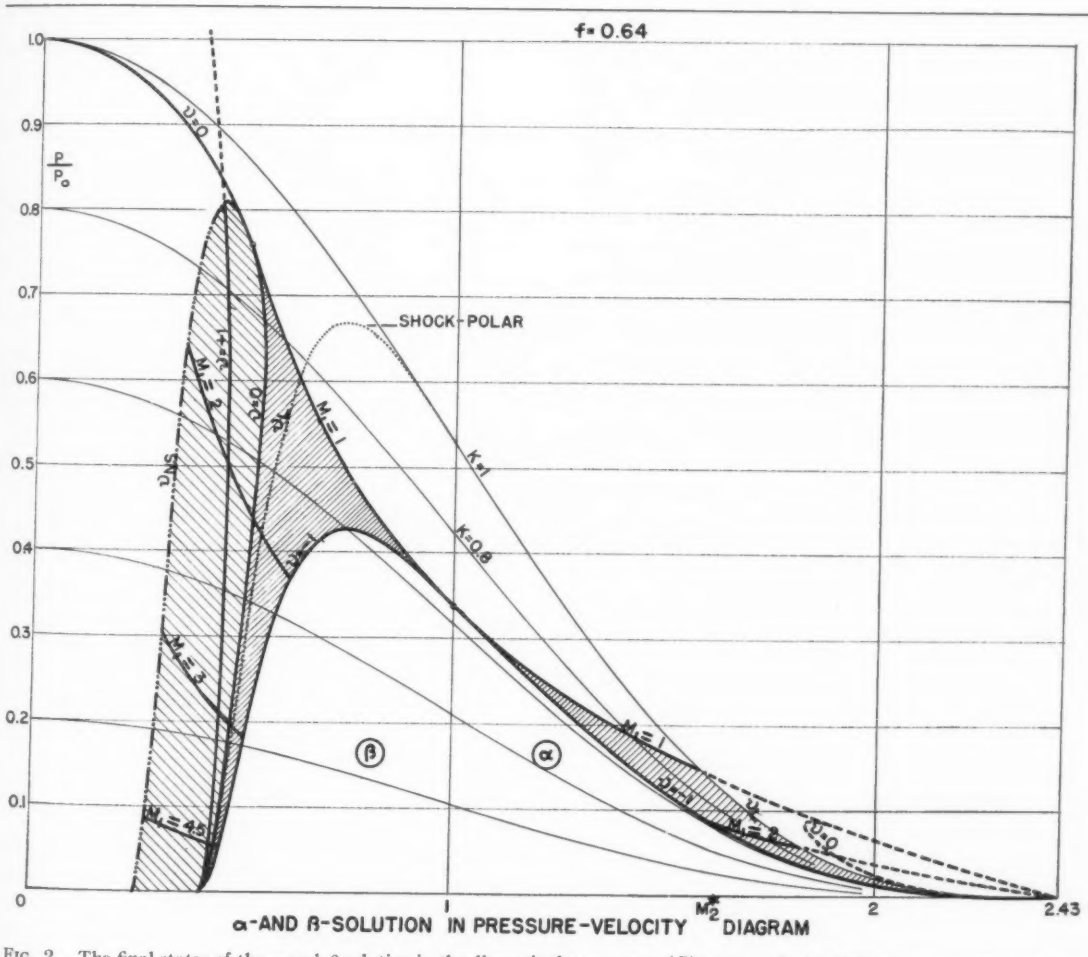

FIG. 2. The final states of the α and β solution in the dimensionless pressure (P) versus velocity (M^*) diagram. Parameters are Mach Numbers M_1 and chamber pressure ν.

This equation is valid even under consideration of the work of the turbulent shearing stresses, because such work represents no exterior work. Since the air in the test chamber is in permanent energy exchange with the jet, it belongs to the system under consideration. The walls of the tunnel, including the test chamber, have to be insulated.

(3) Solution of the System of Equations

The fundamental Eqs. (01), (05), and (11) are a system of three independent equations for the determination of the three unknown variables—w_2, p_2, ρ_2 of the final state. They can be calculated if the three variables w_1, p_1, and ρ_1 of the initial state, the test chamber pressure p_e, and the geometric boundaries F_1, F_2 are given. We now have the general case $p_e \neq p_1$ with one more variable than the former special case $p_e = p_1$.

In order to simplify the set of equations, we introduce the area ratio f and the dimensionless test chamber pressure difference ν,

$$f = F_1/F_2 < 1 \tag{03}$$

$$\nu = (p_e - p_1)/p_1 \tag{07}$$

$\nu = 0$ corresponds to pressure equilibrium. $\nu \gtrless$ corresponds to test chamber pressure above or below the equilibrium. The minimum possible test chamber pressure is the absolute vacuum $p_e = 0$ or $\nu = -1$. Certainly, the jet will expand into the vacuum with considerable increase in cross section, and the one-dimensional analysis will not hold up to this mathematical limit. The maximum test chamber pressure permitted will be discussed later [see Section (5B)]. For practical wind-tunnel purposes, $\nu = +1$ represents a reasonable positive limit that is physically possible above $M = 1.362$ [see Eq. (64)].

The momentum Eq. (05) becomes, with Eqs. (01), (03), (07),

$$f \cdot w_1\rho_1(w_1 - w_2) = p_2 - p_1[1 + (1 - f)\nu] \tag{10}$$

We introduce the following dimensionless values for velocity, pressure, and mass flux:

$$\frac{w}{a^*} = M^*, \qquad \frac{p}{p_0} = P, \qquad \frac{w\rho}{a^*\rho^*} = \Theta \tag{13}$$

where P and Θ are well-known functions of M^* and the entropy s [see reference 2, Eq. (5)]. Using

$$a^{*2}\rho^*/p_0 = \gamma[2/(\gamma + 1)]^{\gamma/(\gamma-1)} \tag{12}$$

Eqs. (10) and (01) become

$$\frac{P(M_2^*, s_2) - P(M_1^*, s_1)\,[1 + (1 - f)\nu]}{M_1^* - M_2^*} = \gamma\left(\frac{2}{\gamma + 1}\right)^{\gamma/(\gamma-1)} \cdot f \cdot \Theta(M_1^*, s_1) \tag{14a}$$

$$\Theta(M_2^*, s_2)/\Theta(M_1^*, s_1) = f \tag{14b}$$

In order to eliminate s_2, we further introduce the total pressure ratio of the transformation process

$$K_P = p_0'/p_0 \tag{15}$$

which is connected with the entropy increase by

$$(s_2 - s_1)/R = -\ln K_P \tag{16}$$

The energy Eq. (11) gives, after some conversions and with Eqs. (15) and (16),

$$P(M^*, s_2) = K_P \cdot P(M^*, s_1) \tag{17}$$

$$\Theta(M^*, s_2) = K_P \cdot \Theta(M^*, s_1) \tag{18}$$

We put Eqs. (17) and (18) in Eqs. (14a) and (14b), eliminate K_P, omit s_1, and obtain

$$K_P = f[\Theta(M_1^*)/\Theta(M_2^*)] \tag{20}$$

$$f\frac{P}{\Theta}(M_2^*) - [1 + (1 - f)\nu]\frac{P}{\Theta}(M_1^*) = \gamma\left(\frac{2}{\gamma + 1}\right)^{\gamma/(\gamma-1)} \cdot f \cdot (M_1^* - M_2^*) \tag{23}$$

Here and in the following, the P and Θ have to be taken at the entropy s_1. Using the abbreviation

$$f' = f/[1 + (1 - f)\nu] \tag{24}$$

Eq. (23) becomes

$$f'\frac{P}{\Theta}(M_2^*) - \frac{P}{\Theta}(M_1^*) = \gamma\left(\frac{2}{\gamma + 1}\right)^{\gamma/(\gamma-1)} \cdot f'(M_1^* - M_2^*) \tag{25}$$

while in Eq. (20) the value f remains. Comparison of Eq. (25) with the corresponding equation of the former report [reference 2, Eq. (7)] gives the following results. For $\nu = 0$, $f' = f$ and Eq. (25) becomes identical with former Eq. (7), which is a necessary agreement. Beyond that, former Eq. (7) becomes identical with Eq. (25) if f is replaced by f'. This fact is not trivial but allows a reduction of the solution for the velocity at $\nu \neq 0$ to that at $\nu = 0$. Thus we obtain

$$M_{2\alpha,\,2\beta}{}^* = \frac{\left(\frac{2\gamma}{\gamma + 1}\right) - \frac{1}{f'}\frac{\gamma - 1}{\gamma + 1}M_1^{*2} + \frac{1}{f'}}{2M_1^*} \pm \sqrt{\left(\frac{\left(\frac{2\gamma}{\gamma + 1} - \frac{1}{f'}\frac{\gamma - 1}{\gamma + 1}\right)M_1^{*2} + \frac{1}{f'}}{2M_1^*}\right)^2 - 1} \tag{29}$$

This equation is identical with the former velocity relation [reference 1 or 2, Eq. (10)] at pressure equilibrium if f is replaced by f'. However, this reduction is valid only for the velocities after the transformation. The pressure relation (20) contains f and cannot be reduced. We use subscript α for the positive sign and subscript β for the negative sign of the root. Exclud-

ing special cases for $M_1^* = 1$ and $f' = 0$, it follows from Eq. (29)

$$M_{2\alpha}^* \cdot M_{2\beta}^* = 1 \tag{30}$$

where

$$M_{2\alpha}^* > 1; \qquad M_{2\beta}^* < 1 \tag{31}$$

and both are always real and positive.

Mathematically, our problem has two solutions—one supersonic α-solution and one subsonic β-solution. Their velocities are interconnected in the same way as the velocities before and behind a normal shock. These results are the same as those obtained in the case of pressure equilibrium.

Analysis of the total pressure belonging to the α- and β-solution will show if and under which conditions they will be permitted by the second law of thermodynamics. Eq. (20) furnishes the total pressure ratio of the α- and β-solution

$$K_{P\alpha} = f[\Theta(M_1^*)/\Theta(M_{2\alpha}^*)] \tag{32}$$

$$K_{P\beta} = f\,[\Theta(M_1^*)/\Theta(M_{2\beta}^*)] \tag{33}$$

The diffuser efficiency or pressure recovery factor is defined again by

$$\eta = K_P/K_{NS}(M_1^*) \tag{34}$$

where $K_{NS}(M_1^*)$ is the total pressure ratio of the normal shock at the test section velocity M_1^*. Introducing for $M^* \geq 1$ the function

$$\vartheta(M^*) = \Theta(M^*)/K_{NS}(M^*) \tag{37}$$

with the characteristic relation

$$\vartheta(M^*) = \Theta(1/M^*) \tag{38}$$

and a finite limiting value for Mach Number infinity [see reference 1 or 2, Eq. (14c)], the diffuser efficiency of the α- and β-solution results in

$$\eta_\alpha = f[\vartheta(M_1^*)/\Theta(M_{2\alpha}^*)] \tag{39}$$

$$\eta_\beta = f[\vartheta(M_1^*)/\vartheta(M_{2\alpha}^*)] \tag{42}$$

In order to characterize the diffuser losses it is sufficient to use either K_P or η. For the α-solution, $K_{P\alpha}$ is preferred because the condition $K_{P\alpha} \lesseqgtr 1$ is significant if the α solution is or is not thermodynamically allowed. For the β-solution, η_α is preferred because $K_{P\beta}$ is, in general, smaller than 1 and for high Mach Numbers is inconveniently small.

(4) Discussion of the Final State of the α- and β-Solution in the Pressure-Velocity Diagram

General Remarks.—The discussion of the results in Sections (4) to (7) is made for the purpose of presenting this paper without further mathematical deductions simply by description of the graphs, obtained by numerical evaluation of the formulas above. They are calculated with the arbitrary value of the area ratio $f = 0.64$, which represents a good average for supersonic wind tunnels with a free-jet length between one and one-half and two times the nozzle exit height. It was used in the design of the two supersonic wind-tunnel test sections (40 by 40 cm.) at Peenemuende and Kochel, Germany—now in operation at Naval Ordnance Laboratory, White Oak, Md. However, the equations allow the calculations with any f-value.

The final states of the α- and β-solution are represented in the diagram of dimensionless pressure (P) versus velocity (M^*) (Fig. 2). Each point represents one thermodynamic state. The initial states lie on the supersonic part of the upper isentropic line. The isentropic lines below the initial one designate higher entropy—states that are allowed by the second law of thermodynamics. States above the initial isentropic line are thermodynamically forbidden. Each final state is designated by the intersection of two lines, one line of Mach Number M_1 and one line of test chamber pressure ν. The net at the right-hand side ($M_2^* \geq 1$) contains the α-solution; the net at the left-hand side ($M_2^* \leq 1$) contains the β-solution. Each final α-state point is connected with the corresponding final β-state point by a normal shock process at the velocity $M_{2\alpha}^*$. It might be emphasized, however, that the transition from one initial state to either one of the final states is never a normal shock, as this graph demonstrates. The diffuser transformation process is a different process of a more general nature than a normal shock.

The régime of the β-solution lies almost completely below the initial isentropic line. The few points at low Mach Number and ν around $+1$, which lie above, are situated at the same time beyond the positive pressure limit ν_{NS} [see Section (5B)]. Hence, all β-solutions within this limit are also permitted by the second law of thermodynamics. The régime of the α-solution extends to a large degree above the initial isentropic line ($K_{P\alpha} = 1$) into the forbidden area. Therefore, only the α-solutions for low chamber pressure smaller than the negative pressure limit $\nu_L(M_1)$ are permitted. The β-solution at this ν_L coincides with the lower portion of the well-known normal shock polar. The line for $\nu = -1$ in the α-solution is identical with the isentropic line for $K_{P\alpha} = f = 0.64$. In the β-solution this line is affine to the normal shock polar by the factor f, which means $\eta_\beta = f$, valid for all M_1.

(5) Diffuser Efficiency of the β-Solution

(A) *Variation with Mach Number*

The diffuser efficiency η_β of the β-solution is shown in Fig. 3 as a function of the initial Mach Number with test chamber pressure ν as the parameter. The general trend of the curves with different chamber pressure is the same as the curve for pressure equilibrium ($\nu = 0$), which at Mach Number 1 has the value $\eta_\beta = 0.888$ and then decreases. All curves approach, for infinite Mach

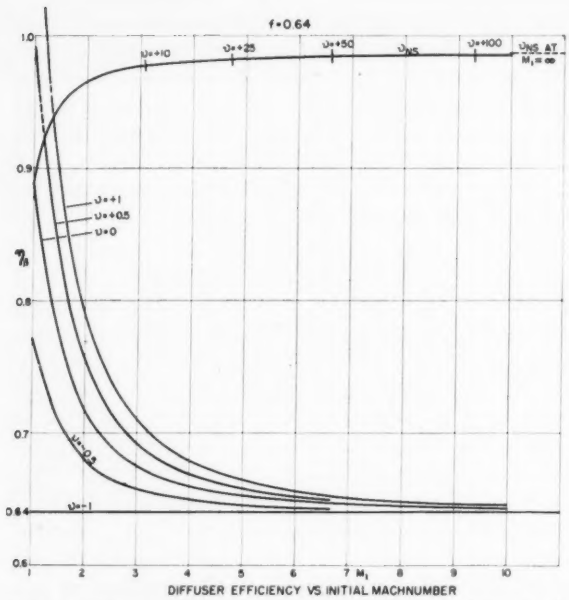

FIG. 3. Diffuser efficiency η_β of the β solution as a function of Mach Number M_1 with chamber pressure ν as the parameter.

Number, the limiting value $\eta_\beta = f$. Positive test chamber pressure improves the diffuser efficiency; negative chamber pressure diminishes the efficiency. At $\nu = -1$, η_β is always equal to f. The influence of test chamber pressure on the efficiency decreases considerably with high Mach Number.

(B) *The Positive Pressure Limit ν_{NS} of the Normal Shock*

The upper curve (Fig. 3) designated with ν_{NS} is the positive pressure limit, beyond which the β-solution has no physical meaning. It is the test chamber pressure at which a normal shock is established in the exit cross section F_1 of the Laval nozzle, followed by a free parallel jet with subsonic velocity and pressure equilibrium. ν_{NS} is calculated from the theory of the normal shock, with p_1 equal to the static pressure before and p_e equal to the static pressure behind the shock at Mach Number M_1. This furnishes

$$\nu_{NS} = [2\gamma/(\gamma + 1)]\,(M_1^2 - 1) \qquad (64)$$

Obviously, this positive pressure limit is large at high Mach Numbers.

Fig. 3 shows that the curve for $\eta_\beta(\nu_{NS})$ starts at Mach Number 1 at the point for $\eta_\beta(\nu = 0)$, then increases, and soon approaches a limiting value. Using an incompressible approximation for $K_{P\beta}(1/M_{max.}{}^*)$ given in the former analysis [reference 2, Eq. (26)] furnishes the formula

$$\lim_{M=\infty} \eta_\beta(\nu_{NS}) = 1 - (1 - f)^2 \cdot \frac{\gamma(\gamma - 1)}{(\gamma + 1)^2} \qquad (70)$$

This limit is always smaller than unity, and for $f = 0.64$ its value is 0.987. Considering only the normal shock in the exit cross section would furnish $\eta_\beta = 1$. The fact that $\eta_\beta(\nu_{NS})$ is always below 1 is due to the transformation losses of the following subsonic jet.

A free-jet wind tunnel can be started "slowly" (quasi-steady) by means of gradually opening the diffuser throat [(see Section (7B)]. The chamber pressure is hereby reduced from a high positive pressure $\nu \leq \nu_{NS}$ gradually down to pressure equilibrium $\nu = 0$ (Fig. 7). Hence, the diffuser efficiency decreases continuously (according to Fig. 3 or 4) down to the value for operation. No jump occurs; no swallowing of the shock happens. No special reserve of compression ratio of the blowers for the starting process is required. In a tunnel of this type, the running compression ratio is higher than the compression ratio needed during the "slow-starting" period.

(C) *Variation with Chamber Pressure*

Fig. 4 shows the same η_β as in Fig. 3, but it is plotted as a function of chamber pressure and with Mach Number as the parameter. η_β increases with increasing test chamber pressure. In the ν range between -1 and $+1$, the change in efficiency is nearly linear. Only the beginning of the positive pressure limit curve $\nu_{NS}(M_1)$ is shown in this diagram. The negative pressure limit $\nu_L(M_1)$, below which the α-solution is permitted by the second law, is also plotted in this graph of the β-solution.

(D) *Linearized Approximation for High Mach Numbers*

An approximation of η_β was obtained, which is linear in the term $1/M^2$. The calculations are carried out in the neighborhood of $M_{max.}{}^*$, linearized in terms of $\Delta M^* = M_{max.}{}^* - M^*$. First, $M_{2\alpha}{}^*$ according to Eq.

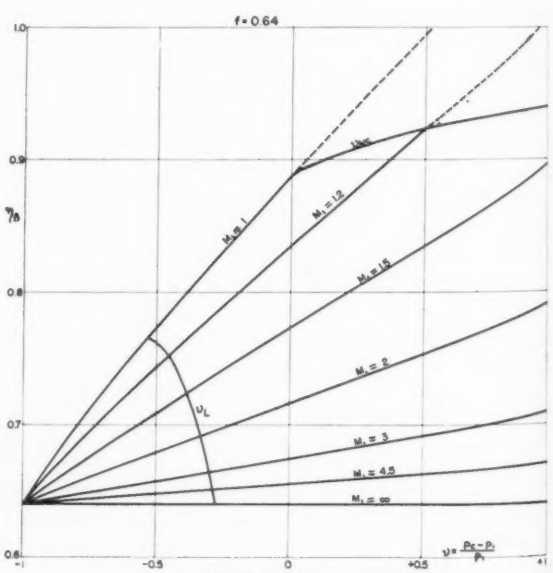

FIG. 4. Diffuser efficiency η_β of the β solution as a function of chamber pressure ν with Mach Number M_1 as the parameter.

(29), is expanded as a function of $M_{max.}{}^*$ in terms of ΔM^* for $\nu = 0$. Second, the functions of $\vartheta(M_1{}^*)$ and $\vartheta(M_{2\alpha}{}^*)$ are expressed by $\vartheta(M_{max.}{}^*)$ and are expanded in terms of ΔM^*. Third, η_β is calculated with those functions according to Eq. (42) valid for $\nu = 0$. Fourth, $\nu \neq 0$ is introduced by means of the relation between f and f' according to Eq. (24). Fifth, conversion is made from $M_{max.}{}^*$ and ΔM^* to $1/M_1{}^2$. The result of the extended calculation is

$$\eta_\beta(M_1;\ f;\ \nu) = f\left\{1 + \frac{1-f}{f}(1+\nu)\cdot\frac{\gamma+1}{2\gamma}\cdot\frac{1}{M_1{}^2}\right\} \quad (97)$$

This equation shows the approach toward the limiting value $\eta_\beta = f$ with $1/M^2$ at a given finite chamber pressure; the linear variation of η_β with the test chamber pressure at a given Mach Number; and the value $\eta_\beta = f$ at $\nu = -1$ for all Mach Numbers. The accuracy of this equation is very good. For $f = 0.64$ and $\nu = 0$ the deviation between Eq. (97) and the exact numerical values are 0.5 per cent at Mach Number 1.5 and smaller than 0.1 per cent from $M = 2$ up to infinity. Later, the partial derivative of Eq. (97) with respect to ν is needed,

$$\frac{\partial\eta_\beta}{\partial\nu}(M_1;f;\nu) = (1-f)\frac{\gamma+1}{2\gamma}\cdot\frac{1}{M_1{}^2} \quad (98)$$

The influence of the chamber pressure on the diffuser efficiency decreases with $1/M_1{}^2$. For $f = 0.64$, the derivative becomes Eq. (98a) with an accuracy of about 0.5 per cent from Mach Number 2 up,

$$\partial\eta_\beta/\partial\nu = 0.3081/M_1{}^2 \quad (98a)$$

(E) *Stability of Test Chamber Pressure at the β-Solution*

Eq. (98) shows that there is always

$$\partial\eta_\beta/\partial\nu > 0 \quad (99)$$

The positive sign, which is not only valid in the linearized equation but in the total Mach Number range from 1 to infinity and for all ν between $\nu_{min.} = -1$ and $\nu_{max.} = \nu_{NS}$, is of great importance. We make a "quasi-steady" stability consideration as follows: A small positive pressure change in the test chamber ($d\nu > 0$) will cause an increase in efficiency η_β and in total pressure behind the transformation zone. Hence, the mass flow determined by the Laval nozzle now has a smaller volume flow in the sonic diffuser throat $F_\beta{}'$ [see Section (7A)] than before. Therefore, the throat is able to take additional mass flow which is drawn out of the test chamber, whereby the chamber pressure is reduced and the positive pressure disturbance disappears. A small negative pressure change in the chamber also vanishes in the corresponding manner. The opposite assumption of a negative sign in Eq. (99) would result in a completely unstable test chamber pressure against disturbances.

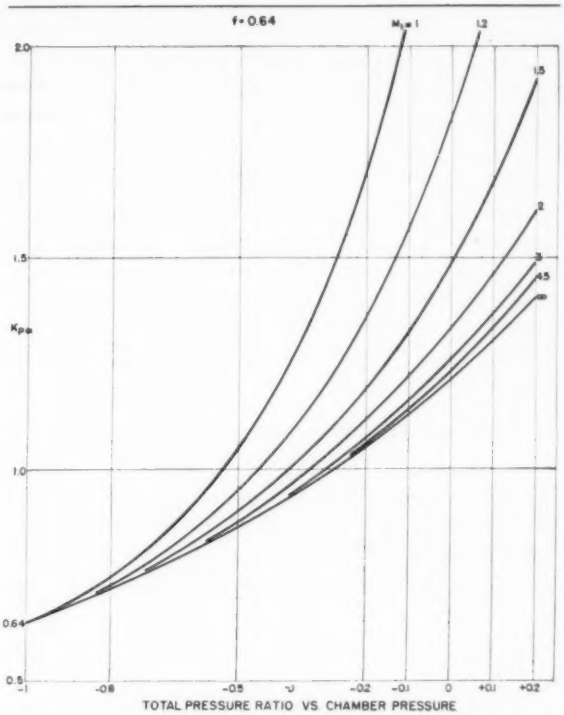

FIG. 5. Total pressure ratio $K_{P\alpha}$ of the α solution as a function of chamber pressure ν with Mach Number M_1 as the parameter.

Obviously, the positive sign of $\partial\eta_\beta/\partial\nu$ is the physical reason for the stable behavior of the test chamber pressure in supersonic free-jet wind tunnels as observed in actual operation. For subsonic free-jet wind tunnels, such reasoning is not valid. It is restricted completely to supersonic tunnels with a diffuser efficiency dependent on test chamber pressure. It is known that subsonic free-jet tunnels have a tendency for pulsation flow originating at the diffuser inlet, while in the supersonic free-jet tunnels at Aachen, Peenemuende, and Kochel, the author never observed any unstable flow phenomena.

(6) TOTAL PRESSURE RATIO OF THE α-SOLUTION

(A) *Variation with Mach Number and Chamber Pressure*

In order to describe the transformation losses of the α-solution, we use the total pressure ratio $K_{P\alpha}$. Fig. 5 shows $K_{P\alpha}$ as a function of ν with Mach Number as the parameter. At a given Mach Number positive chamber pressure improves $K_{P\alpha}$, and negative chamber pressure diminishes $K_{P\alpha}$. For $\nu = -1$, we have $K_{P\alpha} = f = 0.64$ independent of M. For a given chamber pressure, $K_{P\alpha}$ decreases with Mach Number. The line $K_{P\alpha} = 1$, identical with no change in entropy, divides the solution into two régimes. The lower régime with $K_P < 1$ means an entropy increase and is permitted by the second law of thermodynamics. The upper

TABLE 1

f	0	0.1	0.2	0.35	0.5	0.64	0.80	0.99	1
$\nu_{L\infty}$	−1	−0.834	−0.704	−0.540	−0.396	−0.274	−0.147	−0.0070	0

régime with $K_{P\alpha} > 1$ is connected with entropy decrease, and therefore the corresponding flow processes are forbidden. Evidently a certain limiting chamber pressure ν_L belongs to each Mach Number at and below which the α-solution is permitted. ν_L ranges from $\nu_L = -0.536$ at Mach Number 1 to $\nu_L = -0.275$ at Mach Number 10. At pressure equilibrium, $\nu = 0$, a supersonic solution is not possible at all. This important result was obtained formerly (see references 1 and 2, Sections 4C, 2).

(B) *Linearized Approximation for High Mach Numbers*

At Mach Number infinity, the exact formula (32) for $K_{P\alpha}$ fails and becomes indeterminate. An expansion linearized in $1/M^2$ is then helpful and is made in the same way as described for η_β in Section (5D). The final formula gives the limiting value of $K_{P\alpha}$ for Mach Number infinity,

$$\lim_{M=\infty} K_{P\alpha}(f, \nu) = \frac{f}{\{\gamma - (\gamma-1)(1/f)[1 + (1-f)\nu]\}^{1/(\gamma-1)}} \quad (120)$$

The curve for $M = \infty$ in Fig. 5 is calculated according to Eq. (120). The negative pressure limit $\nu_{L\infty}$ for Mach Number infinity is now calculated by the requirement that Eq. (120) is equal to unity, which gives

$$\nu_{L\infty} = -\frac{1 - f[(\gamma - f)^{\gamma-1}/(\gamma-1)]}{1-f} \quad (129)$$

Evaluation of Eq. (129) for various f gives the values for $\nu_{L\infty}$ as shown in Table 1.

For conventional wind-tunnel application, $\nu_{L\infty}$ has a finite, not vanishing, value. A definite negative chamber pressure is needed until the supersonic solution is permitted by the second law.

(C) *Regions of Existence of the α- and β-Solution*

The total pressure ratio of both solutions $K_{P_{\alpha,\beta}}$ are shown in Fig. 6 with logarithmic ordinate. The curves for $K_{P\alpha}$ are essentially the same as in Fig. 5. The line $K_{P_{\alpha,\beta}} = 1$ separates the upper forbidden region from the lower region permitted by the second law. Also included are the boundaries for $\nu_{NS}(M_1)$, above which our system of fundamental equations becomes invalid. It is seen that for the α-solution the function $\nu_L(M_1)$ is the effective upper ν-limit, while for the β-family the upper ν-limit is given by the function $\nu_{NS}(M_1)$. The following results are obtained:

(1) The β-solution is permitted for all negative chamber pressures, for pressure equilibrium, and for positive chamber pressure up to $\nu_{NS}(M_1)$, where the normal shock is established in the nozzle exit.

(2) The α-solution is permitted for low negative chamber pressure with the upper limit $\nu_L(M_1) < 0$. The α-solution is forbidden for higher negative pressure above $\nu_L(M_1)$, for pressure equilibrium, and for all positive chamber pressures.

(3) Thus, in the negative chamber pressure range at and below the limit $\nu_L(M_1)$, both the α- and the β-solution are permitted. Which one will be established actually cannot be decided by this analysis alone. It requires a study of the continuation of the α-solution through the diffuser under consideration of friction. The experimental data [see Section (7B)] can be understood qualitatively.

Fig. 6 may suggest the opinion that it is desirable to establish the α-solution, if possible, because of its much higher total pressure ratio. However, the flow through the total diffuser must be considered [see Section (7A)] up to the region, where the supersonic velocity is finally converted into low subsonic velocity. $K_{P\beta}$ is small but represents practically all losses, while $K_{P\alpha}$ is higher but does not include the additional large losses downstream of the transformation zone with the Mach Number $M_{2\alpha} > M_1$.

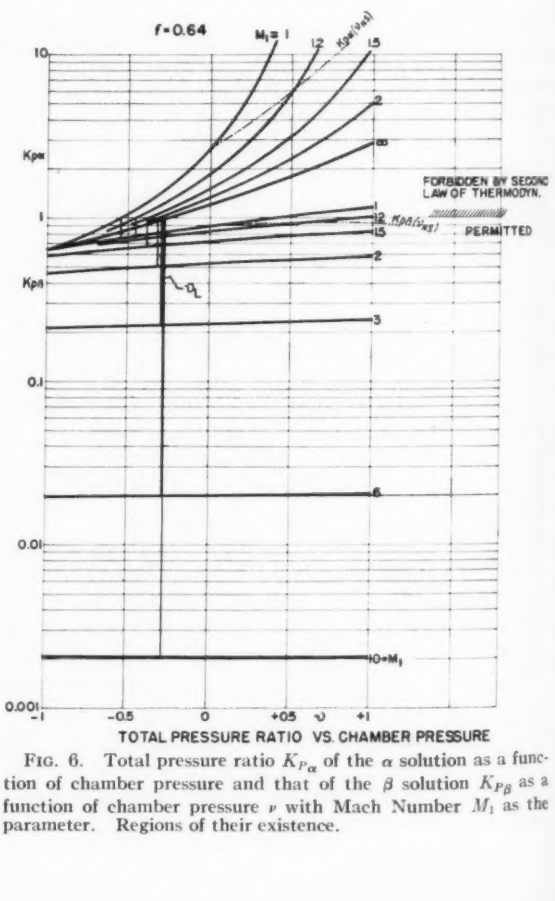

FIG. 6. Total pressure ratio $K_{P\alpha}$ of the α solution as a function of chamber pressure and that of the β solution $K_{P\beta}$ as a function of chamber pressure ν with Mach Number M_1 as the parameter. Regions of their existence.

(7) Diffuser Throat Cross Section of the β-solution and Test Chamber Pressure Control

(A) *Conditions of the Second Throat*

In order to calculate the diffuser throat and discuss pressure control by means of the adjustable diffuser we have to follow the flow further downstream of the transformation zone through the diffuser. In case of the β-solution, the subsonic flow in the entrance region of the diffuser will be accelerated within its convergent part, connected with small boundary layers and negligible losses by friction. If the pressure downstream of the diffuser is low enough, the flow attains sonic velocity in the minimum cross section and supersonic velocity in the divergent part. (Subsonic velocity is finally obtained by a normal shock whose location can be adjusted by the compression ratio of the blowers close downstream of the minimum section, hence encountering negligible losses.) The diffuser acts as an accelerating conventional Laval nozzle, not as a decelerating reverse nozzle as in the case of a closed test section. The mass flow passing the second throat with sonic velocity must be equal to the mass flow entering through the Laval nozzle, when steady state is present, furnishing the equation

$$\frac{F_\beta^{*\prime}}{F_1}(M_1^*, f, \nu) = \frac{\vartheta(M_1^*)}{\eta_\beta(M_1^*, f, \nu)} \qquad (105)$$

If M_1^* and f are given, a certain chamber pressure ν causes a certain efficiency [Eq. (42)] and thus requires in a steady motion a certain throat area according to Eq. (105). If now the diffuser throat is made smaller than given by Eq. (105), for instance, by voluntary throat control, the mass flow coming from the Laval nozzle is not able to flow completely through the throat. The difference in mass flow must accumulate in the test chamber, raising the test chamber pressure, which increases the diffuser efficiency. ν and η_β rise until Eq. (105) is fulfilled. When the diffuser throat is made larger than given by Eq. (105), the opposite is valid.

In case of the α-solution, the convergent diffuser part causes a deceleration of the supersonic flow with pressure rise. This will produce strong increase in boundary-layer thickness, maybe separation or oblique shocks, all processes connected with considerable losses. Evidently, one-dimensional frictionless analysis is not applicable for the continuation of the α-solution through the diffuser. According to present experience, the velocity can be decelerated only partly, and no sonic velocity is attained in the minimum area. Thus it does not act as a second throat, and chamber pressure control by means of the adjustable diffuser is not possible.

(B) *Variation with Mach Number and Chamber Pressure; Operation of Pressure Control*

Fig. 7 shows the second throat area of the β-solution $F_\beta^{*\prime}/F_1$ as a function of Mach Number with the cham-

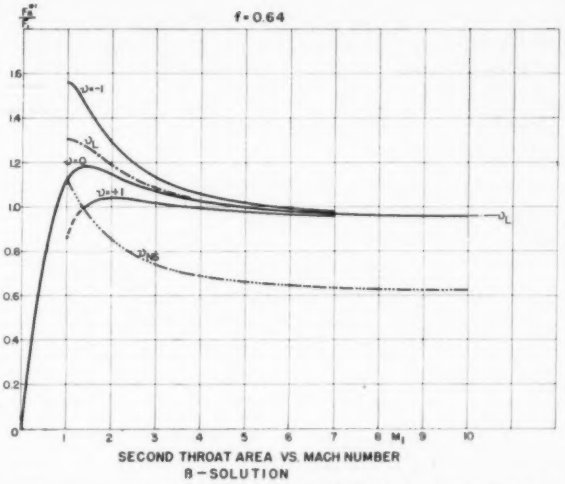

Fig. 7. Relative second throat $F_\beta^{*\prime}/F_1$ of the β solution as a function of Mach Number M_1 with the chamber pressure ν as the parameter.

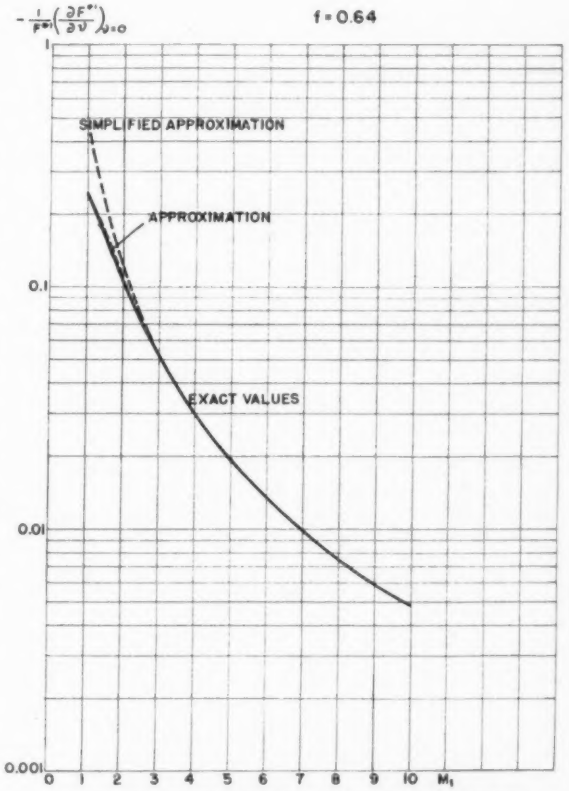

Fig. 8. Chamber pressure control term of the β solution $1/F_\beta^{*\prime} \cdot \partial F_\beta^{*\prime}/\partial\nu$ as a function of Mach Number M_1. Exact values, linearized approximation, and simplified linearized approximation.

ber pressure ν as the parameter. It also gives the complete curve for pressure equilibrium through the subsonic region down to Mach Number zero (taken from references 1 and 2) and the curve for ν_{NS}. The parts of the ν curves below curve ν_{NS} have no physical meaning.

The test chamber pressure control operates the following way: Assuming a fixed Mach Number we may start with a diffuser throat belonging to the positive pressure limit ν_{NS}, which produces a normal shock in the nozzle exit. Now we open up the diffuser throat gradually and pass one ν-line after the other, designated with decreasing but still positive chamber pressure. Finally, we reach pressure equilibrium at the line $\nu = 0$. Further enlargement of the diffuser throat produces decreasing negative chamber pressure until the negative pressure limit ν_L is reached. In this whole range, only the β-solution exists and the chamber pressure control works perfectly. This control is important for actual model testing and has been used for about 20 years in supersonic wind tunnel practice, but it never before was understood. At ν_L we have the alternative [see Section (6C)] of the β-solution with continued chamber pressure control or of the α-solution, where chamber pressure control by the adjustable diffuser throat no longer exists. According to the author's former experience in operation of free-jet supersonic wind tunnels, the latter will probably occur, at least at Mach Numbers above the order of 2 to 3.

(C) *Chamber Pressure Control Term—Linearized Approximation*

For some purposes of design and operation of wind tunnels, it is valuable to have quantitative data of the pressure control which are more explicit than those given in Fig. 7. Therefore, the rate of change of the throat area with the chamber pressure, called the "chamber pressure control term," was calculated with the aid of Eq. (105) and is represented in Fig. 8 for $f = 0.64$, designated as "exact values." It is sufficient to present the control term for $\nu = 0$ only because the influence of ν is extremely small as long as we stay within $\nu = \pm 1$ for wind-tunnel purposes. Obviously, the sensitivity of pressure control increases considerably with high Mach Numbers. A linearized approximation is obtained by using η_β (97) and $\partial\eta_\beta/\partial\nu$ (98),

$$\left(\frac{1}{F_\beta^{*\prime}}\cdot\frac{\partial F_\beta^{*\prime}}{\partial\nu}\right)_{\nu=0} = -\frac{1-f}{f}\cdot\frac{\gamma+1}{2\gamma}\cdot\frac{1}{M_1^2}\left(1-\frac{1-f}{f}\cdot\frac{\gamma+1}{2\gamma}\cdot\frac{1}{M_1^2}\right) \quad (114)$$

Fig. 8 shows Eq. (114) as "Approximation." If we set the bracket equal to unity, we obtain the "simplified approximation." The first equation is exact within 3 per cent and better from Mach Number 1 to 10. The simplified equation is exact within 2 per cent and better from Mach Number 4.5. Eq. (114) allows fast calculations of the chamber pressure control term for any f value.

Conclusions

The flow process in the diffuser and its efficiency are investigated for the general case, when the pressure in the test chamber surrounding the free jet is different from the pressure in the exit cross section of the Laval nozzle. An exact solution for one-dimensional nonviscous steady flow is obtained. Velocity and pressure after the transformation process, total pressure ratio, diffuser efficiency, and diffuser throat area are calculated for variable chamber pressure. The exact mechanism of test chamber pressure control by means of the adjustable diffuser throat is shown. Other results are the proof of the stability of the test chamber pressure, the existence of two different types of flow at low negative chamber pressure, and the quantitative description of a "slow-starting" process of the tunnel.

References

[1] Hermann, R., *Theoretical Calculation of the Diffuser Efficiency of Supersonic Wind Tunnels with Free Jet Test Section*, Heat Transfer and Fluid Mechanics Institute, 1949, Berkeley, Calif.; published by the American Society of Mechanical Engineers, May, 1949, New York, pp. 255–270 (this paper contains a bibliography of ten references).

[2] Hermann, R., *Diffuser Efficiency and Flow Process of Supersonic Wind Tunnels with Free Jet Test Section*, Air Force Technical Report No. 6334, Wright Field, December, 1950 (this paper contains a bibliography of 24 references).

Free-Flight Air-Drag Measurement Techniques

A. B. J. CLARK* AND F. T. HARRIS†

Naval Research Laboratory

With an Appendix by R. E. Roberson‡

SUMMARY

Using the ballistic pendulum air-drag technique with pendulums of several different lengths, the air-drag coefficient, C_D, has been determined for cal. .50 spheres in the region of Mach Numbers 1.4 to 5.4. A conventionally suspended pendulum with a period of 3.2 sec. was used to obtain most of the data; the values of C_D so obtained were consistently about 6 per cent low. It was suspected that the time of momentum transfer covered too great a fraction of the pendulum period. For this reason, pendulums having seismographic suspensions with periods from 17.5 to 30 sec. were installed. After correction for end effects, the values of C_D then obtained agreed closely with the results of other methods. The influence of baffle-hole size and correction for end effects are discussed.

SYMBOLS

α = air-drag coefficient uncorrected for end effect
ρ = air density
ω = $2\pi/P$
A = area of projectile normal to trajectory
C_D = air-drag coefficient corrected for end effect
D_1 = base length between first and second screen
D_2 = base length between second and third screen
E = $(1/2)mV^2$ kinetic energy of projectile (no spin)
ΔL = apparent additional length of pendulum, representing end effect
L = physical length of the pendulum
m = mass of projectile
P = period of the pendulum
S = displacement of projectile in direction of trajectory
T_1 = transit time over D_1
T_2 = transit time over D_2
V = projectile velocity
V_E = velocity of projectile at pendulum exit
V_L = projectile velocity loss to pendulum over path $L + \Delta L$
V_1 = velocity over first base length
V_2 = velocity over second base length
X = $\rho AS/m$
X' = $\rho AL/m$
X'' = $\rho A(L + \Delta L)/m$

INTRODUCTION

Origin of the Ballistic Pendulum Air-Drag Technique

INCIDENTAL TO STUDIES OF ARMOR for resistance to fragment penetration, questions arose during the summer and fall of 1944 as to the reliability of estimates of remaining velocity of fragments. The desire to check fragment drag coefficients in current use coincided with completion of a new high-speed spark chronograph, which gave sufficient precision to permit the measurements being made on an improvised 20-ft. range in a basement laboratory room. The results of these chronograph drag measurements were satisfying with respect to the immediate issues in question. This brief activity in ballistic aerodynamics preceded and helped stimulate the conception of making laboratory measurements of air drag with a ballistic pendulum.

In 1943, personnel from the Naval Ordnance Laboratory sought assistance from the Naval Research Laboratory in their studies of mechanical fuze development. Dr. G. R. Irwin, Superintendent of the Mechanics Division and Acting Head of the Ballistics Branch of the Naval Research Laboratory, proposed that the momentum loss in plates be precisely determined using a special ballistic pendulum technique. This technique consisted of mounting a plate in a ballistic pendulum and determining the momentum lost by the projectile to the plate by computing, from the pendulum deflection, the momentum gained by the plate. The success of this method led Dr. Irwin to believe that momentum lost by a projectile to air could be measured in a similar manner.

In March, 1945, at the Bureau of Ordnance, Dr. Irwin discussed with Lieutenants Hunt and Hoffman the possibility of measuring air drag with a ballistic pendulum. It was agreed that the method was promising, and active experimental work was initiated in August, 1945, using $^5/_{16}$-in. steel spheres in a cal. .30 smooth bore gun. In August, 1947, pendulums were installed for work with cal. .50 projectiles. All the cal. .50 work has been concerned with spheres. Attention is directed to the advantages of this system:

(1) The pendulum method measures momentum rather than velocity loss and, for equal precision, utilizes a much shorter trajectory than any of the known chronograph techniques for determining resistance of gases to penetration by projectiles.

(2) About 1 per cent precision is obtainable readily enough so that the experiment can remain simple and convenient.

Received August 29, 1951. Final copy received February 25, 1952.

* Physicist.

† Physicist. Now, Biophysicist, Naval Medical Research Institute, Bethesda, Md.

‡ Physicist, Naval Research Laboratory. Now with North American Aviation, Inc.

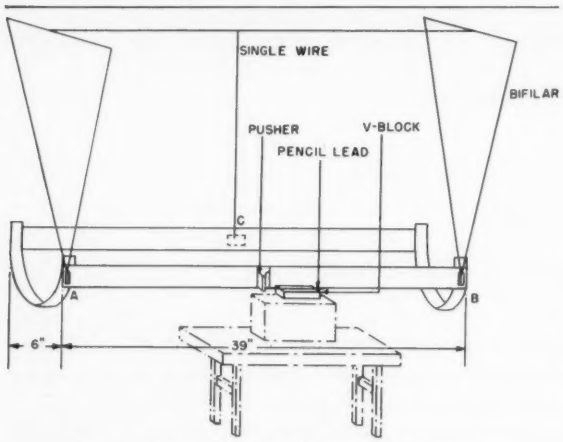

FIG. 1. Conventional cradle pendulum support.

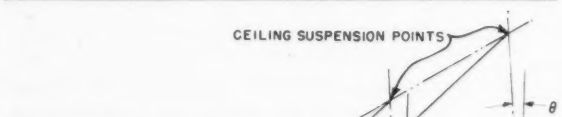

FIG. 2. Seismographic-type pendulum showing the angle θ between the line from ceiling suspension points to cone pivots and the vertical. The period $p = \sqrt{l/g} \sin \theta$, where l is the length of the arms.

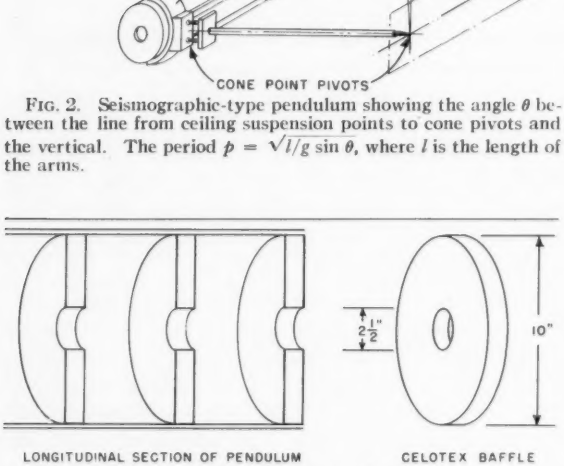

FIG. 3. Arrangement of baffle discs.

(3) The transonic and subsonic ranges are not too low for use of the pendulum air-drag technique. In contrast to chronograph methods, accuracy will improve with increasing velocity of the test missile.

(4) Missiles may be of any shape that can be fired in proper orientation through a 100-cal.* path in air.

(5) The pendulum method is adaptable for study of such features as head shape, the effect of yaw upon drag, scale effect, and the effects of various physical conditions of the resisting medium. Adaptations of the method to the study of lift are possible but will require a considerable amount of experimental development.

* That is, 100 projectile diameters.

EXPERIMENTAL PROCEDURE

Measurement Technique.—When a missile is fired through a hollow, partly closed pendulum, the pendulum acts as a trap for the momentum imparted to the air. The swing of the pendulum increases in a known way with its momentum gain. In a way not fully understood (since details of momentum transfer from air to pendulum are still obscure), the pendulum deflection increases with momentum loss of the missile. There are three principal trajectory sections: (1) the path of the missile which creates pressure differential against the entrance face of the pendulum; (2) the interior path; and (3) the path that may cause transfer of momentum through the exit-face opening. To measure the air-drag coefficient successfully, it is desirable to design the experiment so that sections (1) and (3) are independent of pendulum length, so that the wall or choking effects along section (2) are negligible, and so that the air motion inside the pendulum becomes random in a time less than one-thirtieth of a quarter period of the pendulum. When these requirements are satisfied, firings at the same measured velocity with several pendulum lengths will serve to determine the end correction and will, therefore, permit absolute determination of the air-drag coefficient.

The pendulums were constructed so that the entrance and exit faces were similar. All firings were made with spheres; choice of this shape eliminated the yaw problem and reduced expense, since commercial ball bearings were used.

Equipment.—Outside the pendulum room: A cal. .50 sphere was given a horizontal velocity by firing through a cal. .50 gunbarrel. The amount of gun powder used provided the desired velocities. After leaving the gun, the sphere passed through a steel cylindrical silencer 3 ft. in diameter and 10 in. long. Attached to the silencer on the side facing the pendulum was a blast deflector $1\frac{1}{2}$ ft. long with 14 square aluminum plates 2 in. apart; each plate measured 1 by 1 ft. and had a 1-in. diameter hole for the passage of the sphere.

Inside the pendulum room: Pendulum bodies, whether of the conventional Fig. 1 or seismographic-type Fig. 2 suspension, were identical in construction. Aluminum, 0.032 in. thick, was formed into a cylinder 10 in. in diameter and of appropriate length. Art board, $\frac{1}{8}$ in., was cut into discs to fit within the pendulum; each disc had at the center a hole 4 or 5 cal. in diameter. Starting at one end, the discs were placed in the cylinder spaced by aluminum frameworks, which served to separate the discs by 4 in. These discs act as baffles as shown in Fig. 3.

On the outer surface of the cylinder, an aluminum projection 1/4 by 1 by 1 in. was fastened so that a normal off the 1- by 1-in. face was parallel to the direction of pendulum travel. This projection, called a "pusher," served to displace a free pencil lead which rested horizontally in two V supports on a stationary block. A traveling microscope was mounted on a solid stationary support in such a manner that the distance between the pusher at the pendulum rest position and the end of the pencil lead after displacement could be determined. The sphere passed through the pendulum without direct contact, and the air disturbed by the projectile and its shock wave caused the pendulum displacement.

After the rest position of the pendulum is determined, the pendulum must be held there until the instant before firing. Restraint was effected by a damper actuated by a solenoid and controlled by push buttons either from the pendulum room or from the firing point.

The period of the pendulum was determined with a stop watch. In the formula $F = -M\omega^2 d$ (where $\omega = 2\pi/P$ and P = the period of the pendulum), the force, F, and the displacement, d, were directly measured by holding back the pendulum by a weight over a low-friction pulley. Thus the mass, M, of the pendulum was determined. To support the 176-in. pendulum two cradles were used, and three cradles were needed for the 273-in. pendulum.

The velocity of the projectile at the center of the pendulum was measured by a 1.6-mc. electronic counter, which is operated from pulses fed to it by two photoelectric screens placed about 2 ft. from each end of the pendulum. The exit velocity is then approximately $V_c - (1/2)V_L$, where V_c is the velocity at the center of the pendulum, computed from the counter observation; V_L is the velocity lost by the projectile through the length of the pendulum, computed from the observed deflection.

Theory

Drag Calculations

Let us define the air-drag coefficient, C_D, by the relationship

$$-dE/dX = C_D E \tag{1}$$

whence

$$E = E_0 \exp(-C_D X) \tag{2}$$

and

$$V = V_0 \exp[(-C_D X)/2] \tag{3}$$

where

E = $(1/2)mV^2$, kinetic energy of the projectile (no spin)
V = projectile velocity
m = mass of projectile
X = $\rho AS/m$
ρ = air density
A = area of projectile normal to trajectory
S = displacement of projectile in direction of trajectory

If $S = L$,

$$X' = \frac{\rho AL}{m} \tag{4}$$

and if $S = L + \Delta L$,

$$X'' = \rho A(L + \Delta L)/m \tag{5}$$

where L = physical length of the pendulum and ΔL = apparent additional length of pendulum, representing the end effect.

For small increments in X and S, the relation may be written

$$1 + \frac{V_L}{V_E} = \exp\frac{(C_D X'')}{2} = \exp\frac{(\alpha X')}{2} \tag{6}$$

where

V_L = projectile velocity loss to pendulum over path $L + \Delta L$
V_E = velocity of projectile at pendulum exit
α = air-drag coefficient uncorrected for end effect
C_D = air-drag coefficient corrected for end effect

Eq. (6) is convenient to use since V_L and V_E may be readily computed, X' is known, and $\alpha X'/2$ can be obtained from a table of the exponential function when the value of $1 + V_L/V_E$ is known. The relation

$$C_D/\alpha = L/(L + \Delta L) \tag{7}$$

follows directly from Eqs. (4), (5), and (6).

Method of Determining C_D

If α is plotted against the reciprocal of the pendulum length, one can extrapolate to C_D at $1/L = 0$. Fig. 4 is plotted in this manner. It is interesting to note that, if this curve is extrapolated so as to intercept the horizontal axis, this intercept will be the reciprocal of the end correction, ΔL.

The equation

$$C_D = (L_1\alpha_1 - L_2\alpha_2)/(L_1 - L_2) \tag{8}$$

where L_1 and L_2 are any two pendulum lengths and α_1 and α_2 are the corresponding values of α, may be more convenient for the determination of C_D than the graphical method. The validity of this equation may be shown at once by plotting αL vs. L for several values of L. The slope of the resulting curve is C_D, the horizontal intercept is ΔL, and the vertical intercept is $\alpha\Delta L$.

Air Drag of Cal. .50 Steel Spheres by a Conventionally Suspended Ballistic Pendulum

The values of α were investigated to determine the effect of baffle-hole size and pendulum length. As was

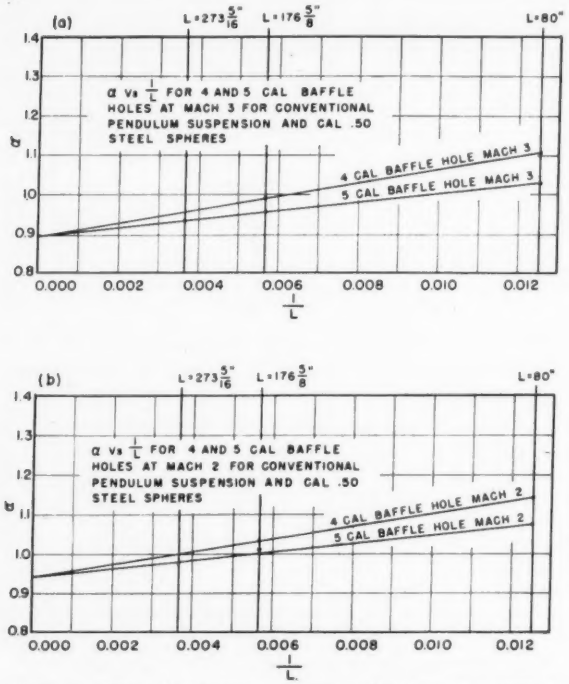

FIG. 4. Graph (a) shows α values at Mach = 3.0 plotted against the reciprocal of the pendulum length. Data for 4 and 5 cal. baffle hole diameters is plotted. Graph (b) is the same except that the α values were obtained at Mach = 2.0. For comparison, the values read from graph (a) and (b) at $1/L = 0$ are shown on Fig. 5d and are indicated at 4A and 4B. The values were obtained using a conventionally suspended pendulum.

expected, the larger the baffle hole, the smaller the α for the same Mach Number. Curves of α vs. Mach Number for the 5-cal. baffle-hole diameter were made for pendulum lengths of 80, 176.6, and 273.3 in., as shown in Fig. 5.* Data were taken for a 4-cal. baffle-hole diameter at Mach Numbers 2 and 3, using 80- and 176.6-in. pendulums. Values of C_D, obtained by plotting the values for the 4- and 5-cal. baffle-hole diameters against $1/L$ and extrapolating to $1/L = 0$, were the same (Fig. 4) and shown in Fig. 5.

Air Drag of Cal. .50 Aluminum Spheres by a Velocity-Difference Method

To have data with which to compare results of the ballistic pendulum air-drag technique, C_D was determined by the velocity-difference method. Cal. .50 aluminum spheres were used, since their low density made their velocity loss over a given distance almost three times that of the steel spheres. Screens were set up 25 ft. apart to give two nearly equal base lengths.

In the calculation of C_D, no consideration has been given to the difference in base lengths between screens. As shown in the Appendix, if the experiment is repeated with the direction of firing reversed, the average C_D calculated for the two directions will be identical with the average C_D calculated with base-length differences taken into consideration. That is, averaged C_D values obtained by this method, ignoring possible errors in the location of the center screen, will not be in error.† The values of C_D obtained by this method are quoted in the report and are averages of this kind. The velocity of the projectile was measured over each base length, and values of C_D were computed using the equation

$$V_1/V_2 = \exp(C_D X/2) = T_2/T_1 \qquad (9)$$

where V_1 and V_2 are the velocities of the projectile over the first base length D_1 and the second base length D_2, respectively, and where T_1 and T_2 are the correspond-

* A, B, and C, respectively. In Fig. 5d these curves are compared with the values of C_D obtained by Charters and Thomas and the values of C_D from Fig. 4A and 4B.

† Actually, this statement is correct only insofar as the computation method outlined earlier in the report is used. A more exact treatment shows that this averaged C_D value will be correct within second-order terms in $(D_1 - D_2)/(D_1 + D_2)$. See Appendix for further discussion.

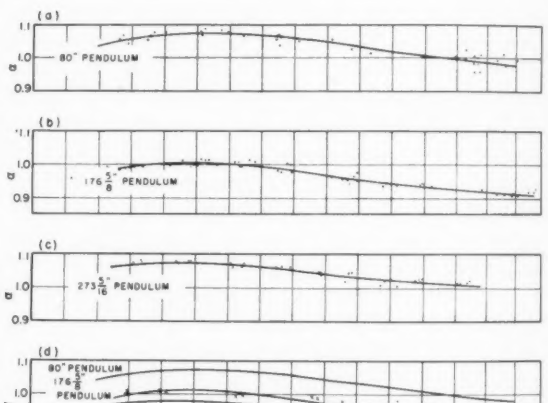

FIG. 5. α vs. Mach Number for cal. .50 steel spheres, 5-cal. ($2^1/_2$-in.) baffle hole, conventional pendulum suspension. x represents values obtained by Charters and Thomas in (d). $4A$ and $4B$ are values of C_D obtained from Fig. 4a and 4b.

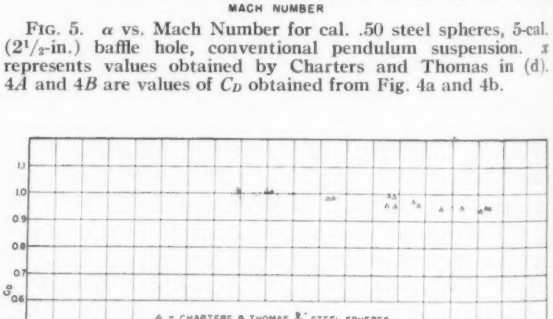

FIG. 6. C_D from N.R.L. free-flight velocity difference method compared with Charters and Thomas values.

ing transit times. Again, time was measured by Potter 1.6-mc. electronic counters. Photocell light screens were used for triggering. Data obtained in this manner are plotted in Fig. 6, together with values obtained by A. C. Charters and R. N. Thomas* for $^9/_{16}$-in. steel spheres. It will be noted that the values of C_D obtained by these two methods agree closely.

Discrepancy in C_D Values Obtained by Different Methods

Values of C_D obtained by extrapolation after plotting α vs. $1/L$ are given in Fig. 5d, together with values obtained by Charters and Thomas, as well as curves obtained by the ballistic pendulum method at N.R.L. It will be noted that the values of C_D corrected in this way are about 6 per cent lower than those reported by Charters and Thomas.

Probable Cause of Lower C_D Values

Since the period of the conventionally suspended pendulum was 3.2 sec., it seemed probable that the time of momentum transfer was long enough to affect the deflection reading. An analog of the pendulum was set up using a ballistic galvanometer, a charged condenser, and a resistor. The RC product of the condenser and the resistor, plus the resistance of the galvanometer, was used as a measure of the time required for the charge to be transferred through the coil of the galvanometer. The capacity of the condenser and the voltage applied were adjusted to obtain a nearly full-scale reading with no external resistance.

The period of the galvanometer was 8.6 sec. Fig. 7 shows the per cent of maximum deflection plotted against the time expressed as the per cent of the total period of the galvanometer.

From Fig. 7, 94 per cent of the maximum deflection corresponds to having an RC product that is 4 per cent of the galvanometer period. Analogously, with the period of the conventionally suspended pendulum equal to 3.2 sec., the momentum reading would be 94 per cent of maximum if the time of momentum transfer were 4 per cent of 3.2 sec. or 0.128 sec. If a 99.5 per cent momentum reading is desired, the time of momentum transfer, judging from Fig. 7, should be about 0.7 per cent of the period of the pendulum or about one-sixth of the time that gave 94 per cent of the maximum deflection.

Since increasing the period of the pendulum would have the same effect as decreasing the time it takes for the momentum transfer, increasing the pendulum period by a factor of 6 should give values of C_D which agree closely with established ones.

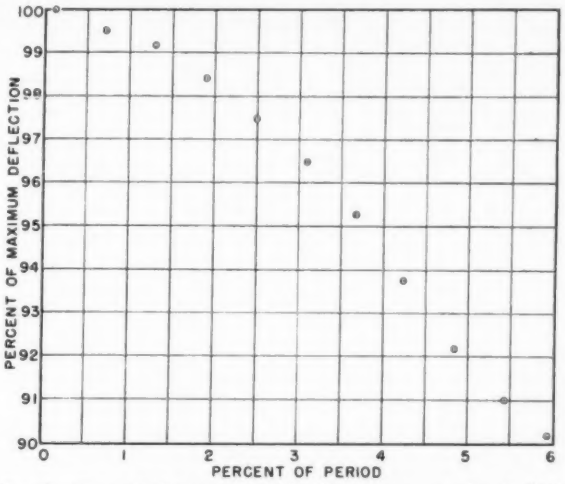

FIG. 7. Per cent of maximum deflection vs. per cent of period of galvanometer for various RC products.

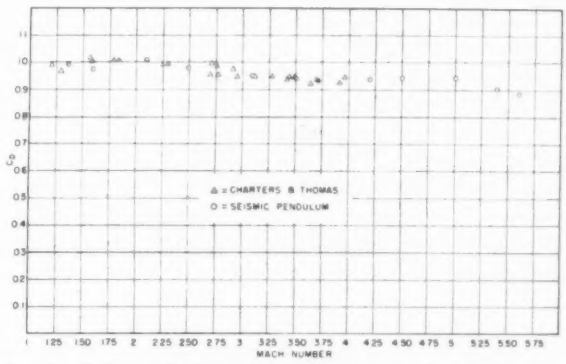

FIG. 8. C_D from seismic pendulum data compared with Charters and Thomas values.

Use of Seismographic-Type Suspensions to Obtain Longer Period Pendulums

Seismographic-type suspensions† (Fig. 2) were tried using pendulums with periods of 17 to 30 sec. The values of C_D thus obtained agree closely with those obtained by Charters and Thomas and with values obtained at N.R.L. by taking velocity differences. For comparison Fig. 8 shows these C_D values, as well as those obtained by Charters and Thomas. Good agreement will be noted, except at Mach Number = 1.6 where the pendulum values are about 2.5 per cent low.

Conclusion

The ballistic pendulum method of determining the air-drag coefficient is particularly applicable to extremely high Mach Numbers, provided the arrangements include suitably reduced baffle-hole sizes and a sufficient reduction of muzzle blast. Since the base

* Aberdeen Proving Ground, Ballistic Research Laboratory Report 514; Charters, A. C., and Thomas, R. N., Journal of the Aeronautical Sciences, Vol. 12, p. 468, October, 1945.

† Use of seismographic-type suspensions for this work was suggested to the writers and given initial trials at N.O.L. by Dr. George Shue.

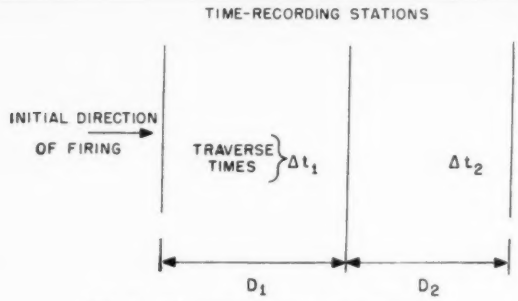

FIG. 9. The experimental arrangement.

length over which the projectile velocity is determined is large and since the deflection of the pendulum increases with projectile velocity, no decrease of precision in the determination of projectile velocity or momentum loss is noted at high Mach Numbers. Because the total length of trajectory need be only 30 ft., somewhat higher Mach Numbers can be maintained than are possible with the customary spark chronograph ranges.

This method of determining the air-drag coefficient can be used with missiles of any shape which can be projected through the pendulum, provided the yaw and drift, if present, can be controlled to prevent contact between the missile and the pendulum. The convenience of this method makes it adaptable for use in universities either for the determination of the air-drag coefficient or for instructing students in aerodynamics.

APPENDIX

By Robert E. Roberson

Referring to Fig. 9 for experimental arrangement, let D_1 and D_2 denote distances between screens, defining $D = (1/2)(D_1 + D_2)$, and let Δt_1 and Δt_2 be the transit times between screens of a projectile fired in the direction indicated by the arrow. It is desired to find the error made by calculating C_D as if $D_1 = D_2$ and to show how it is reduced by reversing the direction of firing and using the average value of C_D calculated for the two directions.

Let us represent by C_D the value of the drag coefficient calculated recognizing the difference between D_1 and D_2 and by $C_D{}^*$ the approximation to this value calculated upon the assumption that $D_1 = D_2$. Postulate that (1) the value C_D is calculated from the equation†

$$C_D = \frac{2m}{\rho A D} \ln \frac{D_1 \Delta t_2}{D_2 \Delta t_1} \tag{10}$$

and (2) that, except for the errors in the approximation $C_D{}^* \simeq C_D$, the errors of the experiment are the same for the two directions of firing.

The first of these postulates makes it unnecessary to examine in this Appendix the rationale of the calculation procedure. The second allows the errors in the location of the center screen to be considered aside from the various other experimental errors.

An additional notation, let subscripts f and r represent forward and reversed directions of firing and a bar above any quantity represent its average value for the f and r experiments.

From the definition of C_D and Eq. (10), there result immediately

$$(C_D)_f = \frac{2m}{\rho A D} \ln \frac{D_1 \Delta t_2}{D_2 \Delta t_1} \tag{11}$$

$$(C_D{}^*)_f = \frac{2m}{\rho A D} \ln \frac{\Delta t_2}{\Delta t_1} \tag{12}$$

$$(C_D)_f - (C_D{}^*)_f = \frac{2m}{\rho A D} \ln \frac{D_1}{D_2} \tag{13}$$

Clearly, in the reversed firing, the roles of D_1 and D_2 are effectively interchanged. Therefore, by analogy with Eq. (13),

$$(C_D)_r - (C_D{}^*)_r = \frac{2m}{\rho A D} \ln \frac{D_2}{D_1} \tag{14}$$

Taking one-half the sum of Eqs. (13) and (14), one has

$$\bar{C}_D = \bar{C}_D{}^* \tag{15}$$

That is, if the C_D value of the experiment is the average of the C_D values obtained by firing through the screens in two directions, it contains no error by virtue of being calculated on the assumption that $D_1 = D_2$.

A somewhat more sophisticated argument, constructed upon a less restrictive base than postulate (1), shows that actually the error made in C_D by considering $D_1 = D_2$ is of second order in $(D_1 - D_2)/(D_1 + D_2)$.

† The listing of the more basic assumptions that lead to this formula is beyond the scope of this Appendix.

Impingement of Spherical Water Droplets on a Wedge at Supersonic Speeds in Air

MYRON TRIBUS* AND ARMAND GUIBERT†

University of Michigan and University of California at Los Angeles

SUMMARY

The water-drop interception characteristics of a wedge in a supersonic flow field are investigated analytically for the case of flows in which the shock wave is not detached. The results indicate that, contrary to the subsonic flow cases considered previously, there is no limiting position on the wedge beyond which the droplets cease to strike, but rather icing may occur along the entire wedge surface.

INTRODUCTION

ANALYTICALLY and experimentally determined icing characteristics for various objects have been previously reported in the literature.[1–6] All of the previous reports have been concerned with subsonic flow at velocities where the compressibility of the fluid is not important. Because the present trend in aircraft design is toward supersonic flight speeds, it is of interest to consider the icing characteristics that will occur at these higher velocities. At these very high velocities, small changes in wing profile, for example, are expected to produce much greater changes in flying characteristics than occur at subsonic speeds.

Although at very high flight speeds it is certain that the effects of aerodynamic heating are sufficient to prevent icing, there still exists a combination of low supersonic speeds and low ambient temperatures at which icing may occur. This icing may occur even though the stagnation temperature in dry air is above freezing, because the presence of the moisture on the wing will cause a depression in temperature (similar to wet bulb depression) with the result that the wing may fall below the freezing temperature. This effect has been discussed in a previous report.[8]

Even when no ice forms, it is of interest to compute the rate at which water droplets strike, since the results may be of value in erosion studies.

As an initial contribution to the solution of the overall problem, there is presented an analysis of the water interception characteristics of a wedge in a supersonic flow field.

NOMENCLATURE

a = acoustic velocity (ft. per sec.)
$\bar{a}$ = acceleration vector (ft. per sec.^{2})
b = distance from centerline of wedge (ft.)
C_D = drag coefficient (dimensionless)
F = force vector (lbs.)
m = mass (slugs)
M = Mach modulus (dimensionless)
P = pressure (lbs. per sq.ft.)
r = radius of droplet (ft.)
R = Reynolds modulus (dimensionless); $R = 2\frac{|\bar{U}|r\rho_a}{\mu}$
t = time (seconds)
T = absolute temperature (°R.)
$\bar{U}$ = relative velocity vector (ft. per sec.)
$\bar{V}$ = velocity vector (ft. per sec.)
x = distance (ft.)
α = wedge half angle (deg.)
λ = "range" of a drop in still air (ft.)
μ = viscosity of air (lbs. sec./ft.^{2})
ρ = density (slugs per cu.ft.)
ω = shock wave angle (deg.)

Subscripts

a = air
w = water
0 = initial value
1 = before shock wave
2 = after shock wave

Superscripts

Dots = differentiation with respect to time

ANALYSIS

The water interception characteristics of a wedge at supersonic velocities may be computed in a rather simple fashion subject to the following postulates:

(a) The water drops are spherical.

(b) The airflow about the wedge corresponds to two-dimensional frictionless flow of a perfect gas with constant heat capacities.

(c) The drag force exerted by the air on the drop is that experienced by a sphere in a real fluid.

(d) The shock wave is not detached.

(e) No condensation shock occurs.

(f) No heat transfers or mass transfers occur to or from the drop.

These postulates have been used in the idealized treatment of icing at subsonic speeds with good agreement between measured and predicted behavior. Of the above list, postulate (e) most likely will cause deviations between predicted and observed performance.

For the case of a wedge, the supersonic flow field (Fig. 1) is simpler than the subsonic flow field. If the flow ahead of the shock wave is uniform and parallel to the chord line of the wedge, after the shock wave it will

Received April 16, 1951.

* Director of Icing Research.
† Associate Engineer.

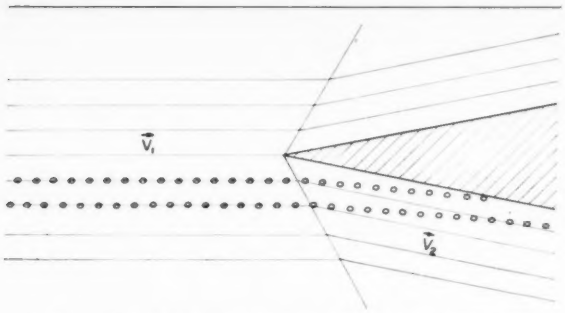

FIG. 1. The field of flow about a wedge in uniform flow

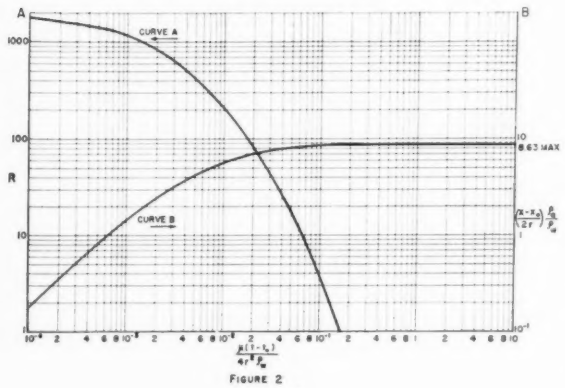

FIG. 2.

again be uniform but parallel to the wedge surface. Because disturbances cannot be felt upstream, the flow over a finite wedge is initially the same as that over a wedge that extends an infinite distance downstream.

Fig. 1 reveals the interesting fact that all the droplets describe identical trajectories until they either strike the wedge surface or flow with the air stream parallel to it. The drops arrive at the shock wave with the initial velocity $\bar{V}_1$. Relative to the airflow after the shock wave, they have a velocity $(\bar{V}_1 - \bar{V}_2)$. Therefore, as a consequence of the fact that the flow field is uniform before and after the shock, the trajectory of a drop relative to still air may be determined, and the trajectory of the drop relative to the wedge may be obtained by adding the air velocity $\bar{V}_2$.

The "range" of a sphere projected into still air has been computed by Langmuir.[3] Because some of the intermediate data indicated but not presented in his analysis are needed here, the derivation and computation are presented in the following.

If a drop of radius r and density ρ_w be projected into still air of density ρ_a and viscosity μ, then, according to Newton's Law, there will be a deceleration because of the drag—i.e.,

$$\bar{F} = m\bar{a} \tag{1}$$

where m, the mass of the drop and $\bar{a}$, the acceleration are given by

$$m = (4/3)\pi r^3\rho_w \tag{2}$$

$$\bar{a} = d\bar{U}/dt \tag{3}$$

The drag force $\bar{F}$ is given by

$$\bar{F} = -(1/2)\rho_a|\bar{U}|^2 C_D \pi r^2(\bar{U}/|\bar{U}|) \tag{4}$$

C_D is the experimentally determined drag coefficient for a sphere. Therefore,

$$\frac{d\bar{U}}{dt} = -\frac{3}{8}\frac{\rho_a}{\rho_w}\frac{C_D}{r}|\bar{U}|^2\frac{\bar{U}}{|\bar{U}|} \tag{5}$$

The drag coefficient is a function of the Reynolds modulus for the droplet R. Replacing the velocity by the Reynolds modulus, one obtains the scalar equation

$$\dot{R} = -\frac{3}{8}\left(\frac{\rho_a}{\rho_w}\right)\left(\frac{C_D(R)}{r}\right)\left(\frac{\mu R^2}{2r\rho_a}\right) \tag{6}$$

Finally, then,

$$\int_{R_0}^{R}\frac{dR}{C_D(R)R^2} = -\frac{3}{16}\frac{\mu(t - t_0)}{r^2\rho_w} \tag{7}$$

Since Stokes' Law (i.e., $C_D = 24/R$) is valid for small values of R, if the upper limit of integration approaches zero, t becomes infinite; the drop never comes to rest. As pointed out by Langmuir, however, the drop travels only a finite distance.

Using the reported experimental data for drag coefficients for spheres, Eq. (7) may be integrated. Curve A of Fig. 2 shows the resultant variation in Reynolds modulus, R, with time when a drop is projected into still air with an initial value for R equal to 1,800. Curve A of Fig. 2 may be used for other initial values of Reynolds modulus by shifting the origin of the time scale—i.e., subtracting the time required for R to change from 1,800 to the given initial value.

To determine the range of a drop projected into still air, Eq. (8) must be integrated

$$|\bar{U}| = dx/dt = (\mu/2r\rho_a)R \tag{8}$$

hence,

$$\left(\frac{\rho_a}{\rho_w}\right)\left(\frac{x - x_0}{2r}\right) = \frac{1}{4}\int_{(\mu t_0/\rho_w r^2)}^{(\mu t/\rho_w r^2)} Rd\left(\frac{\mu t}{\rho_w r^2}\right) \tag{9}$$

The integral on the right-hand side of Eq. (9) is the area under the curve of R plotted versus $(\mu t/\rho_w 4r^2)$ within the limits t and t_0 determined from the first integration. The result of the second integration is shown in Fig. 2 as Curve B.

The results of the foregoing calculations can be used to calculate the water impingement on a wedge at supersonic speeds as follows:

(a) The flow conditions before and after the wedge may be found from Reference 7.

(b) The initial Reynolds modulus of the droplet, with respect to the air flow after the shock wave, is computed using the magnitude of the difference in vector

velocities of the air before and after the shock wave as the relative velocity.

(c) With this value of R, Curve A of Fig. 2 may be used to determine the dimensionless time interval for the droplet to come to the initial Reynolds modulus from $R = 1{,}800$.

(d) Corresponding to this dimensionless time $\mu(t - t_0)/4r^2\rho_w$, a value of dimensionless distance $(x - x_0)\rho_a/2r\rho_w$ may be determined from Curve B of Fig. 2.

(e) The difference between this value of $(x - x_0)\rho_a/2r\rho_w$ and its maximum value (8.63) corresponding to $R_0 = 1{,}800$ is the maximum range, $\lambda_{max.}$, the drop attains with respect to the air.

(f) Superposing a line of length $\lambda_{max.}$ in the direction of the initial relative velocity on the sketch of the wedge flow field (Fig. 5), it is seen that there is a critical starting position, $b_{max.}$, such that the drops just reach the wedge surface. Drops farther from the chord line than $b_{max.}$ do not reach the wedge.

(g) The position at which a particular drop strikes the wedge surface may be obtained by adding, vectorially, the distance traveled by the drop, with respect to the air, to the distance the air moves in the same time.

A sample calculation follows.

Problem Statement

Consider a two-dimensional wedge of half angle 10° traveling at a Mach Number of 1.767 at an altitude of 15,000 ft. and a free air temperature of −25°F. The droplets are 20 microns in diameter (6.56×10^{-5} ft.) and the liquid water content of the cloud is 0.2 Gm. per cu.m. Where do the drops strike the wedge?

From reference 7 it is found that (Fig. 3) $M_2 = 1.417$, $P_2/P_1 = 1.655$, $\rho_{a2}/\rho_{a1} = 1.428$, $a_1 = 1{,}021$ ft. per sec, and the shock wave is at an angle of 45°.

From these data the following are calculated:

$$T_2/T_1 = (P_2/P_1)\,(\rho_{a1}/\rho_{a2}) = 1.655/1.428 = 1.156$$

$$\frac{|\vec{V}_2|}{|\vec{V}_1|} = \frac{M_2}{M_1\sqrt{\dfrac{T_2}{T_1}}} = \frac{1.417}{1.767}\sqrt{1.156} = 0.862$$

$$|\vec{V}_1| = M_1 a_1 = 1.767 \times 1{,}021 = 1{,}802 \text{ ft. per sec.}$$

$$|\vec{V}_2| = 0.862 \times 1{,}802 = 1{,}555 \text{ ft. per sec.}$$

P_1 = 16.88 in. Hg, $\rho_{a1} = 0.00160$ slugs per cu.ft., $T_1 = 435°\text{R}$.

P_2 = 27.9 in. Hg, $\rho_{a2} = 0.00228$ slugs per cu.ft., $T_2 = 504°\text{R}$.

The relative velocity of the droplet ($\vec{V}_1 - \vec{V}_2$) may be computed from the vector diagram of Fig. 4.

$$|\vec{U}| = \sqrt{1{,}555^2 + 1{,}802^2 - 2 \times 1{,}802 \times 1{,}555 \cos 10°}$$

$$|\vec{U}| = 379 \text{ ft. per sec.}$$

The initial Reynolds modulus of the droplet is, therefore,

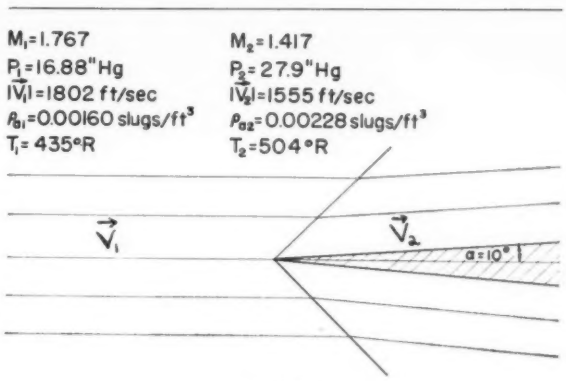

Fig. 3.

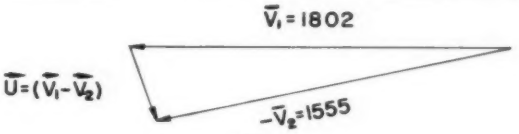

Fig. 4.

$$R = \frac{|\vec{U}|\,2r\rho_a}{\mu} = \frac{379 \times 6.56 \times 10^{-5} \times 0.00228}{0.368 \times 10^{-6}} = 154$$

The dimensionless time required for the drop to come to this value of R from an initial value of $R = 1{,}800$ is read from Fig. 2, Curve A, as

$$\mu(t - t_0)/4r^2\rho_w = 1.25 \times 10^{-2}$$

From Curve B of Fig. 2, the dimensionless distance traveled in this time (from an initial value $R = 1{,}800$) is

$$(x - x_0)\rho_a/2r\rho_w = 6.10$$

hence, the (dimensionless) maximum distance traveled by a drop initially at $R = 154$ is

$$\lambda_{max.}\,\rho_a/2r\rho_w = 8.63 - 6.10 = 2.53$$

(8.63 is the range of a droplet initially at $R = 1{,}800$). In feet, this range is

$$\lambda_{max.} = \frac{2.53(2r)\rho_w}{\rho_a} = \frac{2.53 \times (6.56 \times 10^{-5}) \times 62.4}{32.2 \times 0.00228} =$$

0.141 ft.

The time required for the droplet to traverse half this distance, for example, may be computed from Fig. 2 as follows:

(1) The initial dimensionless position at time zero is 6.10.

(2) Traveling half the "range" increases the dimensionless position by 2.53/2 = 1.26—i.e., the dimensionless position will be 6.10 + 1.26 = 7.36.

(3) The dimensionless time (Curve B) is 2.6×10^{-2} corresponding to position 7.36.

(4) At position 6.10, dimensionless time equals 1.2×10^{-2}.

TABLE 1

Distance Traveled by Droplet Relative to the Air Stream (Dimensionless)	Time Required to Traverse This Distance (Dimensionless)	Time Required (Sec.)	Distance Traveled by Droplet Relative to Air Stream (Ft.)	Distance the Air Stream Moved Parallel to Wedge in This Time Interval (Ft.)
2.53	.....	.....	0.141	...
1.90	3.3×10^{-2}	7.46×10^{-4}	0.106	1.16
1.26	1.4×10^{-2}	3.16×10^{-4}	0.070	0.49
0.63	0.58×10^{-2}	1.31×10^{-4}	0.035	0.20

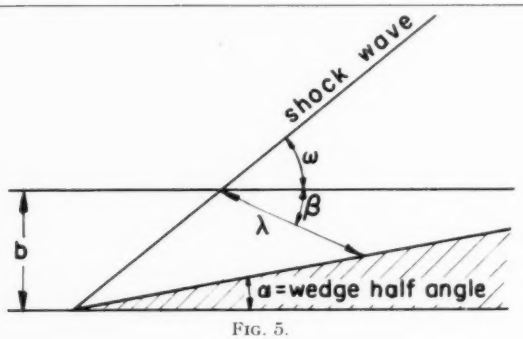

FIG. 5.

(5) Therefore, the time interval is 1.4×10^{-2} (dimensionless).

(6) The actual time is, therefore,

$$t - t_0 = \frac{(1.4 \times 10^{-2})\ (2r)^2 \rho_w}{\mu} = \frac{1.4 \times 10^{-2} \times (6.56 \times 10^{-5})^2 \times 62.4}{32.2 \times 0.368 \times 10^{-6}} = 3.16 \times 10^{-4} \text{ sec.}$$

Table 1 was constructed using the method just described.

From the known shock angle (ω), wedge half angle (α), and direction of the relative velocity vector (β) (Fig. 5), the initial distance from the centerline (b) of a droplet that strikes the wedge by moving the relative distance λ may be computed from trigonometric relations as

$$b = \lambda[\sin \omega \sin (\alpha + \beta)]/[\sin (\omega - \alpha)]$$

The angle (β) of the relative velocity vector may be computed from

$$\sin \beta = \frac{\sin \alpha}{\sqrt{1 + (V_1/V_2)^2 - 2\ (V_1/V_2) \cos \alpha}} = \left|\frac{V_2}{U}\right| \sin \alpha$$

For the case at hand, the angles are $\alpha = 10°$, $\omega = 45°$, $\beta = 45.5°$, and

$$b = \lambda \frac{\sin 45° \sin 55.5°}{\sin 35°} = 1.01\lambda$$

Using these data Table 2 was constructed.

TABLE 2

Initial Distance from Centerline (b, ft.)	Position on Wedge at Which Drop Strikes (Ft. from Nose)	Average Rate of Ice Accretion Between This Point and Nose if Liquid Water Content Is 0.2 Gm. per Cu. M. (Lbs. Hr./Ft.²)	Average Rate of Icing (In. per Min.)
0.035	0.24	12.0	0.043
0.071	0.56	10.2	0.036
0.107	1.27	6.8	0.024
0.143	∞	0	0

The position on the wedge at which the drop strikes differs from the distance traveled by the air stream parallel to the wedge surface (Column 5 of Table 1). This difference is the initial displacement of the drop relative to the nose of the wedge but parallel to the wedge surface. The difference occurs because the shock wave angle is less than a right angle. This initial displacement is equal to $(b/\sin \omega)$ [sin $(90° - \omega)$]. For the case where $\omega = 45°$, the initial displacement is equal to b, the initial distance of a drop from the centerline of the wedge.

For this particular flight speed and free air temperature, it is found (using the methods of reference 8) that icing will not occur because of the aerodynamic heating effects. However, at $-40°$F. and the same flight speed, the aerodynamic heating will be insufficient to prevent icing.

REFERENCES

[1] Glauert, M., *A Method of Constructing the Paths of Raindrops of Different Diameters Moving in the Neighborhood of (1) a Circular Cylinder (2) an Airfoil; Placed in a Uniform Stream of Air and a Determination of the Rate of Deposit of the Drops on the Surface and the Percentage of Drops Caught*, R. and M. No. 2025, British A.R.C., 1940.

[2] Kautrowitz, A., *Aerodynamic Heating and the Deflection of Drops by an Obstacle in an Air Stream in Relation to Aircraft Icing*, N.A.C.A. T.N. No. 779, 1940.

[3] Langmuir, I., and Blodgett, K., *A Mathematical Investigation of Water Droplet Trajectories*, U.S.A.F. T.R. 5418, February 1946.

[4] Bergrun, N. R., *A Method for Numerically Calculating the Area and Distribution of Water Impingement on the Leading Edge of an Airfoil in a Cloud*, N.A.C.A. T.N. No. 1397, 1947.

[5] Guibert, A. G., Janssen, E., Robbins, W. M., *Determination of the Rate, the Area, and the Distribution of Impingement of Waterdrops on Various Airfoils from Trajectories Obtained on the Differential Analyzer*, N.A.C.A. R.M. 9A05, February 1949.

(*Continued on page 403*)

Dynamic Stability of a Missile in Rolling Flight

RAY E. BOLZ*

Case Institute of Technology

ABSTRACT

The paper sets down the equations of motion for a symmetric rolling missile with respect to axes attached to the missile. The missile may be jet (or rocket) propelled or coasting under accelerating or decelerating conditions, respectively, wherein the variable rolling velocity is derived from intentionally or unintentionally "canted" fins and/or wings.

The equations contain a force and moment system that includes, in addition to the usual forces and moments, those due to magnus effects, misaligned surfaces, canted surfaces, jet misalignment, and the linear accelerations in the plane normal to the missile axis.

The results present general stability criteria for a rolling missile which are summarized in the "Discussion of Stability."

LIST OF SYMBOLS

(I) *English Letters*

A = moment of inertia in roll about x axis, ρd^5, lb. sec.^{2} ft.
$\bar{A}$ = $A/\rho d^4$, ft.$^{-1}$
B = moment of inertia about y axis, lb. sec.^{2} ft.
$\bar{B}$ = $B/\rho d^4$, ft.$^{-1}$
C = moment of inertia about z axis, lb. sec.^{2} ft.
C_D = drag coefficient, dimensionless
c = wing or tail chord, ft.
d = diameter of missile, ft.
$\boldsymbol{G}$ = linear momentum vector
$\boldsymbol{H}$ = angular momentum vector
i, j = unit vectors along y and $\bar{z}$ axes, respectively
L, M, N = moments about x, y, and $\bar{z}$ axes, respectively
m = mass of missile, lb. sec.^{2} ft.$^{-1}$
$\bar{m}$ = $m/\rho d^3$, dimensionless
P = rolling velocity of missile about x axis, rad. per sec.
P_z = P/V, rad. per ft.
q, r = angular velocities in pitch (about y axis) and in yaw (about $\bar{z}$ axis)
S = area, sq.ft.
T = thrust force, lbs.
$\bar{T}$ = $T/\rho d^3$, ft./sec.^{2}
t = time, sec.
u, v, w = components of linear velocity of the missile along x, y, $\bar{z}$ axes, respectively, ft. per sec.
$\dot{u}, \dot{v}, \dot{w}$ = derivatives with respect to time
V = scalar velocity of missile along flight trajectory ft. per sec.
X, Y, Z = forces acting along x, y, $\bar{z}$ axes, respectively
$x, y, \bar{z}$ = designations of coordinate axes
z = distance along trajectory

(II) *Definition of Coefficients*

$\bar{K}$ = $\bar{T}/V^2$, 1/ft.
$K_{z_\alpha}, K_{m_\alpha}$ = dimensionless coefficients of force and moment, respectively, due to angle of attack or yaw
$\bar{K}_{z_\alpha}, \bar{K}_{m_\alpha}$ = K_{z_α}/d and K_{m_α}/d, respectively, 1/ft.
K_{z_q}, K_{m_q} = dimensionless coefficients of force and moment, respectively, due to pitching or yawing angular velocities
K_{z_p}, K_{m_p} = dimensionless coefficients of force and moment, respectively, due to combined roll with pitch or yaw
$K_{z_{\dot\alpha}}, K_{m_{\dot\alpha}}$ = dimensionless coefficients of force and moment, respectively, due to accelerations
K_{z_M}, K_{m_M} = dimensionless coefficient of magnus force and magnus moment, respectively
K_D = dimensionless coefficient of axial force (drag)
K_Z, K_Y / K_{m_1}, K_{m_2} = dimensionless coefficients of forces and moments in $\bar{z}$ and y directions, respectively, due to misaligned lifting surfaces
$\bar{K}_Z, \bar{K}_Y$ / $\bar{K}_{m_1}, \bar{K}_{m_2}$ = division of coefficients by d, 1/ft.
K_{m_δ} = dimensionless coefficient of moment due to canted surfaces
$\bar{K}_{m_\delta}$ = K_{m_δ}/d, 1/ft.
Z_T, Y_T / N_T, M_T = forces and moments in $\bar{z}$ and y directions due to jet misalignment, lbs. and lb. ft., respectively
$\bar{Z}_T, \bar{Y}_T$ = $Z_T/\rho d^3$ and $Y_T/\rho d^3$, ft./sec.^{2}
$\bar{N}_T, \bar{M}_T$ = $N_T/\rho d^4$ and $M_T/\rho d^4$, ft./sec.^{2}
$\bar{K}_\lambda$ = $\bar{K}_Y + i\bar{K}_Z$, complex coefficient, 1/ft.
$\bar{K}_\xi$ = $\bar{K}_{m_1} + i\bar{K}_{m_2}$, complex coefficient, 1/ft.
$\bar{F}_T$ = complex force, $\bar{Y}_T + i\bar{Z}_T$, ft./sec.^{2}
$\bar{M}_T{}'$ = complex moment, $\bar{M}_T + i\bar{N}_T$, ft./sec.^{2}
$\bar{K}_1$ = coefficient of the total force due to jet misalignment, 1/ft.
$\bar{K}_2$ = coefficient of the total moment due to jet misalignment, 1/ft.

(III) *Greek Letters*

α = angle of attack (in plane of the velocity vector $\boldsymbol{V}$ and the $\bar{z}$ axis)
β = angle of yaw (in plane of the velocity vector $\boldsymbol{V}$ and the y axis)
δ = angle of cant of surfaces (differential angle of offset)
θ = angle of roll
ρ = mass density
η = complex linear velocity, $v + iw$
ϕ = complex angular velocity, $q + ir$
η_z, ϕ_z = η/v and ϕ/v, respectively
$\eta_z{}', \phi_z{}'$ = derivatives with respect to z, the distance along the trajectory
ω = component of angular velocity of the missile about the x axis due to precessional motion

(IV) *Designation of Derivatives*

Primes (η', etc.) are derivatives with respect to z, the distance along the trajectory.

Dots ($\dot{u}$, etc.) are derivatives with respect to time.

INTRODUCTION

THE STUDY OF THE DYNAMIC STABILITY and of the motion of high-speed missiles and aircraft is the

Received September 17, 1951.

* Associate Professor of Aeronautical Engineering.

subject of constant investigation and analysis. Up to the advent of the supersonic guided missile and the jet-propulsion airplane, the aircraft designer needed reference only to the classical stability theory initiated by Lanchester and developed by Glauert and others. A complete discussion of this may be seen in reference 1. Here, the treatment centers about the ability to separate the six equations of motion into two independent groups of three equations each, the lateral and longitudinal groups, and the stability associated with the symmetric and nonsymmetric planes is easily obtained.

The missile development engineer now is faced with the dynamic problems concerning rolling missiles and the aircraft designer with aircraft having relatively large rotating masses in the form of turbines and compressors. The introduction of a rolling velocity into the equations of motion introduces a coupling term that prohibits the separation of the equations into independent lateral and longitudinal groups, and the six equations of motion must be simultaneously treated.

The problem is by no means new, since the stability theory of spinning shells has been a subject of investigation by the ballistician for the past several decades and ballistic treatments of the subject may be found in references 2 and 3. It is the purpose of this paper to present the stability criteria for a rolling missile with basic symmetry of design but with a limited type of asymmetry in the form of misalignment of the lifting surfaces and of the propelling jet if employed. The analysis includes the effect on stability of the canted surfaces that induce the roll either intentionally or otherwise.

The analysis presented here is in no sense a fundamentally new treatment and may be regarded as a modification to the work by Fowler, et al.,[2] and Nielsen and Synge.[3] In contrast, however, the motion here is referred to a coordinate system fixed in the missile and rotating with it such that certain asymmetries may be most conveniently expressed. The results are not restricted to constant-velocity flight or constant rolling motion, but only to motion wherein the rolling velocity is "self-induced" by canted fins such that it becomes a function of the linear velocity itself.

The results present more general stability criteria than previously derived and indicate some interesting results concerning the effect of rolling velocity, wing or fin cant, accelerations, missile geometry, mass distribution, thrust and drag, misaligned surfaces and jets, magnus moments and forces, and roll-yaw interaction moments.

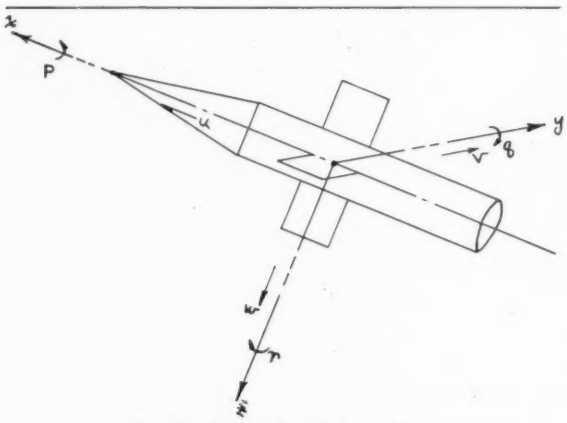

FIG. 1. Axis system for analysis.

DISCUSSION OF THE PROBLEMS AND ASSUMPTIONS

The purpose here is to analyze for the dynamic stability of a rolling finned and/or winged missile in free flight. The missiles will be restricted to essentially symmetrical configurations with nonsymmetry due only to unintentional small angle of incidence settings (in production assembly) of the wings and/or fins or small misalignment of the rocket or jet blast (if any) propelling the missile. In the analysis, the following assumptions are made:

(1) Gravitational effects are neglected for simplicity.

(2) The angular deviations of the missile from its trajectory are small such that the sines and angles are approximately equal and the cosines may be taken as unity.

(3) The linear acceleration is small enough such that the force and moment coefficients may be considered essentially constant over a reasonable period of time in the analysis. For application to flight with a large velocity change, a series of stability calculations may be made for different values of the coefficients selected to cover the whole velocity range in discrete intervals.

EQUATIONS OF MOTION FOR A ROLLING MISSILE

Consider a missile with cruciform tail and wing surfaces, any one of which may be at an angle of incidence with respect to the fuselage. A rectangular coordinate system is attached to the missile at its center of gravity, as shown in Fig. 1. These are the typical stability axes and directions employed in the usual aerodynamic stability treatment of nonrolling aircraft. The use of these axes allows the simple introduction of the effect of wing or fin misalignment angle and the effect of jet misalignment.

The six scalar equations of motion may then be written from the vector forms,

$$\sum \boldsymbol{M} = d\boldsymbol{H}/dt \tag{1}$$

and

$$\sum \boldsymbol{F} = d\boldsymbol{G}/dt \tag{2}$$

and the equations become

$$m(\dot{u} + wq - vr) = \sum X \tag{3a}$$

$$m(\dot{v} + ur - wP_1) = \sum Y \tag{3b}$$

$$m(\dot{w} - uq + vP_1) = \sum Z \tag{3c}$$
$$A\dot{P}_1 + Cqr - Bqr = \sum L \tag{3d}$$
$$B\dot{q} + AP_1r - CP_1r = \sum M \tag{3e}$$
$$C\dot{r} + BP_1q - AP_1q = \sum N \tag{3f}$$

where A, B, C are moments of inertia and the products of inertia vanish because of symmetry of mass distribution. In these equations, P_1 is actually the sum of the roll rate of the missile P and its own axis and the component of angular velocity ω_x about the X axis due to the precessional motion resulting.

$$P_1 = P + \omega_x \tag{4}$$

However, from actual experimental tests of missiles with canted fins, ω_x is, in general, a small magnitude compared with that of P (of the order of $0.001P$). For small values of rolling velocity P, this would not necessarily follow, although no observations indicate otherwise; but here we are in the range of rolling velocities where the roll rate and resultant forces and moments are extremely small and without important influence. Consequently, we neglect ω_x in the equations of motion and replace P_1 by P without significant effect on the stability results.

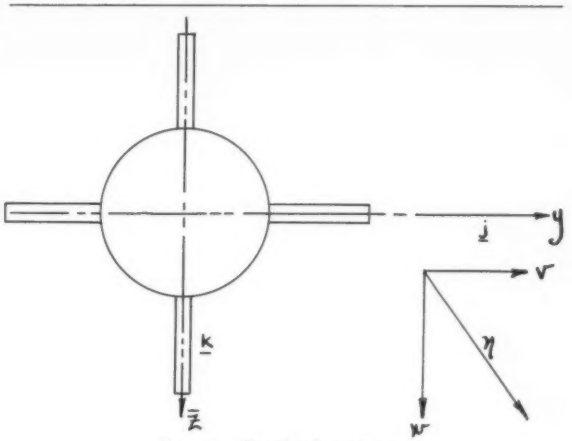

FIG. 2. Sketch of vector η.

In Eqs. (3) the terms wq, vr, and qr may be neglected as second order, since the angular deviation of the missile from its flight path is restricted to small angles and the angular velocities q and r are disturbance velocities.

From the mass symmetry, $B = C$, and we may write the equations of motion now simplified and including the forces and moments involved. We have, as in the usual stability analysis (see reference 1, page 124, for a detailed discussion), neglected the influence of accelerations on the forces and moments involved with the exception of the influence of accelerations $\dot{w}$ and $\dot{v}$.

$$(m/\rho d^3)\dot{u} = (T/\rho d^3) - (K_D/d)V^2 \cos\phi \cong (T/\rho d^3) - (K_D/d)V^2 \tag{5a}$$

$$(m/\rho d^3)(\dot{v} + ur - wP) = (-K_{z_\alpha}/d)vV + K_{z_q}rV + K_{z_p}Pw + K_{z_{\dot\alpha}}\dot{v} - K_{z_M}Pw + (K_Y/d)V^2 + (Y_T/\rho d^3) \tag{5b}$$

$$(m/\rho d^3)(\dot{w} - uq + vP) = (-K_{z_\alpha}/d)wV - K_{z_q}qV - K_{z_p}Pv + K_{z_{\dot\alpha}}\dot{w} + K_{z_M}Pv + (K_z/d)V^2 + (Z_T/\rho d^3) \tag{5c}$$

$$(B/\rho d^4)\dot{q} + [(A - B)/\rho d^4]Pr = (K_{m_\alpha}/d)wV - K_{m_q}qV - K_{m_p}Pv + K_{m_{\dot\alpha}}\dot{w} - K_{m_\beta}Vv + K_{m_M}Pv + (K_{m_1}/d)V^2 + (M_T/\rho d^4) \tag{5d}$$

$$(B\dot{r}/\rho d^4) - [(A - B)/\rho d^4]Pq = (-K_{m_\alpha}/d)vV - K_{m_q}rV - K_{m_p}Pw - K_{m_{\dot\alpha}}\dot{v} - (K_{m_\beta}/d)wV + K_{m_M}Pw + (K_{m_2}/d)V^2 + (N_T/\rho d^4) \tag{5e}$$

Here the coefficients of forces given by the K_z's and the coefficients of moments given by the K_m's are dimensionless coefficients presented mathematically in Appendix (I) and the values of which depend upon the stability derivatives and geometry of the missile used. The stability derivatives may be evaluated theoretically (see, for example, reference 4) or by experiment.

In Eq. (5b), a numerical comparison of the terms $(m/\rho d^3)\dot{v}$ and $K_{z_{\dot\alpha}}v$ shows that a ratio $K_{z_{\dot\alpha}}(\rho d^3/m)$ is of the order of 10^{-3} or 10^{-4} even for extremely low density missiles. A similar comparison in Eq. (5c) shows the ratio $K_{m_{\dot\alpha}}(\rho d^4/B)$ to be of order 10^{-3}. Accordingly, these terms are unimportant and are, henceforth, neglected.

We define, for convenience,

$$\bar{m} \equiv \frac{m}{\rho d^3}, \qquad \bar{T} \equiv \frac{T}{\rho d^3}, \qquad \bar{Z}_T \equiv \frac{Z_T}{\rho d^3}, \qquad \bar{Y}_T \equiv \frac{Y_T}{\rho d^3}$$

$$\bar{A} \equiv A/\rho d^4,\ \bar{B} \equiv B/\rho d^4,\ \bar{M}_T \equiv M_T/\rho d^4,\ \bar{M}_T \equiv N_T/\rho d^4$$

and use a bar notation over the coefficients to indicate division by d. Now multiply Eqs. (5c) and (5e) by i and add, respectively, to Eqs. (5b) and (5d) to obtain

$$\bar{m}u = \bar{T} - \bar{K}_D V^2 \tag{6a}$$

$$\bar{m}(\dot{v} + i\dot{w}) + \bar{m}u(r - iq) - \bar{m}P(w - iv) = -\bar{K}_{z_\alpha} V(v + iw) + K_{z_q} V(r - iq) + V^2(K_Y + iK_Z) + (K_{z_p} - K_{zM})P(w - iv) + (\bar{Y}_T + i\bar{Z}_T) \tag{6b}$$

$$\bar{B}(\dot{q} + i\dot{r}) + (\bar{A} - \bar{B})(r - iq)P = \bar{K}_{m_\alpha} V(w - iv) - K_{m_q} V(q + ir) - \bar{K}_{m_\delta} V(v + iw) - (K_{m_p} - K_{mM})P(v + iw) + V^2(\bar{K}_{m1} + i\bar{K}_{m2}) + (\bar{M}_T + i\bar{N}_T) + K_{m_{\dot{\alpha}}}(\dot{w} - i\dot{v}) \tag{6c}$$

Now we define

$$q + ir = \phi; \qquad v + iw = \eta \tag{7}$$

where η and ϕ are complex values of the linear and angular yaw velocity, respectively.

Eqs. (6b) and (6c) then become

$$\bar{m}\dot{\eta} - i\bar{m}\phi u + i\bar{m}P\eta = -\bar{K}_{z_\alpha} V\eta - iK_{z_q} V\phi - i(K_{z_p} - K_{zM})P\eta + V^2\bar{K}_\lambda + \bar{F}_T \tag{8a}$$

$$\bar{B}\dot{\phi} - i(\bar{A} - \bar{B})P\phi + i\dot{\eta}K_{m_{\dot{\alpha}}} = -i\bar{K}_{m_\alpha} V\eta - K_{m_q} V\phi - (K_{m_p} - K_{mM})P\eta + V^2\bar{K}_\xi + \bar{M}_T - \bar{K}_{m_\delta} V\eta \tag{8b}$$

where

$$\left.\begin{aligned} \bar{K}_\lambda &= \bar{K}_Y + i\bar{K}_Z, & \bar{F}_T &= \bar{Y}_T + i\bar{Z}_T \\ \bar{K}_\xi &= \bar{K}_{m_1} + i\bar{K}_{m_2}, & \bar{M}_T' &= \bar{M}_T + i\bar{N}_T \end{aligned}\right\} \tag{9}$$

are the complex force coefficients due to misaligned surfaces and jet offset, respectively, and the complex moment coefficients due to misaligned surfaces and jet offset, respectively.

By assumption, we have specified that the angle of yaw and the yawing velocities are small disturbance values, and we write $u = V\cos\phi$, where $\cos\phi \to 1$ and $\sin\phi \to \phi$; then

$$\dot{u} = \dot{V} - V\sin\phi\dot{\phi} \cong \dot{V} - V\phi\dot{\phi} \tag{10}$$

or $\dot{u} \cong \dot{V}$ and $u \cong V$.

A final step is now taken—namely, the transformation from the independent variable t to z, the distance along the trajectory—and, since η, ϕ, and P are actual velocities, we define $\eta = V\eta_z$, $\phi = V\phi_z$, and $P = VP_z$, where $\eta_z = \eta/V$, $\phi_z = \phi/V$, and $P_z = P/V$ are velocities per unit distance of travel along z. Then

$$\dot{\eta} = (d\eta/dz)(dz/dt) = V\eta'$$

or

$$\dot{\eta} = (V\eta_z' + \eta_z V')V; \quad \dot{\phi} = (V\phi_z' + \phi_z V')V \tag{11}$$

where the prime refers to a derivative with respect to z. Eqs. (9) become

$$\left.\begin{aligned} &\bar{m}(V^2\eta_z' + VV'\eta_z) - i\bar{m}uV\phi_z + i\bar{m}P_z\eta_z V^2 = -\bar{K}_{z_\alpha} V^2\eta_z - iK_{z_q} V^2\phi_z + V^2\bar{K}_\lambda + \bar{F}_T - i(K_{z_p} - K_{zM})V^2P_z\eta_z \\ &\bar{B}(V^2\phi_z' + \phi_z VV') - i(\bar{A} - \bar{B})V^2P_z\phi_z + i(\eta_z' V^2 + VV'\eta_z)K_{m_{\dot{\alpha}}} = -i\bar{K}_{m_\alpha} V^2\eta_z - K_{m_q} V^2\phi_z - \bar{K}_{m_\delta} V^2\eta_z - (K_{m_p} - K_{mM})V^2P_z\eta_z + V^2\bar{K}_\xi + \bar{M}_T' \end{aligned}\right\} \tag{12}$$

and Eq. (6a) becomes, using Eqs. (10) and (11),

$$\bar{m}VV' = \bar{T} - \bar{K}_D V^2; \quad V'/V = (1/\bar{m})[(\bar{T}/V^2) - \bar{K}_D] \tag{13}$$

Divide Eqs. (12) by V^2 and insert Eqs. (13) and (10),

$$\bar{m}\eta_z' + i\bar{m}P_z\eta_z - i\bar{m}\phi_z + [(\bar{T}/V^2) - \bar{K}_D]\eta_z = -\bar{K}_{z_\alpha}\eta_z - iK_{z_q}\phi_z - i(K_{z_p} - K_{zM})P_z\eta_z + \bar{K}_\lambda + (\bar{F}_T/V^2) \tag{14a}$$

$$\bar{B}\phi_z' + iK_{m_{\dot{\alpha}}}\eta_z' + i(K_{m_{\dot{\alpha}}}/\bar{m})[(\bar{T}/V^2) - \bar{K}_D]\eta_z + (\bar{B}/\bar{m})[(\bar{T}/V^2) - \bar{K}_D]\phi_z = i(\bar{A} - \bar{B})P_z\phi_z - i\bar{K}_{m_\alpha}\eta_z - K_{m_q}\phi_z - \bar{K}_{m_\delta}\eta_z - (K_{m_p} - K_{mM})P_z\eta_z + \bar{K}_\xi + (\bar{M}_T'/V^2) \tag{14b}$$

It has been found, see reference 5, both experimentally and theoretically, that for all of the many geometrical missile configurations investigated the ratio of equilibrium rolling velocity P induced by aerodynamic forces to linear velocity V, $P/V = P_z$, is very nearly a constant over a Mach Number range of 1.3 to 4.0 (see, for example, Fig. 14, reference 6). Then, for conditions where the linear acceleration is not large compared with the resulting angular acceleration in roll, P_z is essentially a constant for supersonic flight.

Furthermore, if the missile is powered by a ram-jet, we may write the thrust approximately as $T \cong K V^2$ and $\bar{T} \cong \bar{K} V^2$ to a good approximation [Appendix (2)] if the changes in velocity are not too great. Then, since

$$\bar{F}_T = \bar{T}\beta = \bar{K}_1 V^2; \qquad \bar{M}_T' = \bar{T} l \beta = \bar{K}_2 V^2$$

where l = moment arm, ft.; $\bar{K}_1 = \beta \bar{K}$, 1/ft.; $\bar{K}_2 = \beta \bar{K} l$, dimensionless; and β is the complex angle of misalignment, Eq. (14) becomes *completely independent of the flight velocity (for supersonic velocities), except for the dependence of the force and moment coefficients on the velocity.*

If the missile is rocket-powered, the thrust is essentially independent of the velocity, and we find the equations dependent to some extent upon the velocity. Here, then, we restrict ourselves to small enough changes in velocity such that $[(\bar{T}/V^2) - \bar{K}_D]$ is negligible and $\bar{K}_T/V^2 \rightarrow$ constant and $\bar{M}_T/V^2 \rightarrow$ constant. However, for a rocket, the mass of the missile usually varies considerably with time or distance, and the solution presented here does not properly treat this case. We shall solve the former case—namely,

$$\left.\begin{aligned} &\bar{m}\eta_z' + (\bar{K} - \bar{K}_D)\eta_z + i\bar{m}P_z\eta_z - i\bar{m}\phi_z = -\bar{K}_{z_\alpha}\eta_z - iK_{z_q}\phi_z - i(K_{z_p} - iK_{z_M})P_z\eta_z + \bar{K}_\lambda + \bar{K}_1 \\ &B\phi_z' + i\eta_z' K_{m_{\dot\alpha}} + (\bar{B}/\bar{m})(\bar{K} - \bar{K}_D)\phi_z - i(\bar{A} - \bar{B})P_z\phi_z + i(K_{m_{\dot\alpha}}/\bar{m})(\bar{K} - \bar{K}_D)\eta_z = \\ &\qquad -i\bar{K}_{m_\alpha}\eta_z - K_{m_q}\phi_z - (K_{m_p} - K_{m_M})P_z\eta_z - \bar{K}_{m_\delta}\eta_z + \bar{K}_\xi + \bar{K}_2 \end{aligned}\right\} \quad (15)$$

Solution of Equations of Motion

Eqs. (15) are two linear differential equations with constant coefficients, which we rewrite for simplicity as

$$\eta_z' + a\eta_z + b\phi_z = s \quad (16a)$$

$$\phi_z' + c\phi_z + d\eta_z + e\eta_z' = t \quad (16b)$$

where

$$\begin{aligned} a &= (1/\bar{m})[(\bar{K} - \bar{K}_D) + \bar{K}_{z_\alpha} + i(K_{z_p} - K_{z_M})P_z] + iP_z \\ b &= i[(K_{z_q}/\bar{m}) - 1] \\ c &= (1/\bar{m})(\bar{K} - \bar{K}_D) + (K_{m_q}/\bar{B}) - i(\bar{A}/\bar{B})P_z + iP_z \\ d &= i(\bar{K}_{m_\alpha}/\bar{B}) + [(K_{m_p} - K_{m_M})/\bar{B}]P_z + (\bar{K}_{m_\delta}/\bar{B}) + i(K_{m_{\dot\alpha}}/\bar{m}\bar{B})(\bar{K} - \bar{K}_D) \\ e &= i(K_{m_{\dot\alpha}}/\bar{B}) \\ s &= \bar{K}_\lambda + \bar{K}_1 \\ t &= \bar{K}_\xi + \bar{K}_2 \end{aligned}$$

Complementary Solution

Solving Eq. (16a) for ϕ_z, differentiating, and substituting these into Eqs. (16) yields

$$\eta_z'' + \eta_z'(a + c - eb) + \eta_z(ac - bd) = cs - bt \quad (17)$$

Let

$$\eta_z = Re^{\lambda z} \quad (18)$$

The complementary part of Eq. (17) becomes

$$\lambda = [-(a + c - eb)/2] \pm (1/2)\sqrt{(a - c + eb)^2 + 4b(d - ae)} \quad (19)$$

The Particular Solution

The particular solution of Eq. (17) is

$$\eta_z = (cs - bt)/(ac - bd) \quad (20)$$

If the denominator becomes extremely small under any circumstances, instability results. We investigate under what conditions, if any, this may occur.

Since $ac - bd = A + iB$,

$$\eta_z = (cs - bt)(A - iB)/(A^2 + B^2) \quad (21)$$

But if $A^2 + B^2 \rightarrow 0$, then $A \rightarrow 0$ and $B \rightarrow 0$.

From an inspection of the coefficients a, b, c, d there appears no feasibility of A and B approaching zero simultaneously.

Stability Criteria

Dynamic stability of a missile implies that, if a small disturbance occurs during flight and causes a displacement of the orientation of the missile axes from their equilibrium position, the effects of the disturbance will damp out and the missile will tend to return toward equilibrium. Mathematically, this means that the real part of Eq. (19) must always be negative. We inspect Eq. (19), and two criteria for stability then arise.

(I) The real part of $(a + c - eb)$ must be positive. This means then that

$$\left\{2\frac{(\bar{K} - \bar{K}_D)}{\bar{m}} + \frac{\bar{K}_{z_\alpha}}{\bar{m}} + \frac{K_{m_q}}{\bar{B}} - \frac{K_{m_{\dot\alpha}}}{\bar{B}}\right\} > 0 \quad (22)$$

and since $\bar{K}_{z_\alpha}$, K_{m_q}, $\bar{K}_D$, $\bar{K}$, and $K_{m_{\dot\alpha}}$ are always positive coefficients, the relationship indicates stability for almost all cases. The only exception here may be conceived under the most unlikely condition of zero thrust, $K = 0$, and extremely high drag coupled with an extremely small lift coefficient (extremely small surfaces) and small damping moment.

(II) The second criterion for stability is that

$$|\text{real}\,(a + c - eb)| > |\text{real}\,\sqrt{(a - c + eb)^2 + 4b(d - ae)}\,| = |\text{real}\,\sqrt{P + iQ}|$$

Then the stability criterion becomes

$$|\text{real } (a + c - eb)|^4 - |\text{real } (a + c - eb)|^2 P + (P^2/4) > (P^2 + Q^2)/4$$

Since $|R(a + c - eb)|$ is a number much smaller than 1, we neglect the fourth-power term and write

$$-P > Q^2/4\,[R\,(a + c - eb)]^2 \tag{23}$$

Inserting the values for P, Q, a, c, etc., we get a stability equation,

$$\frac{1}{4}\left(\frac{\bar{A}}{\bar{B}}\right)^2 + \frac{1}{2}\frac{(K_{zp} - K_{zM})}{\bar{m}}\frac{\bar{A}}{\bar{B}} - \frac{\bar{K}_{m_\alpha}}{\bar{B}P_z^2} > \left[\frac{\frac{\bar{A}}{\bar{B}}\left(\frac{\bar{K}_{z_\alpha}}{2\bar{m}} - \frac{K_{m_q}}{2\bar{B}} + \frac{K_{m_{\dot\alpha}}}{2\bar{B}}\right) - \frac{K_{m_\delta}}{\bar{B}P_z} - \frac{K_{m_p}}{\bar{B}} - \frac{K_{m_{\dot\alpha}}}{\bar{B}} + \frac{K_{mM}}{\bar{B}}}{2\frac{(\bar{K} - \bar{K}_D)}{\bar{m}} + \frac{\bar{K}_{z_\alpha}}{\bar{m}} + \frac{K_{m_q}}{\bar{B}} - \frac{K_{m_{\dot\alpha}}}{\bar{B}}}\right]^2 \tag{24}$$

In this relation the magnitude of the K's for a finned missile is of the order of 10^{-2} or smaller, and, as such, the products of these terms are neglected. The equation therefore is not valid for missiles with near-neutral static stability. In some instances the ratio of the moments of inertia $\bar{A}/\bar{B}$ may be considerably larger than 10^{-2}, and for this reason the product terms involving this ratio are retained.

For the case where the term $\bar{A}/\bar{B}$ is of the same order of magnitude as the K's, Eq. (24) may be further simplified to

$$\frac{-\bar{K}_{m_\alpha}}{\bar{B}P_z^2} > \left[\frac{\frac{\bar{K}_{m_\delta}}{\bar{B}P_z} + \frac{K_{m_p}}{\bar{B}} + \frac{K_{m_{\dot\alpha}}}{\bar{B}} - \frac{K_{mM}}{\bar{B}}}{\frac{2(\bar{K} - \bar{K}_D)}{\bar{m}} + \frac{\bar{K}_{z_\alpha}}{\bar{m}} + \frac{K_{m_q}}{\bar{B}} - \frac{K_{m_{\dot\alpha}}}{\bar{B}}}\right]^2 \tag{25}$$

For cases where the term $(\bar{A}/\bar{B})$ is of the same order of magnitude as the K's but $|\bar{K}_{m_\alpha}/\bar{B}P_z^2|$ is of the order of the square of the other K's (near-neutral static stability), neither equation is valid, and Eq. (23) must be used and analyzed in its entirety.

(III) The third criterion for stability is that Eq. (21) is never satisfied. From an inspection of the coefficients, it appears impossible in a practical sense for this expression to vanish.

Discussion of Stability

From Eq. (24), the following results may be stated as applied to a missile in (a) accelerated or decelerated supersonic flight where the rolling velocity is obtained aerodynamically and varies with the velocity or (b) a supersonic or subsonic missile in essentially constant-velocity flight.

(A) For a statically stable missile with zero or small rolling velocity, dynamic stability is assured, since $\bar{K}_{m_\alpha}$ is a negative coefficient and $\bar{K}_{m_\delta}$ is zero or extremely small corresponding to the rolling velocity.

(B) For a statically unstable missile with zero or small rolling velocity, dynamic instability results.

(C) For rolling rates in the range of $^1/_4$ to 2 or so rad. per ft. travel, dynamic stability is not at all assured for a statically stable missile unless relatively large numerical values of $\bar{K}_{m_\alpha}$ are employed. The left side of the inequality has an order of magnitude of the cube of the coefficients (K's) compared with the square on the right, although the coefficients retained need not themselves be of the same order of magnitude.

(D) For large roll rates, dynamic instability can be induced for a statically stable missile, whereas for a statically unstable missile, dynamic stability can be approached and in some cases obtained by large roll rates.

(E) Large values of thrust have a stabilizing influence, while large values of drag have a destabilizing influence.

(F) An increase in missile size (diameter) for given values of the linear and roll velocities decreases the terms

$$\frac{\bar{K}_{m_\alpha}}{\bar{B}P_z^2} \sim \frac{1}{d^2}; \qquad \frac{\bar{K}_{m_\delta}}{\bar{B}P_z} \sim \frac{1}{d^2}$$

by the square of the diameter with no effect on the remaining terms. Increasing the size of the missile rapidly decreases the stability because of the major importance of the $\bar{K}_{m_\alpha}$ term in Eq. (24). It should be noted, however, that for a missile with a rolling velocity induced by cant on the fins, $P_z \sim 1/d$ and the *stability is independent of missile size.*

(G) For a statically stable rolling missile with small $\bar{A}/\bar{B}$ values (as is usual), the coefficients arising from the (1) canted surfaces, (2) rolling motion, and (3) linear cross accelerations contribute toward instability tendencies. It is interesting to note that the magnus moment opposes this tendency.

TABLE I

FORCE EQUATIONS USED IN STABILITY DISCUSSION

1	Forces due to angles of attack and yaw, respectively	$Z = \frac{\partial C_z}{\partial \alpha} \alpha \frac{\rho V^2}{2} S = -K_{z_\alpha} wV(\rho d^2)$ $Y = -K_{z_\alpha} vV(\rho d^2)$	$K_{z_\alpha} = \frac{\partial C_z}{\partial \alpha} \frac{S}{2d^2}$ • Always positive
2	Forces due to pitching and yawing angular velocities, respectively	$Z = \frac{\partial C_z}{\partial \left(\frac{qc}{2V}\right)} \frac{qc}{2V} \frac{\rho V^2}{2} S = -K_{z_q} qV(\rho d^3)$ $Y = K_{z_q} rV(\rho d^3)$	$K_{z_q} = \frac{-\partial C_z}{\partial \left(\frac{qc}{2V}\right)} \frac{cS}{4d^3}$ • Always positive
3	Forces due to rolling combined with pitching and yawing angular velocities, respectively	$Z = \frac{1}{\beta} \frac{\partial C_z}{\partial \left(\frac{Pb}{2V}\right)} \frac{Pb}{2V} \beta \frac{\rho V^2}{2} S = -K_{z_p} Pv(\rho d^3)$ $Y = K_{z_p} Pw(\rho d^3)$	$K_{z_p} = \frac{1}{\beta} \frac{\partial C_z}{\partial \left(\frac{Pb}{2V}\right)} \frac{Sb}{4d^3}$ • Always positive
4	Forces due to accelerated motion	$Z = \frac{\partial C_z}{\partial \left(\frac{\dot{\alpha} c}{2V}\right)} \frac{\dot{\alpha} c}{2V} \frac{\rho V^2}{2} S = K_{z_{\dot{\alpha}}} \dot{w}(\rho d^3)$ $Y = K_{z_{\dot{\alpha}}} \dot{v}(\rho d^3)$	$K_{z_{\dot{\alpha}}} = \frac{\partial C_z}{\partial \left(\frac{\dot{\alpha} c}{2V}\right)} \frac{Sc}{4d^3}$ • Always positive
5	Magnus pitching and yawing forces	$Z = K_{z_M} Pv(\rho d^3)$ $Y = -K_{z_M} Pw(\rho d^3)$ Note: Derived from Kutta-Joukowski lift equation $Z = \rho \Gamma v l$ where $\Gamma \sim P$	K_{z_M} is a dimensionless positive or negative experimental coefficient
6	Forces due to mis-aligned lifting surfaces	$Z = \frac{\partial C_z}{\partial \alpha} \alpha_m \frac{\rho V^2}{2} S = K_z V^2(\rho d^2)$ $Y = K_Y V^2(\rho d^2)$	$K_z = \frac{\partial C_z}{\partial \alpha} \alpha_m \frac{S}{2d^2}$ $K_Y = \frac{\partial C_Y}{\partial \beta} \beta_m \frac{S}{2d^2}$
7	Axial force or drag	$X = -C_D \frac{\rho V^2}{2} S = -K_D V^2(\rho d^2)$	$K_D = C_D \frac{S}{d^2}$ Always positive
	• The stability derivatives may be evaluated theoretically; see Ref. 4 for rectangular fins (for example) and Ref. 6 for fuselage.		

(H) For a supersonic missile (coasting or ram-jet-powered), the dynamic stability is independent of the linear flight velocity magnitude; whereas, in subsonic flight this independence does not exist. The moment due to accelerated motion in the (y-z) plane results in decreased stability, although this could be important only for large roll rates.

Eq. (24) derived from the particular solution results in the following conclusions:

(1) Misalignment of the fins or wings has no effect on stability.

(2) Jet offset for a propelled missile also has no effect on stability.

It is known that asymmetry in mass distribution or in lifting surface area can result in instability for a rolling missile, as shown in the restricted method of reference 7. However, such asymmetry cannot be treated by the methods of this paper.

Appendix (I)

The forces and moments acting on a rolling finned and/or winged missile are given in Table I and for the most part need no further discussion. The stability derivatives may be evaluated theoretically (see refer-

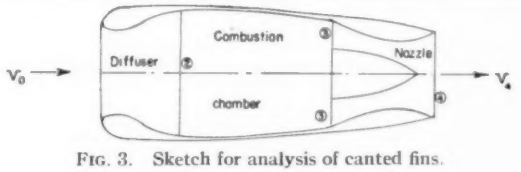

Fig. 3. Sketch for analysis of canted fins.

TABLE II

MOMENT EQUATIONS USED IN STABILITY DISCUSSION

1	Moments due to angles of attack and yaw, respectively	$M = \frac{\partial C_m}{\partial \alpha} \propto \frac{\rho V^2}{2} Sc = K_{m_\alpha} wV(\rho d^3)$ $N = -K_{m_\alpha} vV(\rho d^3)$	$K_{m_\alpha} = \frac{\partial C_m}{\partial \alpha} \frac{Sc}{2d^3}$ • Always positive for statically *unstable*
2	Moments due to pitching and yawing angular velocities, respectively	$M = \frac{-\partial C_m}{\partial\left(\frac{qc}{2V}\right)} \frac{qc}{2V} \frac{\rho V^2}{2} Sc = -K_{m_q} qV(\rho d^4)$ $N = -K_{m_q} rV(\rho d^4)$	$K_{m_q} = \frac{\partial C_m}{\partial\left(\frac{qc}{2V}\right)} \frac{c^2 S}{4d^4}$ • Always positive
3	Moments due to rolling combined with pitching and yawing angular velocities, respectively	$M = -K_{m_p} Pv(\rho d^4)$ $N = -K_{m_p} Pw(\rho d^4)$	$K_{m_p} = \frac{1}{\beta} \frac{\partial C_m}{\partial\left(\frac{Pb}{2V}\right)} \frac{Sb^2}{4d^4}$ • Always positive
4	Moments due to accelerated motion	$M = K_{m_{\dot\alpha}} \dot w(\rho d^4)$ $N = -K_{m_{\dot\alpha}} \dot v(\rho d^4)$	$K_{m_{\dot\alpha}} = \frac{\partial C_m}{\partial\left(\frac{\dot\alpha c}{2V}\right)} \frac{Sc^2}{4d^4}$ • Always positive
5	Magnus pitching and yawing moments	$M = K_{m_M} Pv(\rho d^4)$ $N = K_{m_M} Pw(\rho d^4)$	K_{m_M} is a dimensionless, positive or negative experimental coefficient
6	Moments due to misaligned lifting surfaces	$M = K_{m_1} V^2(\rho d^3)$ $N = K_{m_2} V^2(\rho d^3)$	$K_{m_1} = \frac{\partial C_m}{\partial \alpha} \alpha_m \frac{Sc}{2d^3}$ $K_{m_2} = \frac{\partial C_n}{\partial \beta} \beta_m \frac{Sc}{2d^3}$
7	Moments due to canted surfaces	$M = -\frac{\partial C_z}{\partial \alpha} 2\delta\beta a S \frac{\rho V^2}{2} = -K_{m_\delta} Vv(\rho d^3)$ $N = -K_{m_\delta} Vw\rho d^3$	$K_{m_\delta} = \left(\frac{\partial C_z}{\partial \alpha}\right) \delta \frac{Sa}{d^3}$ Positive for positive roll induced by cant angle

• The stability derivatives may be evaluated theoretically; see Ref. 4 for rectangular fins.

ence 4, for example), and the fuselage effects may be included from data such as appear in reference 6.

The moments due to canted fins may be briefly discussed. Consider two canted surfaces as shown in Fig. 3. The moment resulting from the axial components of the lifting forces is a couple—namely,

$$M = -\frac{\partial C_z}{\partial \alpha} [\beta + \delta + (\beta - \delta)]\delta \frac{\rho V^2}{2} aS$$

$$M = \left[-\left(\frac{\partial C_z}{\partial \alpha}\right) \delta\beta \frac{aS}{d^3}\right] V^2 \rho d^3 = -K_{m_\delta} Vv\rho d^3$$

as appears in Table II.

The forces and moments due to jet offset are merely the thrust multiplied by the constant misalignment angle or merely constants expressed as Z_T and Y_T as forces and N_T and M_T as moments.

Appendix (II)—Derivation of the Simple Thrust Equation for a Ram-Jet

Symbols:

- t = static temperature
- T = total temperature
- p = static pressure
- P = total pressure
- C_p = specific heat at constant pressure
- M = Mach Number
- V = velocity

S = area
m = mass flow, slugs per sec.

Derivation:

From Fig. 4 we write

$$F_{\text{net}} = m(V_4 - V_0) \tag{1}$$

where

$$m = \rho_4 S_4 V_4 \tag{2}$$

Then

$$\frac{V_4^2}{2} = C_p T_3 \left(1 - \frac{t_4}{T_3}\right) = C_p T_3 \left[1 - \left(\frac{p_0}{P_0}\right)^{(\gamma-1)/\gamma}\right] \tag{3}$$

Now

$$\left(\frac{p_0}{P_0}\right)^{(\gamma-1)/\gamma} = \frac{t_0}{T_0} = \left(1 + \frac{\gamma - 1}{2} M_0^2\right)^{-1} \tag{4}$$

and it can be shown from simple thermodynamics, assuming no loss in total pressure during combustion, that

$$V_4/V_0 = \sqrt{T_3/T_2} \tag{5}$$

$$\left.\begin{aligned} V_0 &= \sqrt{2C_p T_2[1 - (p_0/P_0)^{(\gamma-1)/\gamma}]} \\ V_4 &= \sqrt{2C_p T_3[1 - (p_0/P_0)^{(\gamma-1)/\gamma}]} \end{aligned}\right\} \tag{6}$$

Use of Eqs. (2) to (6) in Eq. (1) yields

$$F_{\text{net}} = \gamma M_0^2 S_4 p_0 \,(1 - \sqrt{T_2/T_3}) \tag{7}$$

or for relatively small changes in flight speed only where the ratio T_2/T_3 does not change greatly we may write Eq. (7) in the approximate form,

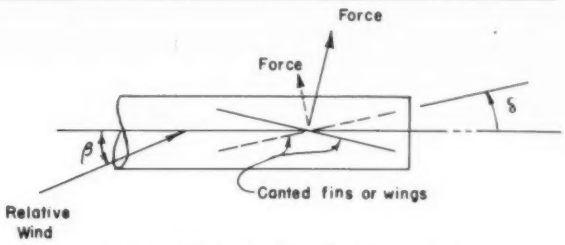

FIG. 4. Schematic of ram-jet power plant.

$$F_{\text{net}} = KV_0^2$$

where $K \cong$ constant.

REFERENCES

[1] Durand, W. F., *Aerodynamic Theory*, Vol. V.; Durant Reprinting Committee, 1943.

[2] Fowler, R. H., Gallop, E. G., Lock, E. N. H., and Richmond, A. W., *The Aerodynamics of a Spinning Shell*, Phil. Transactions of the Royal Society, A, Vol. 221, p. 295, 1921.

[3] Nielsen, K. L., and Synge, J. L., *On the Motion of a Spinning Shell*, Quarterly of Applied Math., Vol. IV, No. 3, p. 201, 1946.

[4] Harmon, S. M., *Stability Derivations of Thin Rectangular Wings at Supersonic Speeds*, N.A.C.A. T.N. No. 1706, November, 1948.

[5] Nicolaides, J. D., and Bolz, R. E., *On the Rolling Motion of Finned Missiles in Supersonic Flight*, Ballistic Research Laboratories Report in Process of Publication, Aberdeen Proving Ground, Md.

[6] Bolz, R. E., and Nicolaides, J. D., *A Method of Determining Some Aerodynamic Coefficients from Supersonic Free-Flight Tests of a Rolling Missile*, Journal of the Aeronautical Sciences, Vol. 17, No. 10, p. 609, October, 1950.

[7] Phillips, W. H., *Effect of Steady Rolling on Longitudinal and Directional Stability*, N.A.C.A. T.N. No. 1627, June, 1948.

[8] Walcher, O., *Systematic Wind-tunnel Measurements on Missiles*, N.A.C.A. T.M. No. 1122, March, 1947.

Impingement of Spherical Water Droplets on a Wedge at Supersonic Speeds in Air

(*Continued from page 394*)

[6] Guibert, A. G., and Hurty, H. C., *Determination of the Rate, the Area, and the Distribution of Impingement of Waterdrops on Various Airfoils from Trajectories Obtained on the Differential Analyzer, Addendum I*, University of California at Los Angeles, Department of Engineering, April, 1949.

[7] Keenan, J. H., and Kaye, J., *Gas Tables—Thermodynamic Properties of Air, Products of Combustion and Component Gases, Compressible Flow Functions;* John Wiley & Sons, Inc., New York, 1948.

[8] Tribus, M., Tessman, J., *et al.*, *Report on the Development and Application of Heated Wings, Addendum I*, U.S.A.F. T.R. 4972, Add. I., January, 1946.

Two-Dimensional Losses in Turbine Blades*

CHARLES A. MacGREGOR†
Propulsion Research Corporation

SUMMARY

Tests have been made on three typical turbine blades in a two-dimensional cascade tunnel. The tests were run at varying angles of attack, stagger angle, solidity, and downstream survey stations at a Mach Number of about 0.4 and a Reynolds Number of 6.5×10^5. The static pressure distribution about the blade was measured by 27 static pressure taps. The wake behind the blade row was surveyed and the loss determined.

Calculations were made of the boundary-layer loss at the various angles of attack, stagger angle, and solidity using the measured pressure distribution. The calculated loss was found to agree with the measured loss even though the pressure distribution varied greatly. It was found that the loss on the suction side of the blade was about six times as large as the loss on the pressure side. This was the result of the shape of the pressure distribution about the blade.

Discharge measurements made behind the blade row showed that the wake spread out as it moved downstream. The loss did not increase greatly in the first half-chord length behind the blade row, even though the shape parameter did.

INTRODUCTION

THE RAPID DEVELOPMENT of the turbojet and the turboprop engines, with their great dependency upon component efficiencies, has made it necessary to design turbines from an aerodynamic point of view. In order to provide an effective method of doing this, it is necessary to be able to calculate the losses in a turbine. The British[1–3] have made attempts to isolate the losses in turbomachines. The losses are divided into two general groups: two-dimensional losses—i.e., profile losses—and three-dimensional losses—i.e., annulus loss, secondary flow losses, tip clearance loss, etc. It is estimated that the profile and the three-dimensional losses are of about equal magnitude at the design point. This paper shows that it is possible to calculate part of the losses, the two-dimensional losses, with reasonable accuracy.

A boundary layer grows next to the blade surface (the profile loss) because of viscosity effects and regions of adverse pressure gradients as the gas flows through the blade row. In order to find this loss, it is necessary to know the pressure distribution about the blade which may be either measured or calculated. Methods for calculating the velocity distribution about a blade for any solidity or camber have been developed from incompressible potential-flow theory.[4–6] However, these methods do not consider compressibility and are mathematically complex. An alternate approach to calculating the velocity distribution has been the stream-filament theories, where the flow equations are integrated graphically[7] or mathematically.[8, 9] The latter method has been compared with experimental values and has been found to be in close agreement. Thus, a concise, simple method of determining the velocity distribution about turbine blades is available.

The cascade tunnel has been used for a long time in the tests of turbine blade profiles. Knowing the inlet conditions and surveying the discharge, it is possible to find the loss in the fluid as it flows through the blade passage. Three blades of greatly different characteristics were tested in a two-dimensional cascade tunnel in which it was possible to independently vary the angle of attack, stagger angle, and solidity. The static pressure was measured around the blade by static pressure orifices. Calculations were then made, using the measured static pressure distribution about the blade, for the boundary-layer loss. These calculations are compared with the measured values obtained from a discharge wake survey.

SYMBOLS

c = chord, see Fig. 1
H = ratio of displacement thickness to momentum thickness
K = ratio of momentum thickness to energy thickness
k = constant in equation for skin friction
n = constant in equation for skin friction

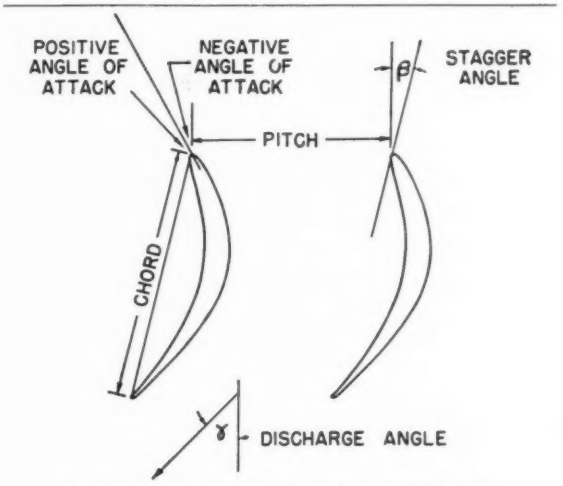

FIG. 1. Diagram of flow through cascade blades.

Received November 27, 1951.

* The research on which this paper is based was done during 1947–1948 while the author was an Aerodynamicist at The Turbodyne Corporation. The author expresses his thanks to Mrs. C. D. Oswalt for performing the computations and reduction of data.

† Aerodynamicist.

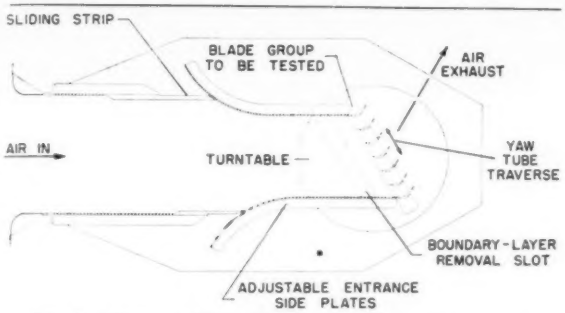

FIG. 2. Cross section of two-dimensional cascade tunnel.

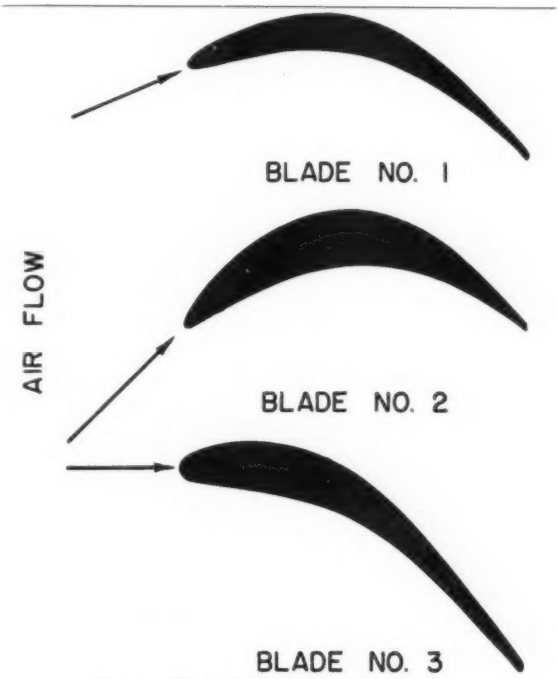

FIG. 3. Blade tested in cascade tunnel.

P = pressure
q = dynamic pressure
R = Reynolds Number based on chord and free-stream velocity
R_θ = Reynolds Number based on boundary-layer thickness
s = distance along blade surface
s_0 = position on surface at start of integration
t = blade pitch, see Fig. 1
u = local velocity inside boundary layer
U = local velocity outside boundary layer
U_0 = free-stream velocity, taken as integrated mean discharge velocity
x = distance normal to discharge flow
α = angle of attack, see Fig. 1
β = stagger angle, see Fig. 1
γ = discharge angle, see Fig. 1

δ^* = displacement thickness, $\int [1 - (u/U_0)]dx$
θ = momentum thickness, $\int (u/U_0)\,[1 - (u/U_0)]dx$
θ_0 = momentum thickness at transition point
ρ = density
σ = solidity, chord/pitch
τ_0 = skin friction per unit area
φ = energy thickness, $\int (u/U_0)^2\,[1 - (u/U_0)]dx$
ω = blade loss factor

Subscripts

a = axial
d = downstream
pr = pressure side
s = static condition
su = suction side
t = total condition
u = upstream

CASCADE BLADE TESTS

Tests have been made on three turbine blades in a two-dimensional cascade tunnel shown schematically in Fig. 2. The tests were made at varying angles of attack, stagger angle, solidity, and four survey stations downstream of the blades. The tunnel discharged into the atmosphere. The blades had a chord of 3 in. and an aspect ratio of 2. The blade sections that were tested are shown in Fig. 3. These three blades are of greatly different shapes and are representative of the blade shapes found in a turbine. The pertinent design data for these blades are given in Appendix (A). The blades were tested in groups of six or seven blades in order to eliminate end effects and simulate the flow through an infinite grid. The center blade of each group was equipped with 27 static pressure taps, which were located at the mid-span position. These taps were used to obtain the velocity distribution about the blade. The tunnel was equipped with boundary-layer removal slots, which were used to remove the boundary-layer air at the inlet of the blade row. A survey made at the discharge of the blade row showed that the flow was uniform and two-dimensional.

A traverse was made with a claw-type yawmeter, used by the null method, at the mid-span height of the discharge of the center passage. In addition, measurements were made of the temperature and total and static pressure upstream of the blade row. The blade loss factor, which is defined as follows:

$$\text{blade loss factor} = \omega = \frac{\text{energy lost}}{\text{energy available}} \qquad (1)$$

which, for incompressible flow, is

$$\text{loss factor} = \omega = \frac{P_{t_u} - P_{t_d}}{P_{t_u} - P_{s_d}} \qquad (2)$$

was found by plotting the survey points and integrating over the blade passage, assuming a uniform discharge static pressure equal to atmospheric pressure.

The tests were all run at a Mach Number of about 0.4 and a Reynolds Number of about 6.5×10^5 based upon the blade chord length.

Method of Calculation

The method used to calculate the boundary-layer momentum thickness about the blade is that of reference 10, where, in order to integrate the von Kármán boundary-layer momentum equation,

$$\frac{d\theta}{ds} + \frac{H+2}{2}\frac{\theta}{q}\frac{dq}{ds} = \frac{\tau_0}{2q} \tag{3}$$

the skin-friction coefficient is expressed as a function of the boundary-layer Reynolds Number,

$$\tau_0/2q = k/(R_\theta)^n \tag{4}$$

and the boundary-layer shape; therefore, H is assumed constant over the chord. The resulting integrated boundary-layer momentum equation is

$$\left(\frac{\theta}{c}\right)_{s/c} = \left[1/\left(\frac{U}{U_0}\right)_{s/c}^{H+2}\right]\left[\frac{(n+1)k}{(R)^n}\int_{s_0/c}^{s/c}\left(\frac{U}{U_0}\right)^{(H+1)(n+1)+1} d\left(\frac{s}{c}\right) + \left(\frac{\theta_0}{c}\right)^{n+1}\left(\frac{U}{U_0}\right)^{(H+2)(n+1)}\right]^{1/(n+1)} \tag{5}$$

This equation was evaluated graphically from the measured pressure distribution in two parts: one for the laminar region and one for the turbulent region. The point of laminar separation was calculated by the method of reference 11 and was assumed to be the transition point. The distance between the velocity peak and the calculated laminar separation point was only about 5 per cent of the chord length. The values of n and k were determined, as recommended in reference 10, from the initial and final values of R_θ for the turbulent region. A value for H of 1.4 was used.

The boundary-layer momentum thickness was calculated from Eq. (5); however, this momentum loss can be expressed in terms of a total pressure defect. The total pressure for incompressible flow at some point in the boundary layer is

$$P_t = P_s + (1/2)\rho u^2 \tag{6a}$$

and the total pressure in the free stream is

$$P_t = P_s + (1/2)\rho U_0^2 \tag{6b}$$

For a uniform discharge static pressure, the loss in total pressure at some point in the boundary layer at the trailing edge is then

$$(\Delta P_t) = (1/2)\rho(U_0^2 - u^2) \tag{7}$$

Integrating this loss across one blade passage at the trailing edge and weighting for flow,

$$\int_0^t (\Delta P_t)u_a\,dt = \int_0^t \frac{\rho}{2}(U_0^2 - u^2)u_a\,dt \tag{8a}$$

and letting

$$\overline{\Delta P_t} = \frac{\int_0^t (\Delta P)u_a\,dt}{\bar{u}_a t} = \frac{\int_0^t \frac{\rho}{2}(U_0^2 - u^2)u_a\,dt}{\bar{u}_a t} \tag{8b}$$

where the bar values represent integrated mean value. It follows, then, from the definition of the loss factor that

$$\omega = \frac{\overline{\Delta P_t}}{(1/2)\rho U_0^2} = \frac{1}{t\cos\gamma}\int_0^t \left(1 - \frac{u^2}{U_0^2}\right)\frac{u_a}{U_0}\,dt \tag{9a}$$

Expressing in terms of the distance normal to the discharge flow instead of parallel to the trailing edges, then

$$\omega = \frac{\int_0^{x/\cos\gamma} \frac{u}{U_0}\left(1 - \frac{u}{U_0}\right)dx}{t\cos\gamma} \times \left\{1 + \frac{\int_0^{x/\cos\gamma} \frac{u^2}{U_0^2}\left(1 - \frac{u}{U_0}\right)dx}{\int_0^{x/\cos\gamma} \frac{u}{U_0}\left(1 - \frac{u}{U_0}\right)dx}\right\} \tag{9b}$$

From the definition of θ, φ, and K and for the values at the trailing edge equal to the sum of the values on the pressure and suction sides, then

$$\omega = \left(\frac{\theta}{c}\right)_{pr+su}\left(\frac{\sigma}{\cos\gamma}\right)\left(\frac{K+1}{K}\right) \tag{10}$$

This then determines the total pressure loss in terms of the sum of the momentum thickness to chord, solidity, discharge angle, and boundary-layer shape parameter K at the trailing edge.

Results

A comparison of measured and calculated momentum thickness for the three blades at various blade settings is shown in Fig. 4. The measured values have been corrected for the traverse not being normal to the discharge flow. The comparison is made using the momentum thickness, since it could be obtained directly from the discharge measurements and calculated directly using the measured pressure distribution. In general, the agreement is good between the calculated and measured momentum thickness and is felt to be within the experimental error. The accuracy of the measured momentum thickness is limited because of the number of points that were taken in the traverse in the wake. There were usually from six to ten points taken within the wake region. This close agreement also indicates that there was no pressure drag loss arising at the trailing edge of the blade or any appre-

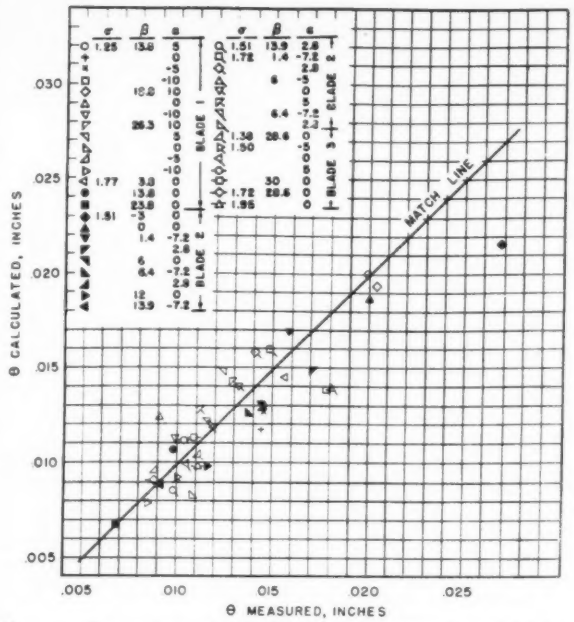

FIG. 4. Comparison of calculated and measured momentum thickness.

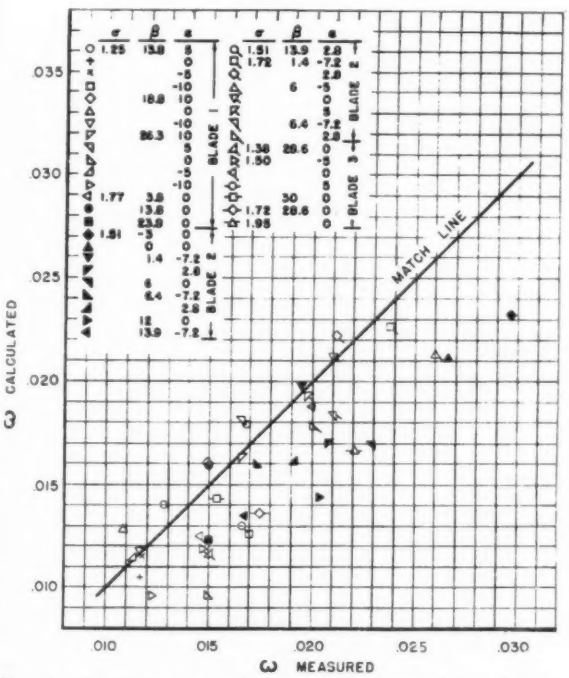

FIG. 5. Comparison of calculated and measured loss factor.

ciable loss when the pressure and suction side boundary layers join.

Fig. 5 shows a comparison of the measured and calculated blade loss factor. The calculated blade loss factor was determined from Eq. (10), which involves the calculated momentum thickness, the discharge angle, and the ratio of the momentum thickness to the energy thickness (K). The value of K used in these calculations was 1.280, which was the average value determined from the measurements made 0.1 chord downstream of the blades. The agreement between the measured and calculated loss factors is not so good as the comparison of the measured and calculated momentum thickness. This is probably the result of using this constant value for K as representative of the average of the pressure and suction surfaces at the trailing edges.

The blade setting shown in Figs. 4 and 5 does not include any where the flow has separated from the surface, since the calculations would not be applicable. The velocity distribution about the blade varied greatly with stagger angle, solidity, and angle of attack. At zero angle of attack, the velocity on the pressure side reached a peak at about 10 per cent of the chord from the leading edge and then accelerated to the free-stream velocity. Only at large negative angles of attack did the velocity at the peak reach the free-stream velocity. On the suction side, the flow accelerated to a velocity peak at about 50 per cent of the chord and then diffused to the free-stream velocity at the trailing edge. In general, the velocity was greater than the free-stream velocity over most of the suction surface. The measured velocity distribution at three angles of attack is shown in Fig. 6. Because of the difference in velocity distribution over the two surfaces, the calculated loss of the suction surface was about six times as large as the loss of the pressure surface. The effect of an increase in stagger angle and solidity was to decrease the velocity peak on the suction surface and, hence, to decrease the loss.

The measured momentum thickness was obtained from the integral of the measurements made in the wake behind the blade. Because of turbulent mixing, as the wake moves downstream, the wake becomes wider and the velocity distribution in the wake changes. The variation of H with downstream distance is shown in Fig. 7 which changes from its trailing-edge value to unity far downstream. The value shown in Fig. 7 is for the sum of the pressure and suction sides, and it changes rapidly in the first half-chord length behind the blades. The variation of momentum thickness with downstream distance is also shown in Fig. 7. The loss increases slightly as the wake spreads out and is mixed up.

CONCLUSIONS

An analysis of turbine blade cascade test data indicates the following conclusions:

(1) The two-dimensional losses of the flow through a turbine blade cascade have been found to agree with the calculated boundary-layer loss. In order to evaluate the loss, it is only necessary to know the pressure distribution about the blade.

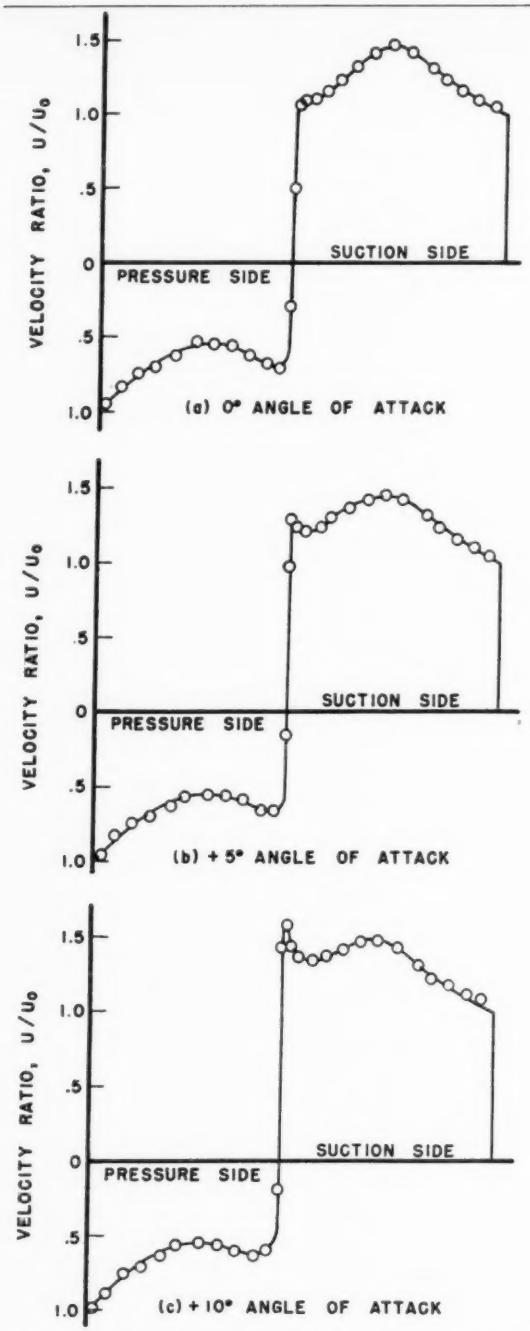

FIG. 6. Velocity distribution about Blade 1 at various angles of attack. β, 13.8°; and σ, 1.25

(2) The loss on the suction side of the blade was about six times as large as the loss on the pressure side. This is because of the shape of the velocity distribution around the blade—i.e., the diffusion of the fluid downstream of the "throat" on the suction side.

TABLE 1
Cascade Blade Design Data

	Blade No. 1	Blade No. 2	Blade No. 3
Typical section of:	Rotor trip	Rotor root	Nozzle
Entrance angle, deg.	22.5	45.8	0
Turning angle, deg.	60	85	52
Surface length, in.	6.85	7.03	7.43
Chord, in.	3.09	3.00	3.42
Trailing-edge thickness, in.	0.045	0.063	0.064

(3) The wake spreads out as it moves downstream from the blade. However, the additional loss is small in the first half-chord behind the blade.

APPENDIX (A)

The three blade sections that were tested correspond to typical turbine blade sections. Blades 1 and 2 correspond to rotor blade section, and Blade 3 to a nozzle blade section. The blades were of die cast aluminum. To obtain a good surface finish, the blades were coated with a primer and then hand polished. Some of the blade design information is given in Table 1.

REFERENCES

[1] Howell, A. R., *Fluid Dynamics of Axial Compressors*, Proceedings Inst. Mech. Engr., Vol. 153, p. 441, 1945.

[2] Howell, A. R., *The Present Basis of Axial Flow Compressor Design*, British Aeronautical Research Council, R. and M. No. 2095, 1942.

[3] Ainley, D. G., *Performance of Axial-Flow Turbines*, Proceedings Inst. Mech. Engr., Vol. 158, p. 230, 1948.

(*Continued on page 432*)

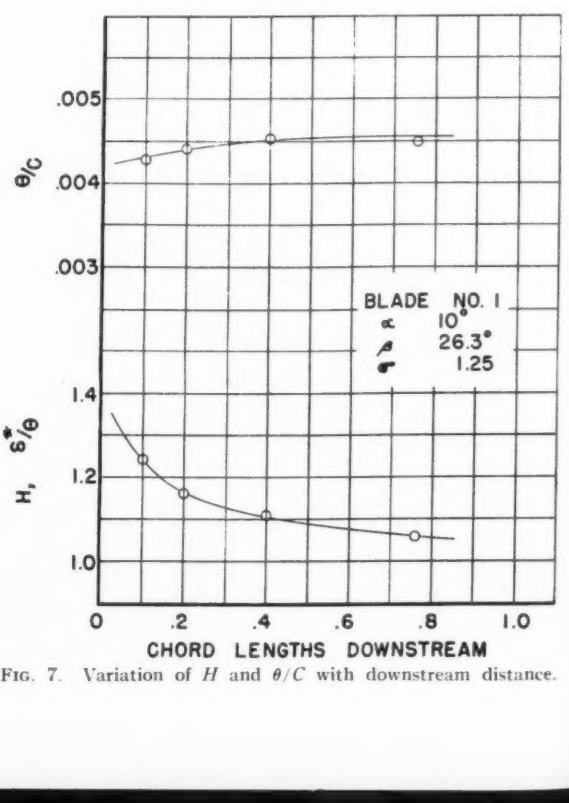

FIG. 7. Variation of H and θ/C with downstream distance.

Ripple-Type Buckling of Sandwich Columns*

A. CEMAL ERINGEN†
Illinois Institute of Technology

SUMMARY

The problem of local instability of thick sandwich columns having orthotropic cores is treated under two different types of loading: (a) axial compressive loads acting at the edges of face plates and (b) bending moments acting at the ends of the sandwich column. End points of the face plates are assumed to be pinned. The present method is, however, applicable to general end conditions and for arbitrary axial and transverse loading. It is shown that the deflected shape is neither symmetric nor antisymmetric, but asymmetric. Numerical calculations and curves are made for various types of cores employed in industry. The results are found to be in good agreement with the experimental data.

NOTATION

E_1, E_2, E_f	=	Young's moduli of faces 1 and 2, or common modulus if they are identical, lbs. per sq.in.
E_x, E_y	=	Young's moduli of core in the x and y direction, respectively, lbs. per sq.in.
G	=	shear modulus of core, lbs. per sq.in.
I_1, I_2	=	moments of inertias of faces 1 and 2 with respect to their median planes, respectively, in.^{4}
L	=	length in x direction, in.
m	=	number of half wave lengths in x direction
o	=	subscript to indicate boundary
s	=	subscript to indicate Fourier sine transform
t	=	thickness in y direction, in.
t_1, t_2, t_f	=	face thicknesses for faces 1 and 2, or common thickness if the faces are identical, in.
u, v	=	components of the displacement vector, in.
x, y	=	Cartesian coordinates
$\mu \equiv \nu_{xy}$ $\nu \equiv \nu_{yx}$	=	Poisson's ratios $\left(\nu_{xy} \equiv \dfrac{\text{contraction in } y \text{ direction}}{\text{extension in } x \text{ direction}}\right)$
σ_{cr}	=	wrinkling stress, lbs. per sq.in.
σ_x, σ_y	=	normal stresses, lbs. per sq.in.
τ	=	shear stress, lbs. per sq.in.

Subscripts after comma indicate differentiation ($\sigma_{x,y} = \partial\sigma x/\partial y$)

INTRODUCTION

DURING THE PAST 10 YEARS, many investigators treated the problem of buckling and bending of sandwich type of beams, plates, and shells.[1–14] In all of these works various simplifying assumptions are made so as to make the problems tractable. These assumptions are mostly concerned with the stress distribution in the core. Otherwise, a boundary value problem of elasticity for a two- or three-dimensional medium under general boundary conditions must be solved. Assumptions made in literature either eliminated or oversimplified the transverse stress components in the core, which in turn either eliminated or oversimplified the local instability. Thus, little attention is devoted to this ripple-type instability. As a result, different authorities seem to hold opposing views regarding the phenomenon of ripple-type instability of wrinkling. In particular, European investigators found that ripple-type instability would always occur in an asymmetric pattern, while other authors obtained wrinkling in a symmetric pattern.[1] The buckling load is known to be largely dependent upon the deflected shape pattern in sandwich structures. Therefore, present work was undertaken to investigate the wrinkling for completely arbitrary deflected shape patterns of faces. Hence, symmetric, antisymmetric, or skew patterns would be special cases of the problem treated. This analysis required the solution of a two-dimensional mixed boundary value problem of elasticity for a rectangular orthothropic medium to obtain the correct stress and deformation distributions in the core in terms of arbitrary distribution of the mixed boundary values.

The present problem became tractable as soon as the foregoing boundary value problem was solved‡ (reference 13 or Navy report footnote, page 1). Thus, the problem of ripple-type buckling of a thick sandwich beam having orthotropic core is solved under axial compressive loads and under end moments. In this way it was possible to prove that the wrinkling should occur in an asymmetric pattern rather than the patterns found by earlier investigators. Experimental evidence is seen to be in favor of this result.[1, 2] Buckling stresses calculated from the present theory were always lower than the ones given by reference 1. Difference between the two theories, while small for lower face and core modulae of elasticity, is considerably larger for higher ones. Experimental results published in reference 6 represent excellent agreement with the present theory (see Fig. 14).

Received October 31, 1951.

* The paper is condensed from the section on application of the author's thesis submitted in partial fulfillment of the requirements for the degree of Doctor of Philosophy in Applied Mechanics at the Polytechnic Institute of Brooklyn, June, 1948. The work contained in this thesis was part of an investigation carried out at the Polytechnic Institute of Brooklyn under contract with the Office of Naval Research of the U.S. Navy (Contract No. N6onr-263-Task Order II). The author is indebted to Dr. N. J. Hoff, his thesis adviser, for the criticism and advice received.

† Research Associate Professor of Mechanics.

‡ Because of the lengthy mathematical analysis involved in this boundary value problem, it is intended to present this part as a separate paper. Consequently, only the necessary formulas will be given here.

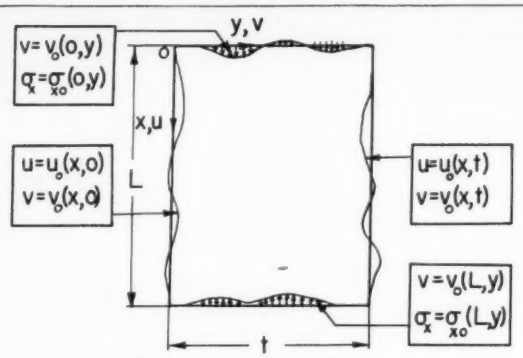

FIG. 1. Boundary conditions.

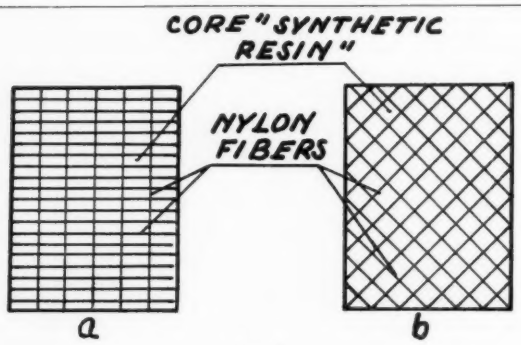

FIG. 2.

(1) STRESS DISTRIBUTION

Consider a rectangular orthotropic elastic medium of length L, width t, and thickness unity, with the axes of orthotropy parallel to the x and y directions (Fig. 1). The differential equations of the boundary value problem without body forces are

$$\left.\begin{aligned} &\frac{A}{\nu}\left(\frac{\partial^2 u}{\partial x^2}\right) + \frac{\partial^2 u}{\partial y^2} + (1+A)\frac{\partial^2 v}{\partial x\,\partial y} = 0 \\ &\frac{\partial^2 v}{\partial x^2} + \frac{A}{\mu}\left(\frac{\partial^2 v}{\partial y^2}\right) + (1+A)\frac{\partial^2 u}{\partial x\,\partial y} = 0 \\ &A = \frac{\mu}{1-\mu\nu}\left(\frac{E_y}{G}\right) = \frac{\nu}{1-\mu\nu}\left(\frac{E_x}{G}\right) \end{aligned}\right\} \quad (1)$$

Eqs. (1) are solved[13] under the following mixed boundary conditions: at $y = 0$,

$$\left.\begin{aligned} &u(x,0) = u_o(x,0); \qquad v(x,0) = v_o(x,0) \\ &\text{at } y = t \\ &u(x,t) = u_o(x,t); \qquad v(x,t) = v_o(x,t) \\ &\text{at } x = 0 \\ &\sigma_x(0,y) = \sigma_{xo}(0,y); \qquad v(0,y) = v_o(0,y) \\ &\text{at } x = L \\ &\sigma_x(L,y) = \sigma_{xo}(L,y); \qquad v(L,y) = v_0(L,y) \end{aligned}\right\} \quad (2)$$

where subscript o denotes the given functions at the boundary.

The result of the analysis in the special case of

$$u_o(x,0) = u_o(x,t) = v_o(0,y) = v_o(L,y) = u_{o,x}(0,y) = u_{o,x}(L,y) = 0 \quad (3)$$

$$E_x/2G > \mu + (\mu/\nu)^{1/2} \quad (4)$$

are

$$\left.\begin{aligned} \sigma_x &= \frac{E_x}{1-\mu\nu}\frac{2}{L}\sum_{m=1}^{\infty}\left\{\left[-\frac{m\pi}{L}U_o(m,y) + \nu V_{o,y}(m,y)\right]v_{os}(m,0) + \left[-\frac{m\pi}{L}U_t(m,y) + \nu V_{t,y}(m,y)\right]v_{os}(m,t)\right\}\sin\frac{m\pi x}{L} \\ \sigma_y &= \frac{E_y}{1-\mu\nu}\frac{2}{L}\sum_{m=1}^{\infty}\left\{\left[V_{o,y}(m,y) - \mu\frac{m\pi}{L}U_o(m,y)\right]v_{os}(m,0) + \left[V_{t,y} - \mu\frac{m\pi}{L}U_t(m,y)\right]v_{os}(m,t)\right\}\sin\frac{m\pi x}{L} \\ \tau &= G\frac{2}{L}\sum_{m=1}^{\infty}\left\{\left[U_{o,y}(m,y) + \frac{m\pi}{L}V_o(m,y)\right]v_{os}(m,0) + \left[U_{t,y}(m,y) + \frac{m\pi}{L}V_t(m,y)\right]v_{os}(m,t)\right\}\cos\frac{m\pi x}{L} \end{aligned}\right\} \quad (5)$$

where $U_o(m,y)$, $V_o(m,y)$, $U_t(m,y)$, $V_t(m,y)$ are known functions (see reference 13, pages 52, 55, and 56 or Navy report, pages 42–45).

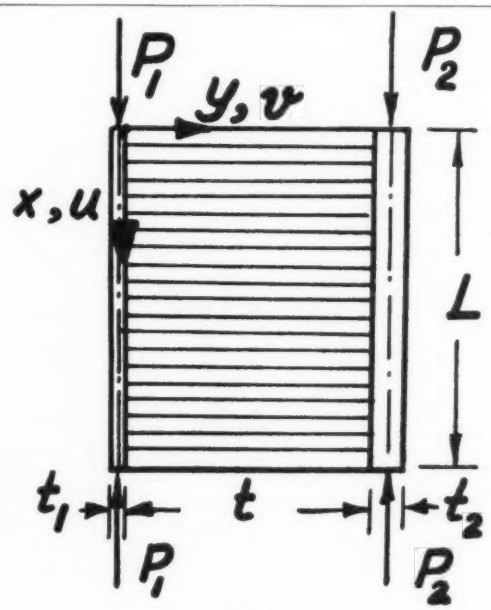

FIG. 3.

(2) Differential Equations

Consider a sandwich column composed of a thick orthotropic core, for which a boundary value problem was previously solved,[13] and the faces, as shown in Fig. 3. Face thicknesses t_1 and t_2 are assumed to be small as compared to core thickness t so that boundary functions $u_o(x, 0)$, $v_o(x, 0)$, $u_o(x, t)$, $v_o(x, t)$ may be taken to coincide with the deformations of median lines of the faces.

The equilibrium condition of faces that are subjected to axial forces P_1, P_2, and reaction stresses σ_y and τ occurring at the contacting surfaces of the faces and the core due to presence of the core leads to the following differential equations:

$$\left.\begin{aligned}(EI)_1\frac{d^4v_o(x,0)}{dx^4}+P_1\frac{d^2v_o(x,0)}{dx^2}+\sigma_y(x,0)-\frac{t_1}{2}\frac{d\tau\ (x,0)}{dx}=0\\(EI)_2\frac{d^4v_o(x,t)}{dx^4}+P_2\frac{d^2v_o(x,t)}{dx^2}+\sigma_y(x,t)-\frac{t_2}{2}\frac{d\tau\ (x,t)}{dx}=0\end{aligned}\right\}\tag{6}$$

The notations and the sign convention are shown in Figs. 3 and 4.

Since it is assumed that the faces are thin, the variations of the shear and normal stresses across their thickness are negligible, and the effect of shear stress on the curvature can be neglected.

In the problem of buckling it is known that the deformations $u_o(x, 0)$, $u_o(x, t)$ are higher order quantities than $v_o(x, 0)$, $v_o(x, t)$. In addition, the end support condition requires that $v_o(0, y) = v_o(L, y) = 0$, since the

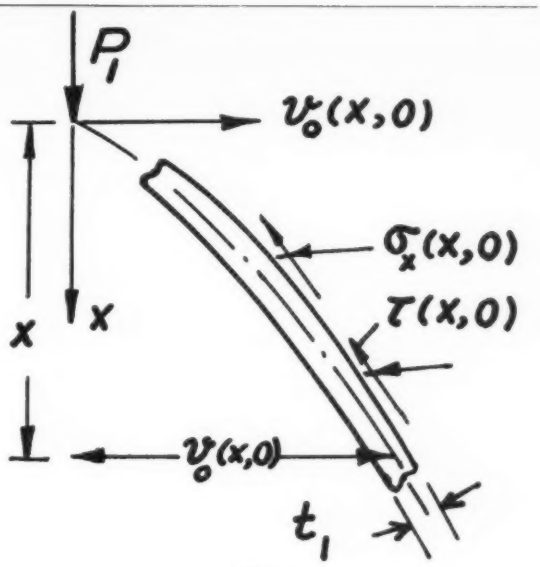

Fig. 4.

friction between ends of the core and the load applying device prohibits any deformation in y direction. Further, $u_{o,\,x}(0, y)$ and $u_{o,\,x}(L, y)$ can also be taken equal to zero, since, as a result of $E_1t_1 \gg E_2t$,

$$\sigma_{xo}(0, y) = \sigma_{xo}(L, y) \cong 0, \quad v(0, y) = v(L, y) = 0$$

and Hooke's Law reducing the boundary condition on stresses in Eqs. (2) to

$$u_{o,\,x}(0, y) = u_{o,\,x}(L, y) = 0$$

Consequently, Eqs. (5) can be used to compute the boundary stresses σ_y and τ needed in Eqs. (6).

Substitution of $\sigma_y(x, 0)$, $\tau(x, 0)$, $\sigma_y(x, t)$, and $\tau(x, t)$ as given by Eqs. (5) into Eqs. (6) leads to

$$\left.\begin{aligned}(EI)_1\frac{d^4v_o(x,0)}{dx^4}+P_1\frac{d^2v_o(x,0)}{dx^2}+\frac{2}{L}\sum_{m=1}^{\infty}\left(\frac{E_y}{1-\mu\nu}\left[V_{o,\,y}(m,0)v_{os}(m,0)+V_{t,\,y}(m,0)v_{os}(m,t)\right]+\right.\\\left.\frac{Gt_1}{L}\left\{\left[U_{o,\,y}(m,0)+\frac{m\pi}{L}\right]v_{os}(m,0)+U_{t,\,y}(m,0)v_{os}(m,t)\right\}\frac{m\pi}{L}\right)\sin\frac{m\pi x}{L}=0\\(EI)_2\frac{d^4v_o(x,t)}{dx^4}+P_2\frac{d^2v_o(x,t)}{dx^2}+\frac{2}{L}\sum_{m=1}^{\infty}\left(\frac{E_y}{1-\mu\nu}\left[V_{o,\,y}(m,t)v_{os}(m,0)+V_{t,\,y}(m,t)\,v_{os}(m,t)\right]+\right.\\\left.\frac{Gt_2}{L}\left\{U_{o,\,y}(m,t)v_{os}(m,0)+\left[U_{t,\,y}(m,t)+\frac{m\pi}{L}\right]v_{os}(m,t)\right\}\frac{m\pi}{L}\right)\sin\frac{m\pi x}{L}=0\end{aligned}\right\}\tag{7}$$

Eqs. (7) are solved for simple-support conditions at $x = 0$ and $x = L$—namely,

$$\left.\begin{aligned}v_o(0,0)=v_o(L,0)=v_{o,\,xx}(0,0)=v_{o,\,xx}(L,0)=0\quad\text{(face 1)}\\v_o(0,t)=v_o(L,t)=V_{o,\,xx}(0,t)=v_{o,\,xx}(L,t)=0\quad\text{(face 2)}\end{aligned}\right\}\tag{8}$$

Eqs. (9) express the fact that the deflection and the bending moments at the supports are zero.

(3) Solution

The definition of finite Fourier sine transform is

$$v_s(m, y) = \int_0^L v(x, y)\sin(m\pi x/L)\,dx \qquad (0 \le x \le L)\tag{9}$$

Application of the finite Fourier sine transform to Eqs. (7) and the use of Eqs. (8) lead to two homogeneous linear equations in $v_{os}(m, 0)$ and $v_{os}(m, t)$.

$$\left.\begin{aligned} W_{11}(m)v_{os}(m, o) + W_{12}(m)v_{os}(m, t) &= 0 \\ W_{21}(m)v_{os}(m, o) + W_{22}(m)v_{os}(m, t) &= 0 \end{aligned}\right\} \tag{10}$$

where

$$\left.\begin{aligned} W_{11}(m) &= E_1I_1(m\pi/L)^4 - P_1(m\pi/L)^2 + (Gt_1/2)\,(m\pi/L)\,[U_{o,\,y}(m, 0) + (m\pi/L)] + \\ &\qquad [E_y/(1 - \mu\nu)]v_{o,\,y}(m, 0) \\ W_{12}(m) &= (Gt_1/2)\,(m\pi/L)\,U_{t,\,y}(m, 0) + [E_y/(1 - \mu\nu)]V_{t,\,y}(m, 0) \\ W_{21}(m) &= (Gt_2/2)\,(m\pi/L)U_{o,\,y}(m, t) + [E_y/(1 - \mu\nu)]\,V_{o,\,y}(m, t) \\ W_{22}(m) &= E_2I_2(m\pi/L)^4 - P_2(m\pi/L)^2 + (Gt_2/2)\,(m\pi/L)\,[U_{t,\,y}(m, t) + \\ &\qquad (m\pi/L)] + [E_y/(1 - \mu\nu)]V_{t,\,y}(m, t) \end{aligned}\right\} \tag{11}$$

To find the nonzero solution of these equations, the determinant of the coefficients is set equal to zero. Hence,

$$P_1P_2 - B_2P_1 - B_1P_2 - C = 0 \tag{12}$$

Here B_1, B_2, and C are expressions that are functions of physical and geometrical quantities related to the faces and the core.

In the case where P_1 and P_2 are both compressive loads, σ_{cr} is the critical value of stress σ defined by

$$P_1 = \sigma t_1, \qquad P_2 = \sigma t_2 \tag{13}$$

When the faces have equal thickness and are made of the same material, $E_1I_1 = E_2I_2$. Thus, Eq. (12) can be simplified to

$$\sigma_{cr} = (1/2)E_f(m\pi t_f/L)^2 + (1/2)Gu_1(m, 0) \pm \left\{[E_y/(1 - \mu\nu)]^2\,(L/m\pi t_f)^2\,[v_1^2(m, 0) - v_2^2(m, 0)] + (G/2)^2u_2^2(m, 0)\right\}^{1/2} \tag{14}$$

provided $E_x/2G > \mu + (\mu/\nu)^{1/2}$, where

$$\left.\begin{aligned} u_1(m, 0) &= 1 + c + dv_2(m, 0)\left[\frac{1}{2}\left(j - \frac{1}{j}\right)\sinh z_1t \sinh z_2t\right](\sinh z_1t - j \sinh z_2t)^{-1} \\ u_2(m, 0) &= dv_2(m, 0)\,(\cosh z_1t - \cosh z_2t)(\sinh z_1t - j \sinh z_2t)^{-1} \\ v_1(m, 0) &= v_2(m, 0)\,(\sinh z_1t \cosh z_2t - j \sinh z_2t \cosh z_1t)(\sinh z_1t - j \sinh z_2t)^{-1} \\ v_2(m, 0) &= e(\sinh z_1t - j \sinh z_2t)\left[1 - \cosh z_1t \cosh z_2t + \frac{1}{2}\left(j + \frac{1}{j}\right)\sinh z_1t \sinh z_2t\right]^{-1} \\ c &= (1/2)\,(1 + A)\lambda^2[(z_1^2 - \lambda^2)^{-1} + (z_2^2 - \lambda^2)^{-1}], \quad \left.\begin{matrix} z_1 \\ z_2 \end{matrix}\right\} = \omega\left\{1 \pm [1 - (\Omega/\omega)^4]^{1/2}\right\}^{1/2} \\ d &= (1 + A)\,(m\pi/L)z_1(z_1^2 - \lambda^2)^{-1}, \quad \omega^2 = [(E_x/2G) - \mu](m\pi/L)^2 \\ e &= (1/2)\,(z_1^2 - z_2^2)\,(z_1^2 - \lambda^2)\,[(1 + A)^2\,(m\pi/L)\lambda^2z_1]^{-1}, \quad \Omega^4 = (\mu/\nu)(m\pi/L)^4 \\ j &= (z_1/z_2)\,(z_2^2 - \lambda^2)\,(z_1^2 - \lambda^2)^{-1}, \quad \lambda^2 = (\mu/A)(m\pi/L)^2 \end{aligned}\right\} \tag{15}$$

A similar procedure can be used to obtain σ_{cr} for the case of orthotropy represented by $E_x/2G < \mu + (\mu/\nu)^{1/2}$. In this case, however, new expressions are needed for σ_y and τ to be used in Eqs. (6), since stresses and strains in the core calculated on the basis of this inequality are different from those given by Eqs. (5). Here, only the resulting σ_{cr} is given [see Navy report, footnote, page 1, reference (13)].

$$\sigma_{cr} = (1/12)\,E_f(m\pi t_f/L)^2 + (1/2)Gu_1'(m, o) \pm \left\{[E_x/(1 - \mu\nu)]^2\,(L/m\pi t_f)^2\,[v_1'^2(m, o) - v_2'^2(m, o)] + (G/2)^2\,u_2'^2(m, o)\right\}^{1/2} \tag{16}$$

provided $E_x/2G < \mu + (\mu/\nu)^{1/2}$, where

$$
\left.\begin{aligned}
u_1'(m,0) &= 1 + c' + d'v_2'(m,0)\,(\sinh^2 z_1't + \sin^2 z_2't)\,(\sinh z_1't\cos z_2't + j'\cosh z_1't\sin z_2't)^{-1}\\
u_2'(m,0) &= h'v_2'(m,0)\,(\sinh z_1't\sin z_2't)\,(\sinh z_1't\cos z_2't + j'\cosh z_1't\sin z_2't)^{-1}\\
v_1'(m,0) &= (1/2)\,v_2'(m,0)\,(\sinh^2 z_1't - j'\sin^2 z_2't)\,(\sinh z'_1t\cos z_2't + j'\cosh z_1't\sin z_2't)^{-1}\\
v_2'(m,0) &= e'(\sinh z_1't\cos z_2't + j'\cosh z_1't\sin z_2't)\,(\sinh^2 z_1't - j'^2\sin^2 z_2't)\\
c' &= (1+A)\,\lambda^2(\omega^2-\lambda^2)\,(\Omega^4 - 2\omega^2\lambda^2 + \lambda^4)^{-1}\\
d' &= -(1+A)\,(m\pi/L)\,z_1'\,(\Omega^2-\lambda^2)\,(\Omega^4 - 2\omega^2\lambda^2 + \lambda^4)^{-1}\\
e' &= 2z_1'(\Omega^4 - 2\lambda^2\omega^2 + \lambda^4)\,[(1+A)^2\lambda^2(m\pi/L)\,(\Omega^2+\lambda^2)]^{-1}\\
h' &= (1+A)\,(m\pi/L)\Omega^2\,[z_2'(\Omega^2+\lambda^2)]^{-1}\\
j' &= (z_1'/z_2')\,(\Omega^2-\lambda^2)\,(\Omega^2+\lambda^2)^{-1}\\
z_1' &= [(1/2)(\Omega^2+\omega^2)]^{1/2}, \qquad z_2' = [(1/2)\,(\Omega^2-\omega^2)]^{1/2}
\end{aligned}\right\} \tag{17}
$$

(4) Buckling of a Sandwich Beam Subjected to Pure Bending

A sandwich beam subjected to bending moments M at both ends can be looked upon as a beam having one face submitted to compression load $P_1 = M/(t + t_f)$, while the other is submitted to tension load $P_2 = -P_1$.

By use of the relations $E_1I_1 = E_2I_2$ and $t_1 = t_2$ and of Eq. (12), σ_{cr} is found to be

$$
\sigma_{cr} = -[E_y/(1-\mu\nu)]\,(L/m\pi t_f)v_1(m,0) \pm \left\{[E_y/(1-\mu\nu)]^2(L/m\pi t_f)^2v_2^2(m,0) + (G/2)^2[u_1^2(m,0) - u_2^2(m,0)] + [(1/12)\,E_f(m\pi t/L)^2]^2 + (1/12)\,E_fG\left(\frac{m\pi t_f}{L^2}\right)u_1(m,0)\right\}^{1/2} \tag{18}
$$

(5) The Deflected Shape for Buckling Under Axial Compression

In the following analysis it will be proved that the ripple-type of buckling occurs according to an asymmetric pattern:*

(a) *Possibility of Symmetric Buckling*

When the buckled shapes of the faces are symmetric with respect to the median line of the sandwich parallel to the x axis, the buckling is called symmetric. Therefore, for symmetric buckling,

$$
v_o(x,0) \equiv -v_o(x,t) \tag{19}
$$

Substitution of Eq. (19) into Eqs. (10) gives

$$
W_{11}(m) = W_{12}(m), \qquad W_{21}(m) = W_{22}(m) \tag{20}
$$

Combining Eqs. (10) and (20), it is found that for symmetric buckling to occur the following equation must be satisfied:

$$
e\left\{\frac{\sinh z_1t\,(\cosh z_2t + 1) - j\sinh z_2t\,(\cosh z_2t + 1)}{1 - \cosh z_1t\cosh z_2t + (1/2)\,[j + (1/j)]\sinh z_1t\sinh z_2t} = 0\right\} \tag{21}
$$

It can be seen that e cannot be zero, since $z_1 \neq z_2$ and $\lambda^2 = z_1^2$ is in contradiction with the inequality $E_x/2G > \mu + (\mu/\nu)^{1/2}$ on the basis of which the solution was derived. Then Eq. (21) reduces to

$$
(z_1^2 - \lambda^2)\sinh z_1t/z_1\,(\cosh z_1t + 1) = (z_2^2 - \lambda^2)\sinh z_2t/z_2\,(\cosh z_2t + 1) \tag{22}
$$

since $j \neq 0$, z_1 and z_2 are finite. Let

$$
F(z) = (z^2 - \lambda^2)\sinh z\,t/z\,(\cosh zt + 1) \tag{23}
$$

It can be seen that $F(z)$ is a monotonically increasing function. Suppose the contrary is true, then $dF/dz = 0$ at some points. Hence, $\sinh zt/zt = (\lambda^2/z^2 - 1)/(\lambda^2/z^2 + 1)$. This, however, is impossible since $|\sinh zt| > |zt|$ and $(\lambda^2/z^2 - 1)/(\lambda^2/z^2 + 1) < 1$. Furthermore, $zt > 0$. Therefore, as was to be proved, $dF/dz > 0$. Hence, $F(z_1) > F(z_2)$ or Eq. (22) cannot hold.

Hence, it may be concluded that *symmetric buckling is not possible.*

* Proof is given here for orthotropic cores satisfying $E_x/2G > \mu + (\mu/\nu)^{1/2}$. A similar method may be used for cores satisfying $E_x/2G \leq \mu + (\mu/\nu)^{1/2}$.

(b) *Possibility of Antisymmetric Buckling*

An antisymmetrically buckled shape is obtained when

$$v_o(x, 0) \equiv v_o(x, t) \tag{24}$$

Following the same procedure as that used in the previous discussion, it is found that

$$\frac{\sinh z_1 t(\cosh z_2 t - 1) - j \sinh z_2 t\ (\cosh z_2 t - 1)}{1 - \cosh z_1 t \cosh z_2 t + (1/2)\ [j + (1/j)] \sinh z_1 t \sinh z_2 t} = 0 \tag{25}$$

This equation is satisfied only for $t = 0$. Otherwise, with $t \neq 0$, it can be seen that the following must be true:

$$F(z_1) = F(z_2) \tag{26}$$

where

$$F(z) = (z^2 - \lambda^2) \sinh zt/z\ (\cosh zt - 1) \tag{27}$$

$F(z)$ is a continuous monotonic function in $0 < z < \infty$. If $F(z)$ is not monotonic, then $dF/dz = 0$ at some points in the interval. This leads to

$$\sinh zt/zt = (1 - \lambda^2/z^2)/(1 + \lambda^2/z^2) \tag{28}$$

Eq. (28) cannot be satisfied except for $t = 0$, for which Eq. (25) must be examined. A limiting process indicates that Eq. (24) is satisfied for $t = 0$. This, however, is obvious since, in this case, the sandwich beam becomes a beam consisting of two faces without core which fails by Euler buckling. Hence, it may be concluded that *antisymmetric buckling is not possible* for a sandwich beam. Therefore, the *buckled shape pattern must be an asymmetric one.*

(6) Numerical Calculations and Discussion

Numerical examples are presented in order to study the effects of variations in the elastic constants of the core: E_x, E_y, G, ν, μ, Young's modulus of the faces, the core thickness, and the face thickness.

The results of these calculations are compared with previous theoretical and experimental results.

The assumed core and face materials and their properties are given in Figs. 5 to 13. A comparison between the present theory and that of reference 1 is shown in Fig. 14.

Some hypothetical materials are chosen with assumed elastic properties as given in Figs. 5 to 13. It is believed that materials similar to these may be produced by using certain synthetic resins in combination with

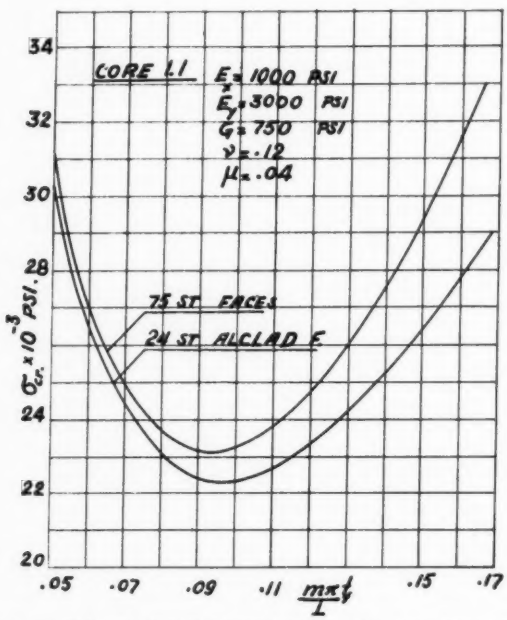

FIG. 5. Buckling of sandwich made of core No. 1.1 and aluminum alloy faces. $E_x/2G > \mu + (\mu/\nu)^{1/2}$.

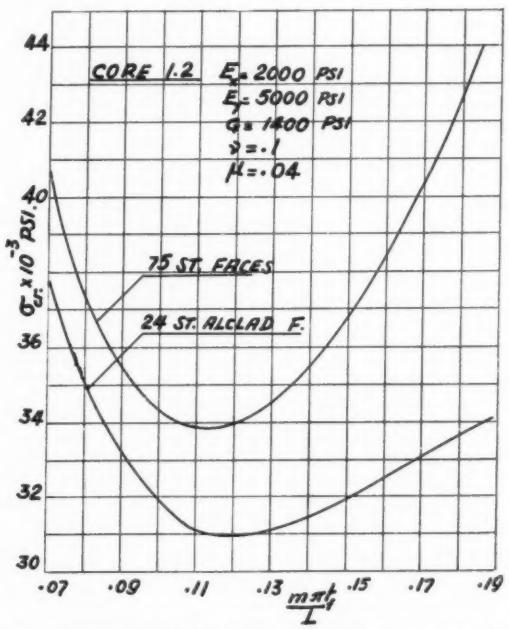

FIG. 6. Buckling of sandwich made of core No. 1.2 and aluminum-alloy faces. $E_x/2G > \mu + (\mu/\nu)^{1/2}$.

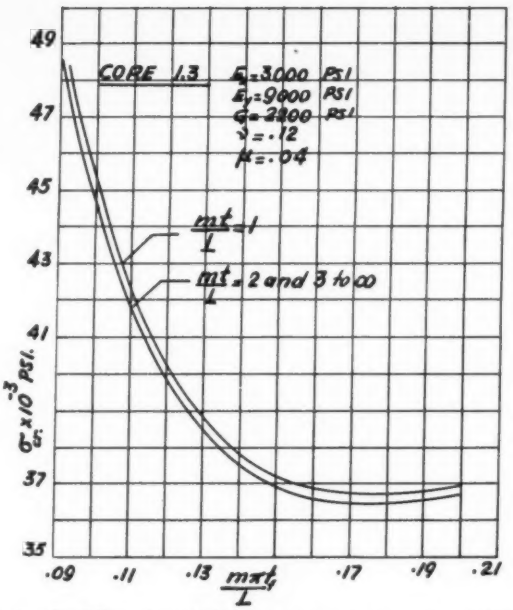

FIG. 7. Buckling of sandwich made of core No. 1.3 and 24ST Alclad faces. $E_x/2G > \mu + (\mu/\nu)^{1/2}$.

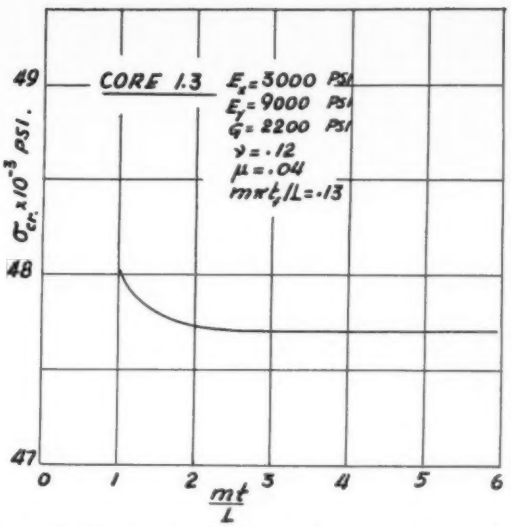

FIG. 9. Buckling of sandwich made of core No. 1.3 and 75ST faces. $E_x/2G > \mu + (\mu/\nu)^{1/2}$.

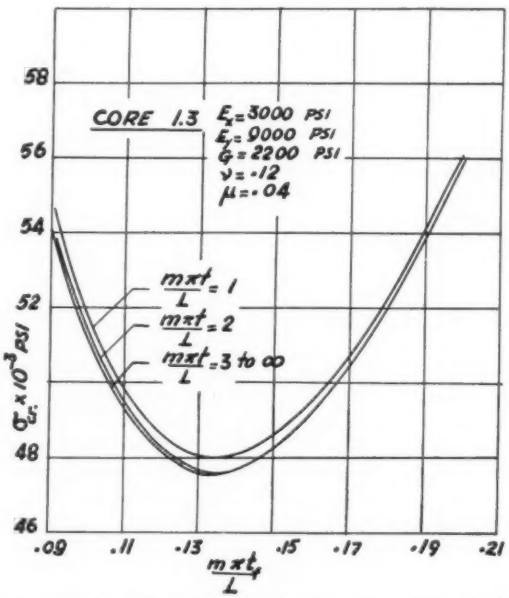

FIG. 8. Buckling of sandwich made of core No. 1.3 and 75ST faces. $E_x/2G > \mu + (\mu/\nu)^{1/2}$.

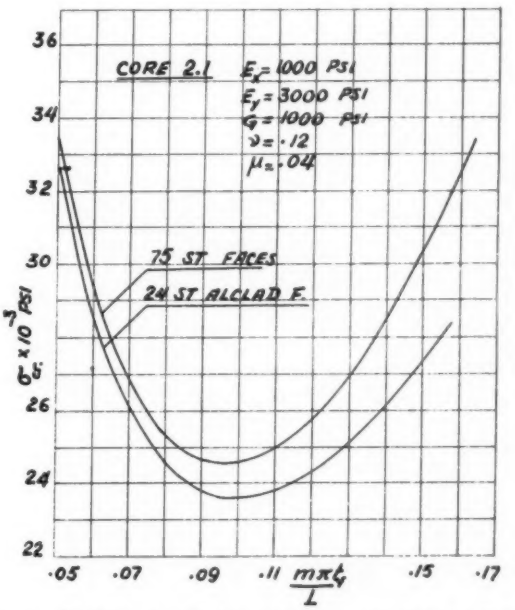

FIG. 10. Buckling of sandwich made of core No. 2.1 and aluminum-alloy faces. $E_x/2G < \mu + (\mu/\nu)^{1/2}$.

nylon fibers arranged in different patterns [see reference 14 and Fig. 2 (a and b)]. These materials may be classified into two groups according to the present theory as:

(a) Elastic materials with elastic properties satisfying the inequality

$$E_x/2G > \mu + (\mu/\nu)^{1/2}$$

(b) Elastic materials satisfying the inequality

$$E_x/2G < \mu + (\mu/\nu)^{1/2}$$

Both cases are studied here. The general conclusion is that the effect of variations in E_y is found to be the most important (see Figs. 5 and 13).

Young's modulus of the faces is also an important factor, but, as can easily be seen, it appears only in the first term of the formula for σ_{cr} which represents Euler buckling of each face [see, for instance, Eq. (14)]. Hence, it becomes more important as the wave length decreases.

The effect of variations in the core thickness is found to be small (see Fig. 9).

The parameter $(m\pi t_f/L)$ is found to be an important factor. Plots of σ_{cr} vs. $(m\pi t_f/L)$ always show a minimum (see Figs. 5 to 8 and 10 to 13).

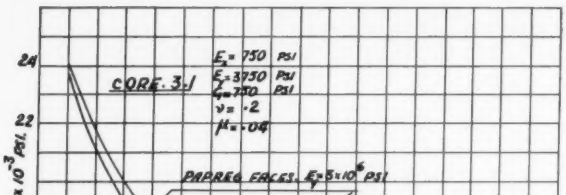

FIG. 11. Buckling of sandwich made of core No. 3.1 and Papreg faces. Use for $\sigma_{cr} \leqq 20{,}000$ lbs. per sq.in. $E_z/2G > \mu + (\mu/\nu)^{1/2}$.

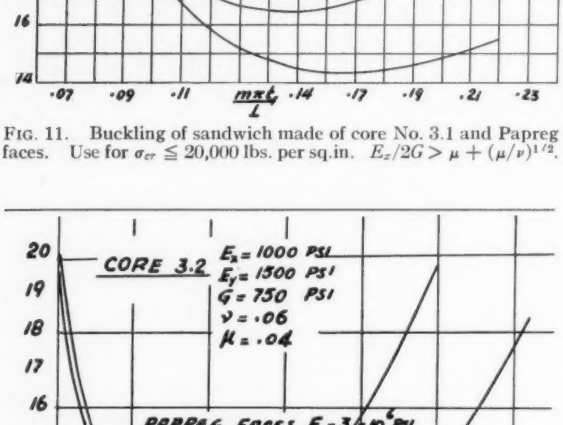

FIG. 12. Buckling of sandwich made of core No. 3.2 and Papreg faces. $E_z/2G \geqq \mu + (\mu/\nu)^{1/2}$.

A comparison between the present theory and test results published in reference 1 is shown in Fig. 14. Good agreement is indicated between the present theory and the tests. The discrepancy does not exceed 6 per cent. The deviation between the two theories is, in general, within 30 per cent of the values given by the present theory for the materials investigated. The present theory always gives lower buckling stress.

The theory of reference 2 agrees well with the experiment for bending of cantilever beams, while a larger discrepancy is noticed in case of buckling.

The method of reference 3 assumes either symmetric or antisymmetric buckling, both of which are proved impossible in the strict sense. However, in experiments it is often difficult to detect the differences in buckled shapes of faces.

Reference 4 considers the Euler type buckling under initial stresses.

The method of reference 5 may be used for sandwich plates and beams when the normal stresses across the thickness of plate are not important. While the assumptions made lead to satisfactory results in the study of overall bending and buckling, they preclude consideration of the wrinkling phenomenon.

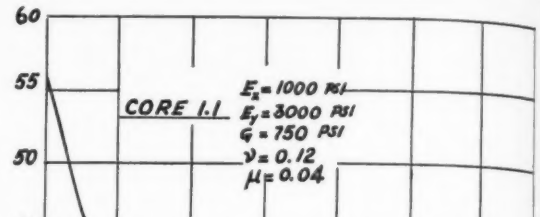

FIG. 13. Comparison of σ_{cr} for pure bending and compression. Core No. 1.1 and 75ST faces. $E_z/2G > \mu + (\mu/\nu)^{1/2}$.

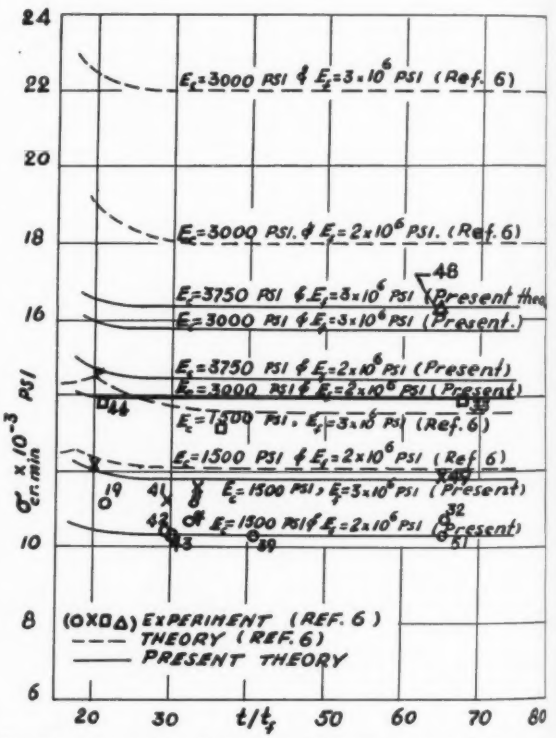
E_c=3000 PSI & E_f=3x10⁶ PSI (Ref. 6)
E_c=3000 PSI. & E_f=2x10⁶ PSI. (Ref. 6)
E_c=3750 PSI & E_f=3x10⁶ PSI (Present theo
E_c=3000 PSI & E_f=3x10⁶ PSI (Present.)
E_c=3750 PSI & E_f=2x10⁶ PSI (Present)
E_c=3000 PSI & E_f=2x10⁶ PSI (Present)
E_c=1500 PSI, E_f=3x10⁶ PSI (Ref. 6)
E_c=1500 PSI & E_f=2x10⁶ PSI (Ref. 6)
E_c=1500 PSI & E_f=3x10⁶ PSI (Present)
E_c=1500 PSI & E_f=2x10⁶ PSI (Present)
(O×□△) EXPERIMENT (REF. 6)
THEORY (REF. 6)
PRESENT THEORY
$\sigma_{cr.min} \times 10^{-3}$ PSI
t/t_f

FIG. 14. Comparison of experimental results, theory of reference 6, and the present theory.

In Fig. 5 of reference 7 a comparison is shown between test and theory which takes the initial waviness into account. However, it is noticed that all experimental points are condensed around the yield stress of the aluminum alloy 75ST faces of the specimens. Therefore, material failure rather than instability may have occurred. However, initial waviness may be important for extremely thin sandwiches having strong cores for which Euler type of buckling occurs.

More recent papers are concerned primarily with the Euler type of buckling of plates[8–10] for which only consideration of average stresses across the core seems to be sufficient to express the overall buckling phenomenon reasonably well for engineering approximation. This, of course, eliminates the type of lengthy analysis given in reference 13. However, ripple-type of wrinkling is excluded because of this oversimplification. Therefore, a correct buckling stress for plates having rather soft thick cores cannot be given. While an analysis similar to that used in reference 13 would be tedious, if not impossible, the method of reference 12 avoids this difficulty with reasonable engineering accuracy.

Finally, it may be of interest to mention that the method of the present paper may be applied to investigate ripple-type buckling of sandwich cylinders.[11]

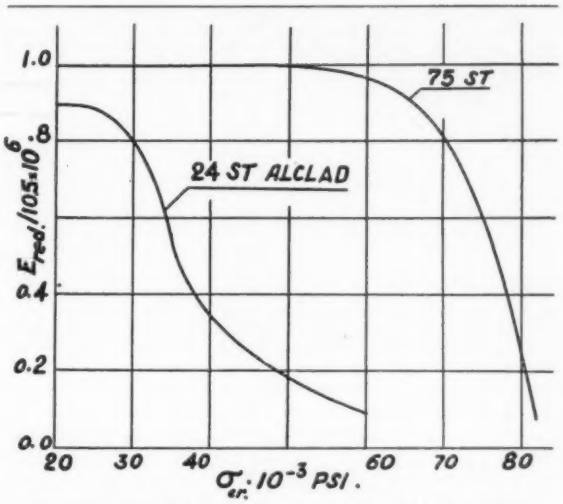

FIG. 15. Reduced modulus of 24ST Alclad and 75ST.

REFERENCES

[1] Hoff, N. J., and Mautner, S. E., *The Buckling of Sandwich-Type Panels*, Journal of the Aeronautical Sciences, Vol. 12, No. 3, July, 1945.

[2] Hoff, N. J., and Mautner, S. E., *Bending and Buckling of Sandwich Beams*, Journal of the Aeronautical Sciences, Vol. 15, No. 12, December, 1948.

[3] Williams, D., Legget, D. M. A., and Hopkins, H. G., *Flat Sandwich Panels Under Compressive End Loads*, Ministry of Aircraft Production, Aeronautical Research Committee Reports and Memoranda, No. 1987, June, 1941.

[4] Goodier, J. N., *Cylindrical Buckling of Sandwich Plates*, Journal of Applied Mechanics, Vol. 13, No. 4, p. A-253, December, 1946.

[5] Reissner, E., *On Bending of Elastic Plates*, Quarterly of Applied Mathematics, Vol. V, No. 1, April, 1947.

[6] van der Neut, *Die Stabilitat Geschichtster Platten*, Pep. No 286. National Luchtvaartlaboratorium, Holland, September, 1943.

[7] Wan, Conrad C., *Face Buckling and Core Strength Requirements in Sandwich Construction*, Journal of the Aeronautical Sciences, Vol. 14, No. 9, September, 1947.

[8] Reissner, E., *Finite Deflections of Sandwich Plates*, Journal of the Aeronautical Sciences, Vol. 15, No. 7, July, 1948.

[9] Libove, Charles, and Batdorf, S. B., *A General Small-Deflection Theory for Flat Sandwich Plates*, N.A.C.A. Report No. 899, 1948.

[10] Stein, M., and Mayers, J., *A Small-Deflection Theory for Curved Sandwich Plates*, N.A.C.A. T.N. No. 2017, February, 1950.

[11] Eringen, A. Cemal, *Buckling of a Sandwich Cylinder under Uniform Axial Compressive Load*, Journal of Applied Mechanics, Vol. 18, No. 2, June, 1951.

[12] Eringen, A. Cemal, *Bending and Buckling of Rectangular Sandwich Plates*, scheduled for publication in the Proceeding of First National Congress on Applied Mechanics.

[13] Eringen, A. Cemal, *Solution of the Two-Dimensional Mixed-Mixed Boundary Value Problem of Elasticity for Rectangular, Orthotropic Media and Application to the Buckling of Sandwich Beams*, Thesis for Ph.D. in Applied Mechanics, Polytechnic Institute of Brooklyn, June, 1948.

[14] Hoff, N. J., *Structural Material, Particularly for Aircraft*, Patent Application Serial No. 734,969, March 15, 1947.

[15] Templin, R. L., Hartmann, E. C., and Paul, D. A., *Typical Tensile and Compressive Stress-Strain Curves for Aluminum Alloy 24 S-T, Alclad 24 S-T, 24 S-RT, and Alclad 24 S-RT Products*, Aluminum Research Laboratories Tech. Paper No. 6, p. 15, Aluminum Company of America, Pittsburgh, 1942.

[16] ANC-5, *Strength of Aircraft Elements*, revised Ed., December, 1942.

[17] Holt, Marshall, and Leary, J. R., *The Column Strength of Aluminum Alloy 75 S-T Extruded Shapes*, N.A.C.A. T.N. No. 1004, January, 1946.

A High-Speed Schlieren Technique for Investigation of Aerodynamic Transients*

WALTER S. BRADFIELD† AND WALTER Y. FISH‡

University of Minnesota

SUMMARY

Development of a simple high-speed schlieren technique for investigation of aerodynamic transients is described, and sample photographs are shown. A spark light source was developed which was capable of delivering bursts of up to 250 photographs at a frequency as high as 16,000 photographs per sec. A simple inexpensive camera for recording the data photographically was devised and constructed in the laboratory. The photographic units were adapted to the schlieren equipment that was on hand, and data were recorded at a Mach Number of 3.5 in an intermittent wind tunnel.

INTRODUCTION

THE ROLE OF TRANSIENT PHENOMENA in supersonic flow has grown in importance during the past few years. The advent of the aerothermodynamic jet engine, flight at supersonic speeds, and the widespread application of the supersonic wind tunnel to research problems have stimulated the modification and further development of basic optical techniques to this end. The technique described herein was developed in connection with a study of wind-tunnel starting transients, which is sponsored by the Air Materiel Command under contract AF 33 (038) 7078.[3]

Specifically, it was desired to study nonstationary shock-wave propagation and reflection and the effect of these transients on the initiation of flow in a "choking" supersonic diffuser. The whole starting process was expected to take place in less than 0.020 sec. It was considered necessary to obtain at least 30 to 50 schlieren photographs during this interval in order to adequately define the flow. With the instrumentation completed, 150 photographs were easily obtained during the specified period (corresponding to 7,500 frames per sec.), and frequencies as high as 15,000 frames per sec. were recorded. The exposure time is roughly 2 microsec

SPARK LIGHT SOURCE

The light source developed to photograph the phenomena discussed above grew out of the basic single spark unit using the Libessart gap as the actual spark head.[1,2] An undesirable feature of these single-shot units proved to be the link that led to the present design—i.e., when the supply potential was raised beyond a critical point, the gap broke down and fired sporadically without a trigger.

The design requirements as indicated by the above discussion can be summarized as follows:

(1) A spark repetition rate upward of 7,500 per sec.

(2) Sufficient intensity for use with schlieren apparatus.

(3) Duration of approximately 20 millisec. per burst.

(4) Individual spark duration short enough to assure sharp exposure of rapidly moving phenomena.

(5) Ability to control beginning and end of spark train or burst.

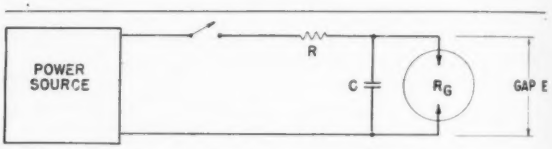

FIG. 1. Simplified circuit diagram.

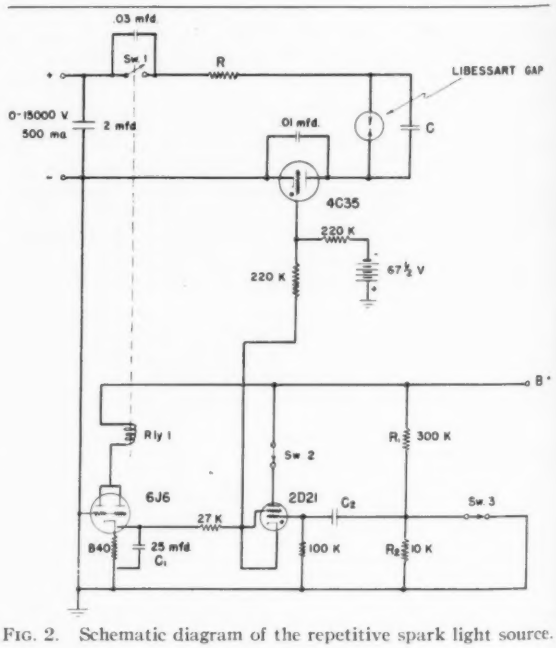

FIG. 2. Schematic diagram of the repetitive spark light source.

Received July 30, 1951.

* The authors acknowledge with thanks the advice and suggestions of Prof. A. R. Kantrowitz, of Cornell University, relative to the development of this technique. Various members of the technical staff of the University of Minnesota Aeronautical Laboratory have made significant contributions.

† Lecturer.

‡ Scientist. Now, Electronics Engineer, Electronics and Guidance Section, Engineering Department, Consolidated Vultee Aircraft Corporation.

These requirements were met using the system to be described; a simplified diagram (Fig. 1) is included for purposes of discussion.

Basically, the repetitive spark light source consists of a power supply of high storage capacity, a switch, resistor-condenser components of the charge-discharge circuit, and a close-spaced gap where the electrical discharge energy is converted into light. With the input voltage adjusted at some point higher than the critical (breakdown) gap voltage, the switch is closed and C charges up toward the source voltage; more, however, when the critical voltage is reached, the gap becomes ionized (breaks down) and the condenser is rapidly discharged through the gap until the voltage (E) can no longer sustain an arc and ionization ceases. The condenser then recharges at a rate determined by R-C and the sequence is repeated. The arc, or spark duration is determined by the value of C and the resistance of the ionized gap. Thus, the repetition rate is established by the R-C constants and input voltage level, while the duration depends on C and R_C.

The actual circuit used is shown schematically in Fig. 2. The power source supplies 0 to 15,000 volts at 500 milliamp., and its storage facilities are augmented by the 2 mfd. condenser at the spark input. The additional vacuum tubes and components are necessary to control the starting time and duration of the burst. To describe a typical operating sequence (with SW-3 closed and the thyratron, 2D21, cut off), the hydrogen thyratron switch tube 4C35 is held nonconducting by the negative battery bias. The 6J6 relay tube is conducting and the relay, Rly 1, is closed. Consequently, the supply voltage would be applied to C and the gap, except for the 4C35 switch. At the moment that it is desired to start the spark pulses, SW-3 is opened and the network R_1 and R_2 becomes a voltage divider that applies a sudden positive bias to the grid of the 2D21, through C-2, as a pulse. Firing of the 2D21 trigger tube causes the 4C35 to ionize, thus allowing full application of the source voltage to the gap and condenser C through charging resistor R. This action initiates the repetitive sparks, which continue until the 6J6 (relay tube) is cut off by action of the positive cathode voltage and at a time later determined by C_1, the 840-ohm cathode resistor, and normal relay inertia. When the relay opens, the high-voltage circuit is broken and the sparks cease. The condenser is shunted across SW-1, and the 4C35 absorbs the transient and prevents arcing in the circuit.

It has been determined experimentally that the spark duration is in the neighborhood of 2 microsec.; this is sufficiently short to ensure good exposures.

In early experiments with the apparatus, it was found difficult to obtain bursts of a high repetition rate for any appreciable length of time (with respect to the desired 20 millisec.) without the gap becoming completely ionized. This difficulty was overcome by piping in air, under pressure, to the enclosed gap area or

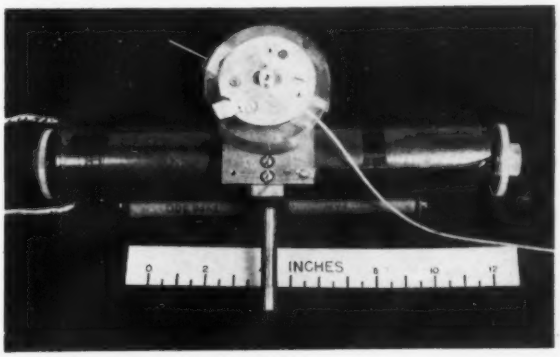

FIG. 3.

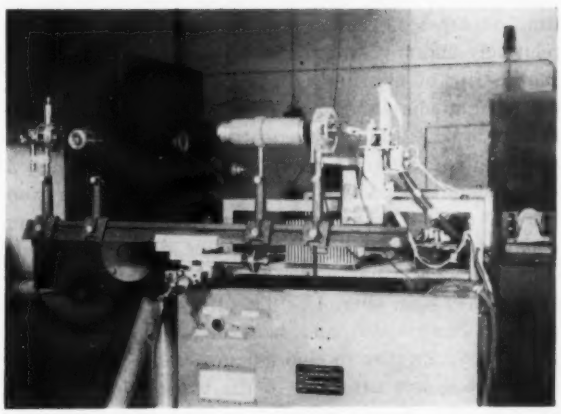

FIG. 4.

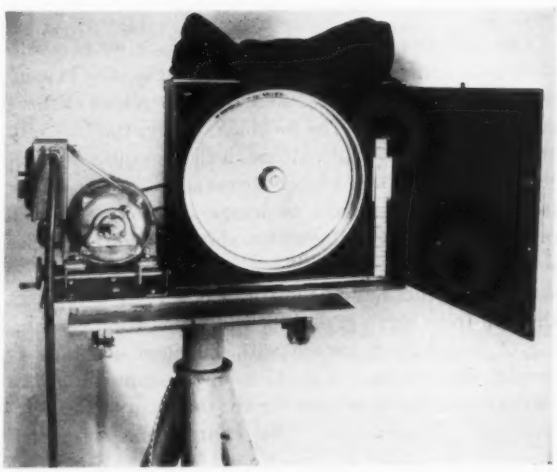

FIG. 5.

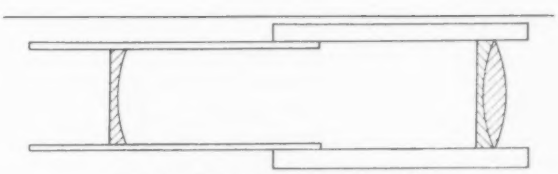

FIG. 6. Drum camera lens assembly.

Fig. 3. It is assumed that the air pressure drives the ionized particles from the enclosure, thus allowing the gap to deionize and extinguish between sparks.

The mechanical construction of the spark head and associated components is such as to facilitate assembly of all high-voltage parts with minimum lead lengths and also to allow its installation on the optical apparatus (Fig. 4).

Camera

It was necessary to devise a camera that would permit recording photographs at the frequencies anticipated and which would be adaptable to the schlieren optical system planned for use with the operation. Since the time duration of the process under investigation was relatively short, it was found possible to utilize fairly short strips of film for recording purposes. This suggested immediately the possibility of using a simple drum camera. The camera constructed consists of an aluminum drum 20 in. in diameter which is rotated at a constant speed by an electric motor. A drive from the motor to the camera is effected by a pulley system in which driving pulleys of variable diameter permit continuous variation of the drum speed between 2,000 and 4,000 r.p.m. (Fig. 4). The drum is enclosed by a plywood box (Fig. 5), and, in order to facilitate loading the film during the daylight hours, a light, tight, felt loading bag was attached to the top of the box. In loading, the film is fastened to the outer perimeter of the drum by means of double-sided Scotch tape. Standard 35-mm. film is cut to length for this purpose.

The objective lens assembly was made up of available optical components as shown in Fig. 6. It consists of one achromat element and one meniscus element arranged as shown. The focal length and the image to object ratio are variable, although the assembly was designed with a 25-ft. object distance in mind. Since the lens system projects an image as small as 4 by 6 mm., the camera will accommodate spark frequencies to 16,000 per sec.

A simple mechanical shutter has served to protect the film from fogging, and for this application the timing of the cycle is known with sufficient accuracy to permit the manual operation of the shutter. The shutter remains wide open for the duration of the aerodynamic phenomenon. The shutter has been left open for periods as long as 3 min. (with the drum running) without objectionable fogging of the film.

Schlieren Optical System

A standard double-pass schlieren optical system was adapted for use with the spark light source and drum camera. A diagram of the optical setup is shown in Fig. 7. The spark light source is of approximately 0.060 in. in diameter, and it emits light as a conical beam due to the shape of its negative electrode. The beam is picked up by the condensing lens, which produces an image of the light source on the aperture of the schlieren optical head. A right-angle prism then directs the beam of light through the tunnel test-section window behind which is situated a spherical mirror whose conjugate focus is located at the knife edge of the schlieren system. Through another set of prisms in the objective head, light is passed into the objective lens system of the drum camera.

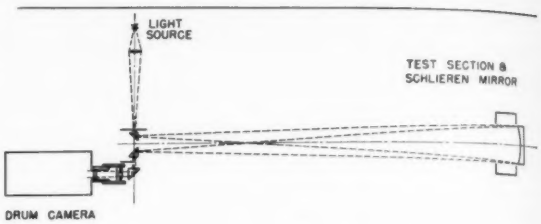

Fig. 7. Schlieren optical diagram

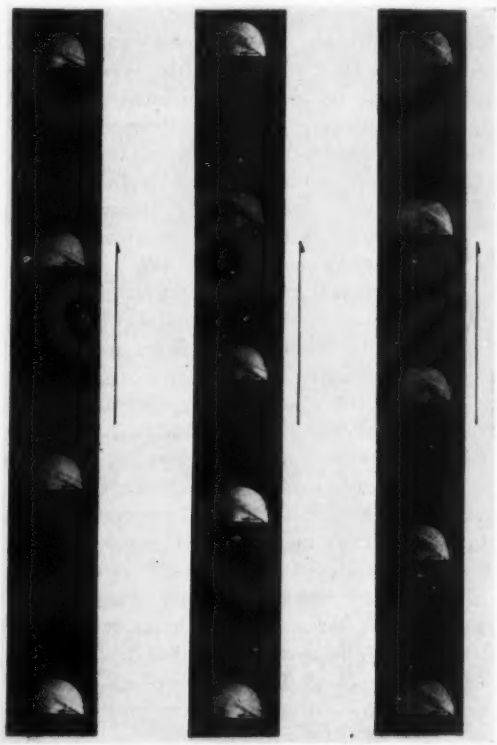

Fig. 8. Drum camera schlieren series showing flow and P-shock passing over 10.88° subcritical diffuser; 7,000 frames per sec.

Application and Results

A schlieren system of this particular type is extremely useful in its application to nonstationary supersonic

(*Continued on page 432*)

Readers' Forum

BRIEF REPORTS of investigations in the aeronautical sciences and discussions of papers published in the JOURNAL are presented in this special department. Publication will be completed as quickly as possible after receipt of the material. The Editorial Committee does not hold itself responsible for the opinions expressed by the correspondents. Contributions should not exceed 800 words in length.

On the General Solution for Unsteady Motion of a Rectangular Wing in Supersonic Flow

John W. Miles*
Fulbright Lecturer, Auckland University College, Auckland, New Zealand
February 28, 1952

WE CONSIDER A WING TIP projecting on the quadrant $z = 0$, $x \geq 0$, $y \geq 0$ in a supersonic flow of Mach Number M directed along the x axis. If the prescribed, normal velocity of the wing is $w(x, y, t)$, *positive down*, a general solution for the velocity potential on the upper surface of the wing is

$$\varphi(x, y, t) = \frac{1}{\pi}\int_0^x d\xi \int_{|\beta^{-1}(x-\xi)-y}^{\beta^{-1}(x-\xi)+y} \frac{w[\xi, \eta, t - (M/\beta^2 a)(x-\xi)]\, d\eta}{[(x-\xi)^2 - \beta^2(y-\eta)^2]^{1/2}} + \frac{1}{\pi^2}\int_0^{\pi} d\psi \int_0^{\pi/2} d\theta \int_0^x d\xi \int_{|\beta^{-1}(x-\xi)\cos\theta - y|}^{\beta^{-1}(x-\xi)\cos\theta + y} \times \frac{w_\theta[\xi, \eta, t - (M + \sin\theta\cos\psi)(x-\xi)/\beta^2 a]\, d\eta}{[(x-\xi)^2\cos^2\theta - \beta^2(y-\eta)^2]^{1/2}} \quad (1)$$

where a is the sonic velocity and

$$\beta = (M^2 - 1)^{1/2} \quad (2)$$

This solution was obtained by carrying out a Fourier transformation with respect to t and a Laplace transformation with respect to x and comparing the result with the Laplace transform of the corresponding problem in steady flow, for which a general solution is available (either by Evvard's method[1] or by the Wiener-Hopf approach[2]). This general procedure, at least for harmonic time dependence, is due to Magnaradze,[3] but the general form of the final result was suggested to us by Stewartson's solution[4] for w of the form $f(x)e^{i\omega t}$.

An alternative approach to the general problem is to expand w in a series of terms like $y^n w_n(x, t)$, for which the corresponding potentials may be derived from solutions of form

$$\psi_n = \left(\frac{\partial}{\partial y}\right)^{n+1} \varphi_n = r^{-n-(1/2)} \cos\left[\left(n + \frac{1}{2}\right)\theta\right] F_n(x, t, r) \quad (3)$$

in the cylindrical polar coordinates (x, r, θ). This method has been applied by Rott[5] in the special case $n = 0$, following Lamb's treatment of the half-plane diffraction problem.[6] Rott discards the higher order solutions ($n \geq 1$) of form (3) in consequence of the order of the singularity exhibited at $r = 0$, but for the more general case φ_n, as obtained by integration of Eq. (3), can be made to vanish as $r^{1/2}$. The $F_n(x, r, t)$ may be determined from a knowledge of the potential on the Mach cone $r = \beta^{-1}x$, but this is quite involved for $n \neq 0$.

We remark that the domain of integration for (ξ, η) in Eq. (1) is bounded by the leading edge and the pseudo Mach lines $\eta = y + [(x-\xi)/\beta]\cos\theta$ and $y - [(x-\xi)/\beta]\cos\theta$, except where the latter is off the wing, in which case it is to be replaced by its reflection (in the side edge) $\eta = [(x-\xi)/\beta]\cos\theta - y$. At the lower limit $\theta = 0$, these lines delimit the "equivalent area" prescribed by Evvard,[1] and the solution appears as a generalization of Evvard's result for a rectangular wing. Unfortunately, this interpretation has no direct extension to more general plan forms, where the lower limit of integration for η depends on x and ξ independently [rather than simply on $(x - \xi)$], in consequence of which the Laplace transform may not be effected by convolution.

Finally, we remark that the result [Eq. (1)] can be extended to any wing having a supersonic leading edge of arbitrary shape and straight subsonic side edges (*not trailing*), provided that there is no interference between the latter. To effect this extension we transform (via a modified Lorentz transformation) the potential equation to the normalized wave equation

$$\phi_{t't'} + \phi_{yy} + \phi_{zz} = \phi_{x'x'} \quad (4)$$

in which form it is invariant after a (true) Lorentz transformation with respect to (x', y). Such a transformation can be used (*cf.* the oblique transformation of Jones,[7] as modified by Hayes[8] to form a group) to bring the port edge to $y = 0$, while the supersonic leading edge can be filled in to $x' = 0$ on the proviso that $w = 0$ over the filled-in portion. We hope to discuss such extensions in more detail in a subsequent paper.

* On leave from University of California at Los Angeles.

REFERENCES

[1] Evvard, J. C., *Distribution of Wave Drag and Lift in the Vicinity of Wing Tips at Supersonic Speeds*, N.A.C.A. T.N. No. 1699, September, 1948.

[2] Miles, J. W., *The Oscillating Rectangular Airfoil at Supersonic Speeds*, Q. Appl. Math., Vol. 9, pp. 47–65, January, 1951.

[3] Miles, J. W., *On the Reduction of Unsteady Supersonic Flow Problems to Steady Flow Problems*, Readers' Forum, Journal of the Aeronautical Sciences, Vol. 17, p. 64, January, 1950.

[4] Stewartson, K., *On the Linearized Potential Theory of Unsteady Supersonic Motion*, Q. J. Mech. & Appl. Math., Vol. 3, pp. 182–199, June, 1950.

[5] Rott, N., *On the Unsteady Motion of a Thin Rectangular Wing in Supersonic Flow*, Readers' Forum, Journal of the Aeronautical Sciences, Vol. 18, No. 11, pp. 775–776, November, 1951.

[6] Bateman, H., *Partial Differential Equations of Mathematical Physics*, pp. 486–488; Dover Publication, New York, 1944.

[7] Jones, R. T., *Thin Oblique Airfoils at Supersonic Speeds*, N.A.C.A. T.N. No. 1107, 1946.

[8] Hayes, W. D., *Linearized Supersonic Flow*, Thesis, California Institute of Technology, Pasadena, Calif., p. 20, 1947; also North American Aviation Rep. AL-222, 1947.

A Nyquist Approach to Flutter

John Dugundji
Republic Aviation Corporation, Farmingdale, N.Y.
February 7, 1952

THE NYQUIST DIAGRAM is a useful tool of servomechanisms theory for determining the stability of linear systems. It would be of interest to see how this Nyquist diagram can be applied to the airplane flutter problem, which is also a problem in stability. For simplicity, the following discussion will deal with the two-dimensional two degree of freedom bending-torsion case.

The aeroelastic equations of motion for bending-torsion flutter are given in reference 1, page 213, as

$$\left.\begin{aligned} M\ddot{h} + S_\alpha\ddot{\alpha} + M\omega_h^2 h - \pi\rho\omega^2(A_{hh}h + A_{h\alpha}\alpha) &= \mathfrak{F} \\ S_\alpha\ddot{h} + I_\alpha\ddot{\alpha} + I_\alpha\omega_\alpha^2\alpha - \pi\rho\omega^2(A_{\alpha h}h + A_{\alpha\alpha}\alpha) &= \mathfrak{M} \end{aligned}\right\} \quad (1)$$

The above equations are in the notation of reference 1. The externally applied force $\mathfrak{F}$ and moment $\mathfrak{M}$ are included here for the sake of completeness, but the structural damping g is assumed zero. Proceeding in the conventional manner the applied force and moment are set equal to zero, and sinusoidal motion* of frequency ω is assumed. The resulting equations are reduced to the form

$$\left.\begin{aligned} \left[1 + \frac{\pi\rho}{M}A_{hh} - \left(\frac{\omega_h}{\omega}\right)^2\right]h + \left[\frac{S_\alpha}{M} + \frac{\pi\rho}{M}A_{h\alpha}\right]\alpha &= 0 \\ \left[\frac{S_\alpha}{I_\alpha} + \frac{\pi\rho}{I_\alpha}A_{\alpha h}\right]h + \left[1 + \frac{\pi\rho}{I_\alpha}A_{\alpha\alpha} - \left(\frac{\omega_\alpha}{\omega}\right)^2\right]\alpha &= 0 \end{aligned}\right\} \quad (2)$$

where the A's represent the aerodynamic coefficients defined by

$$\left.\begin{aligned} A_{hh} &= b^2L_h = b^2\left[1 - \frac{2i}{k}C(k)\right] \\ A_{h\alpha} &= \text{etc.} \end{aligned}\right\} \quad (3)$$

The L_h appearing in the above is a function of reduced frequency $k = \omega b/v$. The values of k and ω which cause the determinant of Eq. (2) to equal zero determine the flutter speed.

For application of the Nyquist criterion, it is more convenient to write the basic equations, including the aerodynamic forces, for arbitrary rather than sinusoidal motion. These can be expressed (see references 2 and 3) as

$$\left.\begin{aligned} &M\ddot{h} + S_\alpha\ddot{\alpha} + M\omega_h^2 h + \pi\rho b^2\left(\ddot{h} + v\dot{\alpha} - ab\dot{\alpha}\right) + \\ &\qquad 2\pi\rho vb\int_0^t \left\{1 - \Phi\left(\frac{v}{b}(t-\tau)\right)\right\} \\ &\qquad \left[\ddot{h} + v\dot{\alpha} + b\left(\frac{1}{2} - a\right)\dot{\alpha}\right]d\tau = \mathfrak{F} \\ &S_\alpha\ddot{h} + I_\alpha\ddot{\alpha} + I_\alpha\omega_\alpha^2\alpha + \pi\rho b^2\left[\left(\frac{1}{2} - a\right)\times\right. \\ &\qquad \left. vb\dot{\alpha} + b^2\left(\frac{1}{8} + a^2\right)\dot{\alpha} - ab\ddot{h}\right] - 2\pi\rho vb^2 \\ &\qquad \left(\frac{1}{2} + a\right)\int_0^t \left\{1 - \Phi\left(\frac{v}{b}|t-\tau|\right)\right\} \\ &\qquad \left\{\ddot{h} + v\dot{\alpha} + b\left(\frac{1}{2} - a\right)\dot{\alpha}\right\}d\tau = \mathfrak{M} \end{aligned}\right\} \quad (4)$$

By changing variables from time t to semichord lengths traveled $s = vt/b$ and then taking the Laplace transform, Eqs. (4) can be put in the form

$$\left.\begin{aligned} \left[1 + \frac{\omega_h^2b^2}{p^2v^2} + \frac{\pi\rho}{M}A_{hh}\right]h + \left[\frac{S_\alpha}{M} + \frac{\pi\rho}{M}A_{h\alpha}\right]\alpha &= \frac{b^2}{v^2}\frac{\mathfrak{F}}{Mp^2} \\ \left[\frac{S_\alpha}{I_\alpha} + \frac{\pi\rho}{I_\alpha}A_{\alpha h}\right]h + \left[1 + \frac{\omega_\alpha^2b^2}{p^2v^2} + \frac{\pi\rho}{I_\alpha}A_{\alpha\alpha}\right]\alpha &= \frac{b^2}{v^2}\frac{\mathfrak{M}}{I_\alpha p^2} \end{aligned}\right\} \quad (5)$$

where p represents the Laplace operator, and the aerodynamic coefficients A's are now defined by†

$$\left.\begin{aligned} A_{hh} &= b^2\left[1 + \frac{2}{p}\left(\frac{0.5p^2 + 0.2808p + 0.01365}{p^2 + 0.3455p + 0.01365}\right)\right] \\ A_{h\alpha} &= \text{etc.} \end{aligned}\right\} \quad (6)$$

To determine the stability of the above dynamic system, the determinant is expanded in powers of p to form the characteristic equation. If any of the roots of this characteristic equation are positive or have positive real parts, the system is unstable.

The Nyquist criterion‡ is a convenient method of determining the stability of a system without the necessity of finding all the roots of the characteristic equation (see, for example, reference 4). Briefly, it states that, for any function $f(p)$,

$$Z = N + P \quad (7)$$

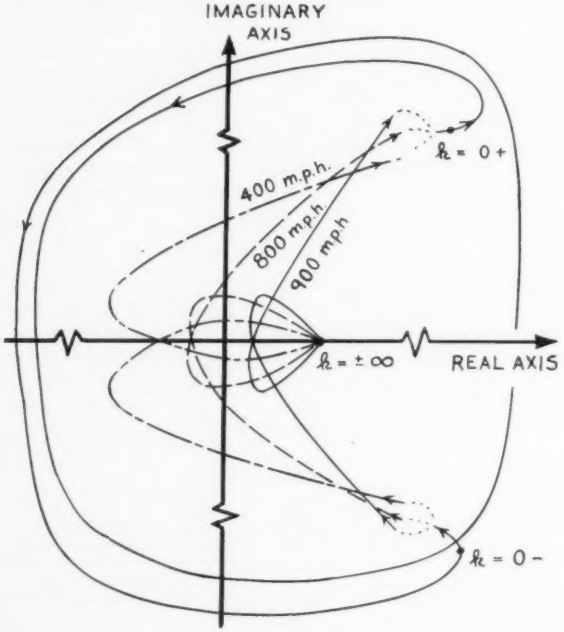

FIG. 1. Nyquist plot for bending-torsion flutter.

* Note that the aerodynamic forces appearing in Eq. (1) already assume sinusoidal motion.

† The R. T. Jones approximation is used here to represent the Wagner Function—i.e., $1 - \Phi(s) \approx 1 - 0.165e^{-0.0455s} - 0.335e^{-0.300s}$—see Reference 2.

‡ Strictly speaking, the criterion used here is the more basic Routh criterion, since it involves encirclements of the origin rather than of the -1 point.

where Z and P are the number of zeros (roots) and the number of poles located in the positive real half of the complex plane, respectively, and where N is the number of encirclements of $f(p)$ about the origin as p maps the boundaries of the positive real half of the complex plane. For the system given by Eqs. (5), the characteristic equation $f(p)$ will be of the form

$$f(p) = K_0 + K_1(1/p) + K_2(1/p^2) + K_3(1/p^3) + K_4(1/p^4) \quad (8)$$

It is to be noted, though, that some of the multipliers K_n will contain the polynomial approximation to the Theodoresen $C(k)$ function

$$C(p) = \frac{0.5p^2 + 0.2808p + 0.01365}{p^2 + 0.3455p + 0.01365} \quad (9)$$

which enters from the aerodynamic coefficients of Eqs. (6). However, since the roots of the denominator of Eq. (9) are both negative real numbers, the characteristic equation $f(p)$ will contain no poles in the positive real half of the complex plane.*

The basic system will therefore be stable if there are no net encirclements of $f(p)$ about the origin as p maps the positive real half of the complex plane.

To apply this Nyquist criterion, a value of velocity v is first set into Eqs. (5). The determinant is then evaluated for various values of $p = ik$ ranging from $p = +i\infty$ to $p = i0^+$, especially in the vicinity of ω near a natural frequency. The counterclockwise circuit of p about the positive half of the real plane is completed by continuing in the conventional manner with due regard for passing from $p = i0^+$ to $p = i0^-$ and from $p = -i\infty$ to $p = +i\infty$. It is to be noted that for this problem, $f(p) \to K_4(1/p^4)$ as $p \to 0$, thus resulting in two counterclockwise encirclements of the origin in passing from $p = i0^+$ to $p = i0^-$. It should be further noted that the value of the determinant of Eqs. (5) for $p = ik$ will be nearly identical to that of Eqs. (2), the only difference being that Eqs. (5) use the R. T. Jones approximation for the $C(k)$ function, while Eqs. (2) utilize the exact expression in terms of Bessel functions.[2] Hence, in plotting the Nyquist diagram, the more familiar sinusoidal form [Eqs. (2)] may be used directly, the less familiar Laplace operator form being used only to investigate the behavior when k approaches zero.

The preceding analysis was applied to a three-dimensional two degree of freedom bending-torsion case. The flutter speed, as worked out by the standard A.M.C. method, resulted in v_F = 855 m.p.h. Three Nyquist plots, two for the stable 400 and 800 m.p.h. speeds and one for the unstable 900 m.p.h. speed, are shown in Fig. 1.

The Nyquist method of solution is convenient when there are many degrees of freedom in the flutter analysis. The method can also be used in synthesizing servo systems where aeroelastic flutter characteristics must be included, since these characteristics can be introduced as the airplane block of a more complicated automatic control system block diagram. However, it should be mentioned that, although stability or instability is definitely determined, the degree of stability is found only in a limited sense. Also, a range of different forward speeds v must be investigated to ensure that the system is stable throughout the flying range of the airplane.

References

[1] Scanlan, R. H., and Rosenbaum, R., *Introduction to the Study of Aircraft Vibration and Flutter;* The Macmillan Company, New York, 1951.

[2] Baird, E. F., and Kelley, H. J., *Formulation of the Flutter Problem for Solution on an Electronic Analog Computer*, Readers' Forum, Journal of the Aeronautical Sciences, Vol. 17, No. 3, pp. 189–190, March, 1950.

[3] Winson, J., *The Solution of Aeroelastic Problems by Electronic Analogue Computation*, Journal of the Aeronautical Sciences, Vol. 17, No. 7, pp. 385–395, July, 1950.

[4] Bollay, W., *Aerodynamic Stability and Automatic Control*, Journal of the Aeronautical Sciences, Vol. 18, No. 9, pp. 569–617, September, 1950.

[5] Sears, W. R., *Operational Methods in the Theory of Airfoils in Non-Uniform Motion*, Journal of the Franklin Institute, Vol. 230, No. 1, pp. 95–111, July, 1940.

* It has been shown by Sears in reference 5 that the exact $C(p)$ in terms of Bessel functions also has no poles in the positive real half of the complex plane.

Comments "On the Deflection of Swept Cantilevered Surfaces"

David B. Hall

Structures Department, The Glenn L. Martin Company, Baltimore

February 26, 1952

In their paper, "On the Deflection of Cantilevered Surfaces," in the December, 1951, Journal of the Aeronautical Sciences, Professor Martin and Mr. Gursahaney have reported finding experimentally that a swept-tapered plate has an "effective elastic axis" and have expressed the belief that this will also be the case for a typical airplane wing. The following analysis indicates that the latter is unlikely.

Essentially, a swept cantilever of high aspect ratio is an ordinary cantilever with a skewed support which produces localized stress disturbances. The stresses in the vicinity of the support may cause the beam, under bending or twisting moments, to rotate about other than the bending or twisting axes. One of the requirements for the existence of an "effective elastic axis" is that in the normal portion of the structure there can be a family of lines such that a twisting moment about any one of them will leave that line straight; some one of them should remain horizontal also.

Consider a symmetrical beam (Fig. 1) having section properties as follows:

$$EI = c_1 x^n; \qquad GJ = c_2 x^n$$

The deflection of a point on a line $y = mx$ will be

$$w = \frac{-M_B}{c_1} \int\int \frac{dx}{x^n}\,dx + \frac{M_T}{c_2}\, mx \int \frac{dx}{x^n}$$

$$= \frac{-M_B}{c_1} \frac{x^{2-n}}{(1-n)(2-n)} + \frac{M_T}{c_2}\, m\, \frac{x^{2-n}}{1-n} + (\text{linear terms})$$

To fulfill the definition of an "effective elastic axis," we must have w = (linear terms only) along a line $y = mx$, and we must have $M_B = mM_T$. Making these substitutions, we find

$$c_2/c_1 = GJ/EI = 2 - n \quad (1)$$

For a trapezoidal plate $n = 1$, and GJ should be equal to EI.* Actual values are approximately as follows:

$$EI = Ebd^3/12(1-\mu^2) = 0.094\, Ebd^3$$

$$GJ \backsimeq Gbd^3/3 = 0.375\, Ebd^3/3 = 0.125\, Ebd^3$$

These values are not exactly equal but may be near enough to account for the results found experimentally. However, for

* Eq. (1) applies even through the equation for w assumes a special form for $n = 1$.

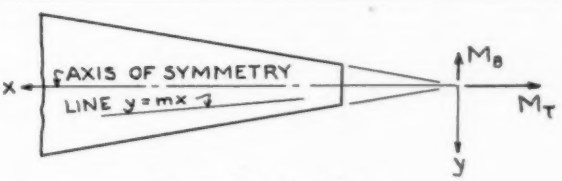

Fig. 1. Plan view of beam.

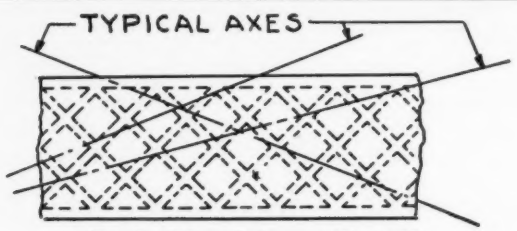

FIG. 2. Prismatic beam—$GJ = 2EI$.

typical wing structure, in which n is approximately 4, the curvature due to twist reverses, and we find that Eq. (1) demands GJ and EI of opposite signs or, more realistically, that under an inclined torque the only straight line on the wing is inclined the opposite way. Thus, the existence of an "effective elastic axis" appears to be a unique property of a special kind of beam of which the tapered plate is an example. Another interesting example would be a prismatic beam so constructed that $GJ = 2EI$. Such a beam could be twisted about a double infinity of axes (Fig. 2) and, when cantilevered from a skewed support, could have a single infinity of effective elastic axes.

On an Extension of Slender-Wing Theory

Mac C. Adams and W. R. Sears
Graduate School of Aeronautical Engineering, Cornell University, Ithaca, N.Y.
February 24, 1952

THE FAMILIAR SLENDER-WING THEORY of Munk and Jones[1] may be interpreted as the result of expanding a solution of the three-dimensional small-perturbation equations in powers of a width parameter and retaining only the leading term. In this note, we shall show how an expansion of this type can be obtained for thin wings in supersonic steady flow. Our procedure makes use of Laplace-transform methods, previously applied by Ward,[2] Stewartson,[3] and others. It gives us higher order terms, which appreciably extend the scope of the slender-body theory.

Consider first the symmetrical (nonlifting) slender wing sketched in Fig. 1. Let x, y, z be orthogonal Cartesian coordinates, as indicated, and let corresponding dimensionless coordinates be defined by $\xi = x/l$, $\eta = y/s$, and $\zeta = z/s$, the constants l and s being defined in Fig. 1. If the thickness distribution is given by $z = \pm t(x, y)$ the slope of the surface is $\sigma = \partial t/\partial x = \sigma(\xi, \eta)$. Further, let the plan form of the wing be defined by the left and right edge curves $\eta = h_1(\xi)$ and $\eta = h_2(\xi)$, respectively. The differential equation satisfied by the velocity potential ϕ is

$$\beta^2 k^2 \phi_{\xi\xi} = \phi_{\eta\eta} + \phi_{\zeta\zeta} \tag{1}$$

where k denotes the width parameter s/l.

In terms of the Laplace transform of ϕ, which we shall call $\bar{\phi}(p, \eta, \zeta)$, Eq. (1) reads

$$(\beta k p)^2 \bar{\phi} = \bar{\phi}_{\eta\eta} + \bar{\phi}_{\zeta\zeta} \tag{2}$$

In Eq. (2) the proper first-order boundary conditions of vanishing velocity components at the leading Mach cone have been introduced. An elementary solution of Eq. (2) which is useful for the construction of nonlifting wings is

$$d\bar{\phi}^{(1)} = \bar{f}(p, \eta_1) K_0(\beta k p r) d\eta_1$$

where $r^2 = \zeta^2 + (\eta - \eta_1)^2$ for any value of η_1 and K_0 is the modified Bessel function of the second kind. In the ξ, η, ζ-space, this solution represents a line source of variable strength, lying along the line $\eta = \eta_1$ in the ξ, η-plane. Its strength is proportional to the inverse Laplace transform of $\bar{f}(p, \eta_1)$, say $f(\xi, \eta_1)$, and a continuous distribution of such line sources in the ξ, η-plane can be used to satisfy the boundary condition at the wing surface.

Similarly, a distribution of line doublets, which is obtained by differentiation with respect to ζ, can be used to construct the flow past a lifting wing without thickness; in this case the elementary solution of Eq. (2) is

$$d\bar{\phi}^{(2)} = -\beta k p \zeta r^{-1} \bar{g}(p, \eta_1) K_1(\beta k p r) d\eta_1$$

The relation between the distribution functions f or g and the surface slope or surface potential, respectively, is found by calculating the behaviors of these elementary solutions at the line singularities; the results, in terms of Laplace transforms, are:

For nonlifting wing:

$$\bar{f}(p, \eta_1) = -\frac{1}{\pi} \bar{\phi}_\zeta(p, \eta_1, +0) = -\frac{s}{\pi} U \bar{\sigma}(p, \eta_1)$$

For lifting wing without thickness:

$$\bar{g}(p, \eta_1) = -(1/\pi) \bar{\phi}(p, \eta_1, +0)$$

In principle, therefore, the superposition of line singularities in this way suffices to construct the flow past supersonic thin wings, either lifting or nonlifting. The velocity potential is obtained by integrating the effects of the elementary solutions across the span and inverting the Laplace transforms; the properties of the Bessel functions are such that only elements in the forecone of any point contribute to the result. In fact, the results of the inversion are just the familiar surface integrals over source or doublet distributions of linearized supersonic wing theory.

To obtain the desired expansion in the width parameter $\beta s/l$, we now restrict ourselves to regions near the wing and expand the Bessel function K_0 for small values of its argument—viz.,

$$K_0(\beta k p r) \approx -[1 + (\beta k p r/2)^2] \ln (\beta k p r/2) - \gamma + (1 - \gamma)(\beta k p r/2)^2 + O[(\beta k p r)^4 \ln (\beta k p r)] \tag{3}$$

where γ denotes the Euler constant. The elementary potential function $d\phi^{(1)}$ can now be obtained by multiplying Eq. (3) by $\bar{f}(p, \eta_1) d\eta_1$ and interpreting the operators term-by-term with the help of the convolution theorem. In the subsequent superposition by integration over η_1, there is some difficulty at the leading edge, but this can be overcome; the result is

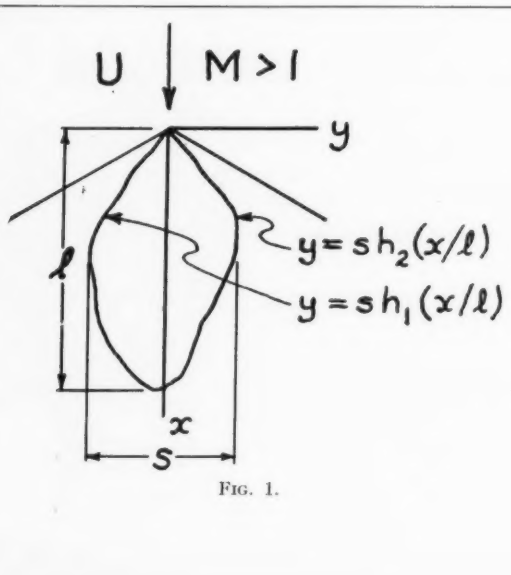

FIG. 1.

$$\phi^{(1)}(\xi, \eta, \zeta) = \frac{U}{2\pi l} S'(\xi) \ln\left(\frac{\beta k}{2}\right) - \frac{U}{2\pi l} \int_0^\xi S''(t) \ln(\xi - t) \times$$
$$dt + \frac{sU}{\pi} \int_{h_1}^{h_2} \sigma(\xi, \eta_1) \ln r \, d\eta_1 - \left(\frac{\beta^2 k^2 s U}{4\pi}\right) \frac{\partial^2}{\partial \xi^2} \times$$
$$\int_{h_1}^{h_2} \sigma(\xi, \eta_1) \left[(1 - \gamma) r^2 - r^2 \ln\left(\frac{\beta k r}{2}\right)\right] d\eta_1 -$$
$$\left(\frac{\beta^2 k^2 s U}{4\pi}\right) \frac{\partial^2}{\partial \xi^2} \int_0^\xi [\gamma + \ln(\xi - t)] \, dt \int_{h_1}^{h_2} r^2 \sigma(t, \eta_1) \, d\eta_1 \quad (4)$$

where $S(\xi)$ denotes the cross-sectional area of the airfoil at ξ—i.e.,

$$S'(\xi) = 2sl \int_{h_1}^{h_2} \sigma(\xi, \eta) d\eta$$

Similarly,

$$\phi^{(2)}(\xi, \eta, \zeta) = -\zeta \int_{\phi \neq 0} g(\xi, \eta_1) \frac{1}{r^2} d\eta_1 - \frac{\beta^2 k^2}{2\pi} \zeta \frac{\partial^2}{\partial \xi^2} \times$$
$$\int_{\phi \neq 0} g(\xi, \eta_1) \left[\gamma + \frac{1}{2} - \ln\left(\frac{\beta k r}{2}\right)\right] d\eta_1 + \frac{\beta^2 k^2}{2\pi} \zeta \frac{\partial^2}{\partial \xi^2} \times$$
$$\int_0^\xi [\gamma - \ln(\xi + t)] \, dt \int_{\phi \neq 0} g(t, \eta_1) d\eta_1 \quad (5)$$

In Eq. (5) we denote the integration across the span by the symbol "$\phi \neq 0$" to remind the reader that contributions of trailing vortices must be included when they are present. Such vortices extend rearward behind all trailing edges, just as in Jones's work.

The first three terms in Eq. (4) have their counterparts in Ward's results[2] for slender pointed (nonplanar) bodies; the last two terms are the additional ones supplied by the present theory for the special case of a thin wing. Similarly, the first term of Eq. (5) is Jones's result, and the other two are the new ones that are expected to extend his theory to broader wings.

For the direct calculation of flow about a specified lifting wing without thickness, Eq. (5), as usual, becomes an integral equation for $g(\xi, \eta_1)$—i.e., the derivative $\phi_\xi(\xi, \eta, 0)/sU$ must be put equal to the slope of the wing surface, say $\alpha(\xi, \eta)$. To solve for $g(\xi, \eta_1)$, we find that a method of successive approximations is useful. We begin by neglecting the second and third terms of the right-hand side [i.e., the terms corresponding to the second and third right-hand terms in Eq. (5)], and thus our first approximation to g is that of Jones's theory, which we designate $g^{(1)}$. This value is subsequently substituted in the second and third terms, yielding a new integral equation for the second approximation, $g^{(2)}$, still of the same form as Jones's integral equation. This can be solved immediately for $g^{(2)}$. The process might be repeated as often as desired, but a consideration of orders of magnitude discloses that further iterations are beyond the accuracy of Eq. (5) itself. An explicit formula for $g^{(2)}$ in terms of $\alpha(\xi, \eta)$ can be written down by means of this procedure, but, in order to conserve space, it will not be reproduced here. (The process is not quite so straightforward for wings for which the Jones solution yields discontinuous pressures on the wing; in such cases a more careful treatment is required in the region of the discontinuity. This will be given in a more complete report.)

An interesting test case is the well-known flat delta wing at incidence. For this case, "exact" results of linearized theory are available,[4] and the results of our present theory are found to be identical with these through terms of the orders carried. In Fig. 2, for example, the lift-curve slope, in the form $C_L/\alpha k$, is plotted against the width parameter $\beta k/2$ for "exact," Jones, and the present theories. Moreover, for this special case, because of the type of dependence of the results on βk, the curves of Fig. 2 actually display the relative accuracies of the three approximations in predicting local pressure coefficient and all the engineering values that are proportional to this coefficient. The new method is seen to extend considerably the slender-wing theory.

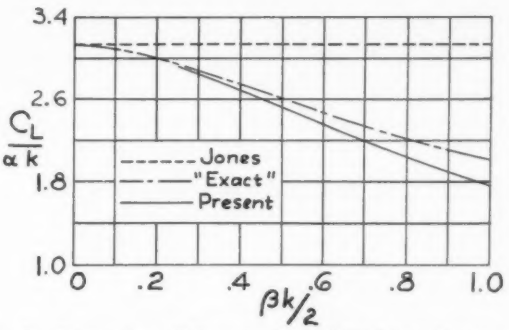

FIG. 2. Comparison of lift-curve slope of flat delta wings as predicted by three approximations.

In a longer paper we intend to present the theory in more detail and to show its application to several typical airfoil problems, including the design of wings for minimum drag. "Exact" linearized theory has not proved tractable for such (nonconical) problems, while Jones's theory is limited to very slender plan forms.

REFERENCES

[1] Jones, Robert T., *Properties of Low-Aspect-Ratio Pointed Wings at Speeds Below and Above the Speed of Sound*, N.A.C.A. Report No. 835, 1946.

[2] Ward, G. N., *Supersonic Flow Past Slender Pointed Bodies*, Quart. Jour. of Mech. & Appl. Math., Vol. 2, pp. 75–97, 1949.

[3] Stewartson, K., *Supersonic Flow over an Inclined Wing of Zero Aspect Ratio*, Proc. Cambridge Phil. Soc., Vol. 46, pp. 307–315, 1950.

[4] Stewart, H. J., *The Lift of a Delta Wing at Supersonic Speeds*, Quart. Appl. Math., Vol. 4, pp. 246–254, 1946.

Diffraction of Blasts by Axisymmetric Bodies*

H. F. Ludloff and M. B. Friedman
Daniel Guggenheim School of Aeronautics, New York University

February 10, 1952

AN ANALYTIC METHOD developed by C. S. Gardner and H. F. Ludloff† and later extended in the thesis of L. Ting,‡ has now been applied to the diffraction of blasts advancing over axisymmetric bodies of arbitrary profile $f(z)$. Besides serving a practical purpose, the computations were undertaken to explore a spatial shock configuration with regard to its Mach effect and its "slipstream." Suppose that the shock front is of arbitrary strength and originally plane and that the blast struck body is relatively slender. Then, during the passage, the blast will consist of a plane incident shock, a spherical weak reflected shock, and a curved diffracted Mach stem. The air stream that has traversed the Mach stem will be rotational and, for sufficiently strong blasts, supersonic with regard to the body. The problem is treated as a time-dependent perturbation, using the method of Lorentz transformation and "reflexion."†' ‡ But in the present problem, the solutions have to be assumed in the form of "retarded potentials." Fixing cylindrical Lorentz coordinates (x, r, t) in the undisturbed air downstream of the shock, the problem may be stated in terms of the disturbance pressure $p^{(1)}$, which is of $0(\epsilon^2)$:

Differential Equation:

$$\Delta p^{(1)} - c^{(-2)} \cdot p_{tt}^{(1)} = 0 \quad (1)$$

* Investigation supported by Navy funds.

† See review article by H. F. Ludloff in *Advances of Applied Mechanics*, Vol. III, 1952.

‡ See article by L. Ting and H. F. Ludloff, JOURNAL OF THE AERONAUTICAL SCIENCES, Vol. 18, p. 143, 1951.

Boundary Conditions: (Surface) at $r = 0, x \leq 0, t > 0$:

$$rp_r^{(1)} = -A_0[f'^2(u) + f(u)\cdot f''(u)] \tag{2}$$

were $u = a(t + \lambda_0 \cdot x)$.

(Shock Front) at $x = 0, r \geq 0, t > 0$:

$$D_{x,\,t}^{(2)}(p^{(1)}) = 0 \tag{3}$$

where $D_{x,\,t}^{(2)}$ is a differential operator of the second order in x and t. The parameters A_0, α, and λ are simple expressions in terms of the shock velocity U_0 relative to the airfoil and the velocity U and Mach Number M of the shock relative to the undisturbed flow behind.

It is necessary to note that at the intersection point of shock and body surface, there is a singularity in the derivative, even for a conical body, characterized by

$$\lim_{r=0,\ x \to 0^-} (rp_r^{(1)} = -A_0[f'^2(at) + f(at)\cdot f''(at)]$$

however,

$$\lim_{x=0,\ r \to 0^+} (rp_r^{(1)}) = -B_0[f'^2(at) + f(at)\cdot f''(at)] \tag{4}$$

In accordance with the "reflexion principle," Eq. (3) can be replaced by a condition on the "extended axis" of the body: At $r = 0, x \geq 0, t > 0$:

$$rp_r^{(1)} = \sum_{i=1}^{3} A_i[f'^2(u_i) + f[(u_i)\cdot f''(u_i)] \tag{5}$$

where $u_i = a(t - \lambda_i x)$. Also, B_0, A_i, and λ_i are simple functions of U_0, U, and M.

It is now essential that, because of the properties of the wave equation, the solution be assumed in the form of a "retarded potential"—integral

$$p^{(1)}(x, r, t) = \frac{1}{2}\left\{\int_{-\infty}^{0} d\xi\, \frac{g_1[\xi, t - (R/c)]}{R} + \int_{0}^{+\infty} d\xi\, \frac{g_2[\xi, t - (R/c)]}{R}\right\} \tag{6}$$

where $R = [(x - \xi)^2 + r^2]^{1/2}$ is the real distance between source point $(\xi, 0)$ and field point (x, r). It turns out that the "retarded temporary source strength's" g_1 and g_2 are equal to expressions (2) and (5), respectively, after x and t have been replaced by ξ and $t - [R(\xi)/c]$. Note that now only one integration is involved.

After substituting Eqs. (2) and (5), Eq. (6) represents the solution for a general profile form $f(z)$.

For the particular case of a blast passing over the conical nose of a missile, the solution in physical (conical) coordinates $\xi = x'/ct$ and $\eta = r'/ct$ reduce to

$$p^{(1)}(\xi, \eta) = K\cdot\sinh^{-1}\left[\frac{1}{\sqrt{1 - M^2}}\cdot\frac{\xi - M}{\eta}\right] + \sum_{i=0}^{3} A_i \sinh^{-1}\left\{\frac{1}{\sqrt{1 - M^2}}\left[\frac{\xi - M - \omega_i}{\eta}\right]\right\} \tag{7}$$

where the ω_i are simple functions of ξ and η.

The density field is given by

$$\rho^{(1)} = (1/c^2)\,[p^{(1)}(\xi, \eta) - \Omega\cdot p^{(1)}(M, \eta)] \tag{8}$$

Also, K and Ω are simple expressions in U_0, U, and M.

In Fig. 1 the surfaces of constant pressure and density are plotted for a blast passing over a cone of half vertex angle $\epsilon = 10^{-1}$. The shock strength is characterized by $(U_0 - U)/c = 1.21$, so that this plot can be compared with the two-dimensional plot in article by Ting and Ludloff.‡ The following features emerge: The rotationality of the flow is again restricted to the domain $T0C$, since the reflected shock, in general, is of $0(\epsilon^4)$; at T, its strength is of even higher order. It is seen that in the present case, the splitting off of corresponding isopycnics and isobars is far less strong, and the density gradient along any isobar is weak. There are no longer singularities at 0 and D; in neither point do several isopycnics end. Thus instead of a contact discontinuity line there is, here, a domain ($T0C$), over which the required entropy change is spread. The isobars are conical surfaces in the Karman-Moore region and follow this general trend, to some extent, also inside the time-dependent domain; apparently the strong singularities located on the axis of the conical body have a dominant influence on the picture.

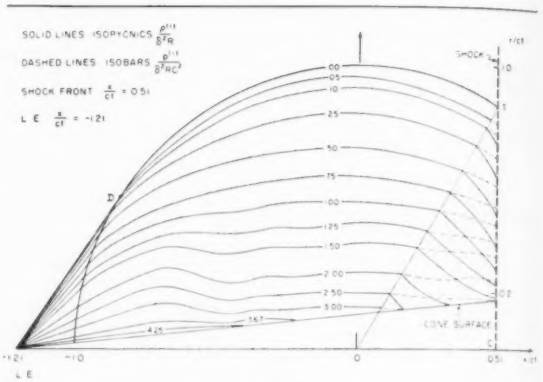

FIG. 1.

Effect of Wind-Tunnel Nozzle on Steady-Flow Nonuniformities

H. S. Ribner and M. Tucker
Lewis Flight Propulsion Laboratory, N.A.C.A.
March 3, 1952

THERE IS AN AREA of common ground between the extension of Prandtl's concepts[1] reported under the above title by Professor Corrsin[2] and another recent investigation.[3] Suppose the velocity in the low-speed section upstream of the nozzle, although purely axial, is not quite uniform across the tunnel. Then, according to an energy consideration by Prandtl,[1] the nonuniformity is considerably smoothed out downstream of the contraction, the more so the greater the contraction ratio. This smoothing effect on longitudinal perturbations (but not on lateral perturbations) is still observed for the unsteady turbulent fluctuations in the wind-tunnel stream. Corrsin has considered the former case of steady perturbed longitudinal filaments, and has extended Prandtl's analysis to include (a) the effect of density ($\sim$ temperature^{-1}) perturbations and (b) the compressibility of the flow. We have concerned ourselves with the latter case of the turbulence carried by the wind-tunnel stream, utilizing the spectrum concept, and have included (b) but not (a).

In the spectral or Fourier integral representation, a turbulent field may be regarded as a superposition of plane, transverse, sinusoidal waves with an apparently random distribution of orientations and wave lengths. The mutual interference of the waves during their transport through the wind-tunnel contraction may be neglected under suitable circumstances;[4] then the contraction effect may be computed for individual plane waves and the overall effect obtained by superposition.

Of this aggregation of plane waves, we now limit attention to those representing purely longitudinal disturbances: The axial velocity varies sinusoidally across the tunnel. These are then

of the steady type considered by Corrsin, since the convection of these waves by the main stream introduces no unsteadiness. It was found that, when the general result was specialized to such waves, there was obtained for any stream line

$$u_2 = (U_1/U_2)u_1 \tag{1}$$

where subscripts 1 and 2 refer to sections upstream and downstream of the contraction, respectively; U is the main-stream velocity; and u is the perturbation velocity. The same relation holds for a rather wider class of waves.[5]

Corrsin's Eq. (8) reduces to the above equation for our case of no temperature perturbation (his $\theta_1 = 0$). The methods of derivation were totally different: He employed considerations of energy, whereas we employed considerations on the transport of vorticity.

When the complete aggregation of plane waves is superposed to represent turbulence the simple relation (1) [applied between root mean square (r.m.s.) values] is, of course, appreciably modified. A rough approximation to our equation[6] in the range $1 \leq U_2/U_1 \leq 20$ is

$$u_2\,(\text{r.m.s.}) \approx (U_1/U_2)^{0.62}u_1\,(\text{r.m.s.}) \tag{2}$$

when the initial turbulence is isotropic (no preferred directions) and the wind-tunnel contraction is axially symmetric. This result is limited to circumstances[4] where the decay of the turbulence during its transport through the nozzle is small in comparison.

References

[1] Prandtl, L., *Attaining a Steady Air Stream in Wind Tunnels*, N.A.C.A. T.M. No. 726, 1933.

[2] Corrsin, Stanley, *Effect of Wind-Tunnel Nozzle on Steady-Flow Non-uniformities*, Readers' Forum, Journal of the Aeronautical Sciences, Vol. 19, No. 2, p. 135, February, 1952.

[3] Ribner, H. S., and Tucker, M., *Spectrum of Turbulence in a Contracting Stream*, N.A.C.A. T.N. No. 2606, January, 1952.

[4] *Ibid.*, Summary, pp. 11–13, 29–32.

[5] *Ibid.*, p. 16.

[6] *Ibid.*, Eq. (34) and Fig. 4.

Comments on "Supersonic Flow of a Two-Dimensional Jet"

E. B. Klunker and Keith C. Harder
Langley Aeronautical Laboratory, N.A.C.A., Langley Field, Va.

January 16, 1952

IN PAI'S[1] PAPER, the mathematical formulation of the problem of the flow of a two-dimensional supersonic jet into subsonic stream appears to be in error, since the boundary conditions given by Eqs. (6) and (7) of his paper are valid only for positive values of x. For negative values of x, the proper boundary conditions are

$$\partial\phi_1/\partial y = \partial\phi_2/\partial y = 0$$

on the boundary $|y| = 1$. No condition can be prescribed for $\partial\phi_2/\partial x$ on this boundary for x negative, since the external flow is subsonic. In addition, the boundary condition given by Eq. (8a) must also be satisfied at $x = -\infty$.

The terms of Eqs. (12) and (13) are solutions for the flow infinitely far downstream of the exit which satisfy the boundary conditions given by Eqs. (5), (6), and (7). Thus, any superposition of these solutions will satisfy the same boundary conditions. As noted, however, these are not the correct boundary conditions for the flow upstream of the jet exit. Consequently, the complete solution cannot be determined through a superposition of only solutions of the type given by Eqs. (12) and (13).

A formal solution satisfying the proper boundary conditions may be formulated by considering the disturbances in the subsonic field to arise from a distribution of sources on the interface for $0 < x < +\infty$. The strength of the source distribution is determined by equating the pressures and flow directions at the interface.

Consider a coordinate system such that one interface lies on the axis $y = 0$ and the jet exit is on the axis $x = 0$. Then, in terms of source distributions,

$$u_2(x, 0) = \frac{1}{\beta_2\pi}\int_{-\infty}^{\infty}\frac{v_2(\xi, 0)}{x - \xi}\,d\xi \tag{1'}$$

and by the Allied integral of Fourier's integral[2]

$$v_2\,(x, 0) = -\frac{\beta_2}{\pi}\int_{-\infty}^{\infty}\frac{u_2(\xi, 0)}{x - \xi}\,d\xi \tag{2'}$$

The supersonic solution may be expressed

$$u_1\,(x, y) = f\,[x + \beta_1\,(1 + y)] + f\,[x - \beta_1\,(1 + y)] \tag{3'}$$

$$v_1\,(x, y) = \beta_1\,\{f[x + \beta_1\,(1 + y)] - f[x - \beta_1\,(1 + y)]\} \tag{4'}$$

where $f(z) = 0$ for $z < \beta_1$. The boundary conditions are satisfied if

$$v_2\,(x, 0) + v_2\,(x + 2\beta_1, 0) = -\frac{\beta_2}{\beta_1}\frac{P_{2\infty}}{P_{1\infty}}\frac{M_{2\infty}{}^2}{M_{1\infty}{}^2}\frac{1}{\pi}\int_0^{\infty}\left[\frac{v_2(\xi, 0)}{x - \xi} - \frac{v_2(\xi, 0)}{x + 2\beta_1 - \xi}\right]d\xi \tag{5'}$$

for $x > 0$. $v_2\,(x, 0) = 0$ for $x < 0$.

The solution of Eq. (5′) together with

$$u_2\,(x, y) = \frac{1}{\beta_2\pi}\int_0^{\infty}\frac{v_2\,(\xi, 0)\,(x - \xi)}{(x - \xi)^2 + \beta_2{}^2y^2}\,d\xi$$

$$v_2\,(x, y) = \frac{\beta_2 y}{\pi}\int_0^{\infty}\frac{v_2\,(\xi, 0)}{(x - \xi)^2 + \beta_2{}^2y^2}\,d\xi$$

determines the subsonic flow.

The functions $f(x + \beta_1)$ and $f(x - \beta_1)$ may be related to the values of u_2 and v_2 on the interface, and the supersonic flow inside the jet may be determined from Eqs. (3′) and (4′).

References

[1] Pai, S. I., *On Supersonic Flow of a Two-Dimensional Jet in Uniform Stream*, Journal of the Aeronautical Sciences, Vol. 19, No. 1, pp. 61–65, January, 1952.

[2] Titchmarsh, E. C., *Introduction to the Theory of Fourier Integrals*, 2nd Ed., p. 119; Oxford University Press, London.

Author's Reply

S. I. Pai
University of Maryland

March 17, 1952

STRICTLY SPEAKING, as Messrs. Klunker and Harder pointed out, my solution for the case of subsonic uniform stream holds true only far downstream of the nozzle. As far as the subsonic stream is concerned, the present problem is similar to the subsonic uniform flow over a wall, which is straight for $-\infty < x \leq 0$ and which is wavy for $0 \leq x < +\infty$. The only difference in these two cases is that the wavy form in my problem is not given but should be determined by the condition on the boundary of the supersonic jet. In my analysis I calculate this wavy form downstream approximately by assuming a solution of the form of Eq. (9) of my paper,[1] which is implicitly for the flow condition far downstream from the nozzle and which should satisfy only the boundary conditions given in my paper. Since I am interested mainly in whether the supersonic jet in a uniform stream has periodic structure or not, my analysis is sufficiently accurate for the purpose, and the main conclusions of my simplified analysis that the supersonic jet in uniform subsonic stream has almost periodic structure and that the approximate wave length in-

creases with the Mach Number of the surrounding stream are correct. However, if one wants to calculate the flow field upstream or near the exit of the nozzle, more refined theory should be used.

My analysis for a supersonic jet in a supersonic uniform stream holds true for all x, because in a supersonic stream the disturbance has no influence upstream.

Reference

[1] Pai, S. I., *On Supersonic Flow of a Two-Dimensional Jet in Uniform Stream*, Journal of the Aeronautical Science, Vol. 19, No. 1, pp. 61–65, January, 1952.

An Approximate Method for the Calculation of the Laminar and Turbulent Boundary Layer by Simple Quadrature for Two-Dimensional and Axially Symmetric Flow

E. Truckenbrodt

Dr.-Ing., Institute of Fluid Mechanics, Technical University, Braunschweig, Germany

January 15, 1952

THE NUMEROUS APPROXIMATE METHODS[1–5] for the calculation of the laminar and turbulent boundary layer have been treated from a common point of view. In this way it has been possible to establish a uniform approximate method for the two-dimensional and axially symmetric case, valid for laminar flow, as well as for turbulent flow. The method consists of calculating the momentum thickness and a shape parameter of the velocity profile, which determines the point of separation. Both are calculated by simple quadrature.

From Prandtl's boundary-layer equations one obtains by a well-known procedure the equations for momentum and energy in the following form for the case of axial symmetry:

$$\frac{(d/dx)\,(U^2R\vartheta)}{U^2R} + H\frac{\vartheta}{U}\frac{dU}{dx} = \frac{\tau_0}{\rho U^2} \tag{1}$$

(equation of momentum);

$$\frac{(d/dx)\,(U^3R\bar{H}\vartheta)}{U^3R} = 2\frac{d+t}{\rho U^3} \tag{2}$$

(equation of energy).

These equations resolve into those of the two-dimensional case by omitting the radius $R(x)$ of the cross section of the body of revolution. $U(x)$ is the potential flow, $\vartheta(x)$ is the momentum loss thickness, δ^* is the displacement thickness, δ^{**} is the energy loss thickness, $H = \delta^*/\vartheta$, $\bar{H} = \delta^{**}/\vartheta$, τ_0 is the shearing stress at the wall, and $(d + t)$ is the work done by the shearing stress.

Subtracting Eq. (2) from Eq. (1), one gets

$$\vartheta\frac{d\bar{H}}{dx} = (H-1)\bar{H}\frac{\vartheta}{U}\frac{dU}{dx} + 2\frac{d+t}{\rho U^3} - \bar{H}\frac{\tau_0}{\rho U^2} \tag{3}$$

Both the shearing stress, $\tau_0/\rho U^2$, and the work of the shearing stress, $(d + t)/\rho U^3$, can be given as functions for the dimensionless quantities $U\vartheta/\nu$ and H. Furthermore, the velocity profiles of the boundary layer are assumed to be one-parametric, and, in consequence of this, there exists a general relation between H and $\bar{H}$. With regard to this, Eqs. (2) and (3) are two equations for the two unknown quantities $\vartheta(x)$ and $\bar{H}(x)$. The momentum loss thickness is calculated from the energy loss equation, Eq. (2), and not from the equation of momentum, Eq. (1), as in most other methods. This brings some advantages for carrying out the integration.

With some simplifications, one gets, for the momentum loss thickness,

$$\frac{\vartheta}{l} = \frac{\left[C_1 + \left(\frac{c_f}{2}\right)^{1+n}\int_{x_1/l}^{x/l}\left(\frac{U}{U_\infty}\right)^{3+2n}\left(\frac{R}{l}\right)^{1+n} d\frac{x'}{l}\right]^{1/(1+n)}}{(U/U_\infty)^3(R/l)} \tag{4}$$

where the constant of integration is

$$C_1 = [(U_1/U_\infty)^3(R_1/l)\,(\vartheta_1/l)]^{1+n} \tag{5}$$

U_1, R_1, and ϑ_1 are the values in the point $x = x_1$.

Here, c_f means the coefficient of skin friction of the flat plate. There is $n = 1$ for laminar flow and $n = 1/6$ for turbulent flow. In the two-dimensional case, R has to be omitted in Eqs. (4) and (5). Eq. (4) can also be used for rough walls by inserting the c_f value of the rough plate.

For the convenience of calculation, it was useful to introduce, instead of $\bar{H}$, the parameter

$$L = \int d\bar{H}/(H-1)\bar{H} \tag{6}$$

This shape parameter of the velocity profile is calculated from Eq. (3). With some simplifications, one obtains

$$L = \frac{\xi_1}{\xi}L_1 + \ln\frac{U}{U_1} + \frac{1}{\xi}\int_{\xi_1}^{\xi}\left[b - \ln\frac{U}{U_1}\right]d\xi' \tag{7}$$

where ξ is obtained from

$$\xi = \left[C_1 + \left(\frac{c_f}{2}\right)^{1+n}\int_{x_1/l}^{x/l}\left(\frac{U}{U_\infty}\right)^{3+2n}\left(\frac{R}{l}\right)^{1+n} d\frac{x'}{l}\right]^c \tag{8}$$

Here, b and c have the following values:

Laminar: $b = 0$; $c = 8.0$

Turbulent: $b = 0.07 lg\frac{U\vartheta}{\nu} - 0.23$; $c = 4.0$

The calculation of ξ can be done very simply, because the expression in brackets in Eq. (8) also occurs in Eq. (4).

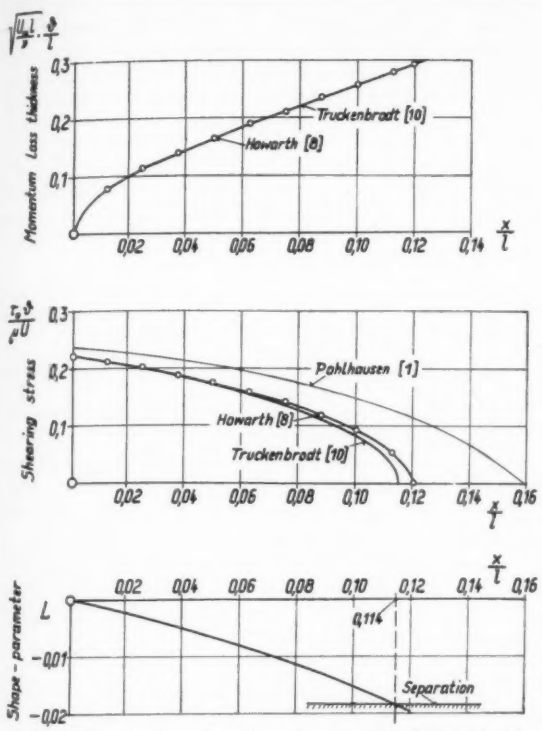

FIG. 1. The laminar boundary layer of the Howarth flow $U(x) = U_\infty [1 - (x/l)]$. 0 = exact solution, Howarth[8]; ——— = approximate solution, Truckenbrodt.[10]

The whole calculation is done in the following way: At first, one gets the momentum loss thickness from Eq. (4); then the shape parameter L from Eq. (7) in connection with Eq. (8).

Separation occurs in the laminar case for $-L > 0.018$ and in the turbulent case for $-L > 0.13$ to 0.18.

The applicability of the method has been shown in the laminar case for the Howarth[8] flow $U(x) = U_\infty [1 - (x/l)]$, Fig. 1, and in the turbulent case[4] for the airfoil NACA 65(216)-222 at an angle of incidence of $\alpha = 10.1°$, Fig. 2. In both cases, there is a comparison with other methods and with measurements. More details of our calculations will be published shortly.[10]

REFERENCES

[1] Pohlhausen, K., *Zur näherungsweisen Integration der Differentialgleichung der laminaren Reibungsschicht*, Zeitschrift für angew. Mathematik und Mechanik, Vol. 1, p. 252, 1921.

[2] Gruschwitz, E., *Die turbulente Reibungsschicht in ebener Strömung mit Drückabfall und Druckanstieg*, Ingenieur-Archiv, Vol. 2, p. 321, 1931.

[3] Kehl, A., *Ueber konvergente und divergente turbulente Reibungsschichten*, Ingenieur-Archiv, Vol. 12, p. 293, 1943.

[4] von Doenhoff, A. E., and Tetervin, N., *Determination of General Relations for the Behavior of Turbulent Boundary Layers*, N.A.C.A. Report No. 772, 1943.

[5] Garner, H. C., *The Development of Turbulent Boundary Layers*, A.R.C. Report No. 2133, 1944.

[6] Rotta, J., *Ueber die Theorie der turbulenten Grenzschichten*, Ingenieur-Archiv, Vol. 19, p. 31, 1951.

[7] Ludwieg, H., and Tillmann, W., *Untersuchungen über die Wandschubspannung in turbulenten Reibungsschichten*, Ingenieur-Archiv, Vol. 17, p. 288, 1949.

[8] Howarth, L., *On the Solution of the Laminar Boundary Layer Equations*, Proc. Roy. Soc., London, Series A 919, Vol. 164, p. 547, 1938.

[9] Schlichting, H., *Grenzschicht-Theorie*; Verlag G. Braun, Karlsruhe, 1951.

[10] Truckenbrodt, E., *Ein Quadraturverfahren zur Berechnung derlaminaren und turbulent Reibungsschlichten bei ebener und rotationssymmetrischer Strömung*, to be published in the Ingenieur-Archiv.

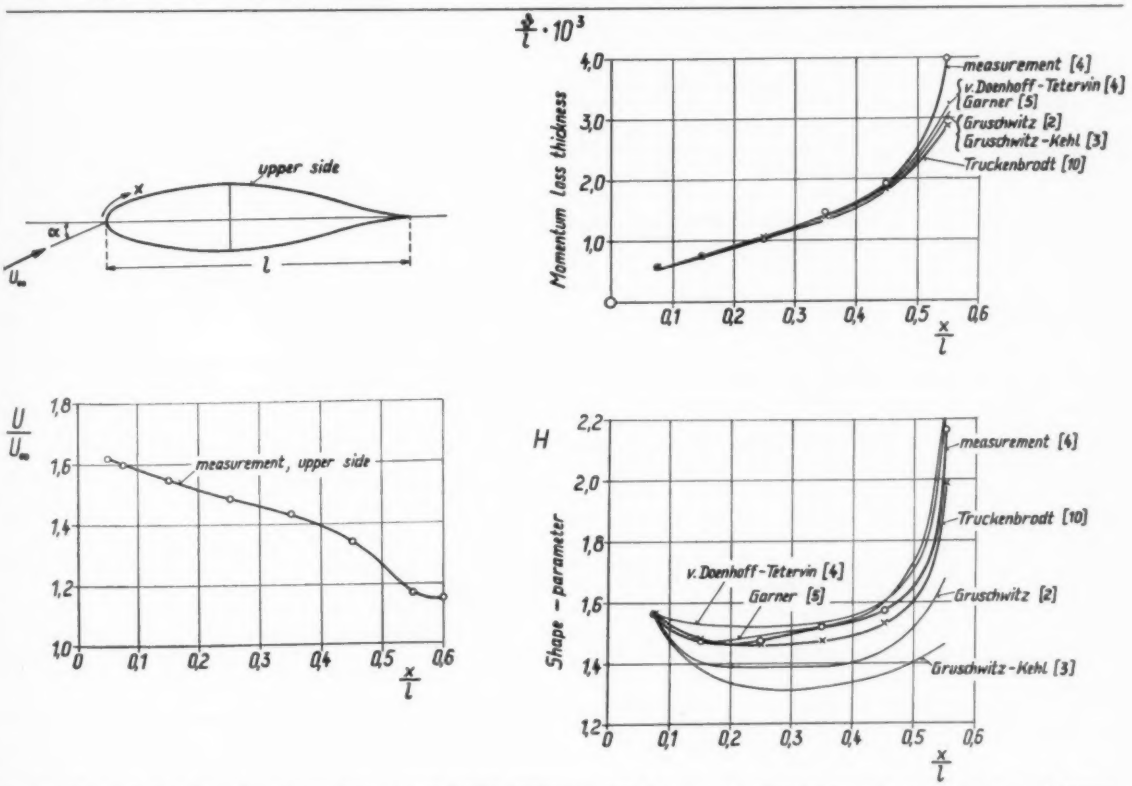

FIG. 2. The turbulent boundary layer of the airfoil NACA 65(216) − 222 at $\alpha = 10.1°$, upper side; $Re = 2.64 \times 10^6$. Measurement from reference 4.

Suggested Way of Comparing Overall Efficiency of Helicopters

W. Z. Stepniewski
Director of Aerodynamics, Piasecki Helicopter Corporation
February 19, 1952

SOME STUDENTS OF THE HELICOPTER still consider the figure of merit of the rotor as a proper measure of the efficiency with which energy brought into the cycle is transformed into the useful work of creating thrust. This approach of evaluating all rotary aircraft on the basis of the aerodynamic merits of the rotor alone can be justified to some extent within selected groups of mechanically driven helicopters equipped with engines of similar specific fuel consumption. However, in such cases as jet helicopters, the variations of propulsive efficiency of jets and the thermodynamic efficiencies of cycles used may be so great that the whole approach based on the figure of merit evaluation becomes of doubtful value. In order to establish a common denominator for the evaluation of the overall energy efficiency (η_{oe}) of all types of helicopters, it is suggested that it should be expressed as the ratio of the ideal power (P_{id}) required to produce a given thrust to the potential power (P_{pot}) represented by the heat energy of the fuel actually used in a unit of time,

$$\eta_{oe} = P_{id}/P_{pot} \tag{1}$$

Denoting hourly fuel consumption of the helicopter by F.C. (lbs. per hour) and assuming that heat value of presently used fuels is 18,500 B.t.u. per lb., the potential heat power can be expressed (in horsepower) as $P_{pot} = 7.27$ F.C. In hovering, the ideal power is simply expressed in terms of gross weight (W), disc loading (w), and air density (ρ), and the overall efficiency becomes

$$\eta_{oe_h} = W\sqrt{w/\rho}/5{,}640(\text{F.C.})_h \tag{2}$$

where the disc loading w (lbs. per sq.ft.) is based on the total swept area of the rotor (s), and $(\text{F.C.})_h$ is the hourly fuel consumption in hovering (lbs. per hour).

In forward flight, the overall efficiency of different helicopters should either be evaluated at some definite speeds (say 100, 120 m.p.h.), or still better at the flying speed, $V_{\text{opt.}}$, corresponding to the longest range. Substituting in Eq. (1) for P_{id}, its expression in horizontal flight and simplifying, the following expression for overall efficiency at optimum flying speed (in m.p.h.) is obtained,

$$\eta_{oe_{\text{opt.}}} = W^2/11{,}800\pi R^2\rho(\text{F.C.})_{\text{opt.}} V_{\text{opt.}} \tag{3}$$

Having the values of η_{oe} (say from statistics or general considerations) for various types of helicopters, together with their useful load/gross weight ratios, it is possible to compare them from the point of view of their pay load carrying capacity in hovering and in forward flight. In the case of hovering this can be done by calculating the hourly fuel consumption from Eq. (2) and comparing it with the amount of fuel available at a given pay load. Similarly, in the case of range, $(\text{F.C.})_{\text{opt.}}$ is computed from Eq. (3); then from the known flying speed, $V_{\text{opt.}}$ and amount of fuel at a given pay load, the corresponding range is obtained. Through this procedure curves showing pay load vs. time in hovering or payload vs. range can be established.

In order to give some feeling as to the order of magnitude of the η_{oe_h} and $\eta_{oe_{\text{opt.}}}$ values, these efficiencies are briefly discussed for the example of mechanically driven helicopters.

Hourly fuel consumption in hovering of this type of helicopter can be expressed as

$$(\text{F.C.})_h = \frac{\text{s.f.c.}}{550\eta_t}\left(kW\sqrt{\frac{w}{2\rho}} + \frac{1}{8}\sigma\pi R^2\rho\bar{c}_{do}V_t^3\right) \tag{4}$$

where new symbols are: η_t = the transmission efficiency (including cooling and antitorque losses), k = the ratio between ideal and actual induced power in hovering (see page 94, reference 1), σ = rotor solidity, $\bar{c}_{do}$ = equivalent profile drag coefficient, V_t = tip speed (ft. per sec.), and s.f.c. = specific fuel consumption of the engine (lbs. per b.hp. per hour). It is easy to show that (see page 104, reference 1) maximum power loading will be obtained when the second term in the brackets of Eq. (4) equals one-half of the first one or, in other words, when the disc loading is

$$w = (1/2)\rho V_t^2\sqrt[3]{(\sigma\bar{c}_{do}/k)^2} \tag{5}$$

Substituting Eq. (4) into Eq. (2) and assuming that the disc loading w is as given by Eq. (5), the following simple expression for the overall efficiency in hovering is obtained:*

$$\eta_{oe_h} = \eta_t/7.27[k + (1/2)]\text{s.f.c.} \tag{6}$$

The following numerical values may be considered as representative for a single-rotored helicopter: $\eta_t = 0.84$, $k = 1.1$, and s.f.c. = 0.5 lb. per b.hp. per hour; hence, $\eta_{oe_h} = 0.145$. It may be of interest to note that for a ram-jet helicopter this efficiency will probably be in the neighborhood of $\eta_{oe_h} = 0.015$ or less, while for a well-designed pressure jet it may reach or exceed $\eta_{oe_h} = 0.08$.

The engine power, P, required in horizontal flight of mechanically driven helicopter when expressed in ft.lbs. per sec. is

$$P = \frac{1}{\eta_t}\left(\frac{1}{2}\rho f V^3 + P_{pr} + \frac{kW^2}{2\pi R^2\rho}\frac{1}{V}\right) \tag{7}$$

where the flying speed V is in ft. per sec. and the new symbols are: f is equivalent flat plate area (including drag component due to the rotor profile drag), P_{pr} is the rotor profile power (in ft.lbs. per sec.), and k is, in this case, the ratio of the ideal to the actual induced power in forward flight. For a constant specific fuel consumption, the best range will be obtained when P/V becomes a minimum. This condition is fulfilled when

$$\frac{1}{2}\rho f V^3 = \frac{kW^2}{2\pi R^2\rho V} + \frac{1}{2}P_{pr} \tag{8}$$

Substituting Eq. (8) into Eq. (7), changing units of power to hp., and multiplying the thus-transformed Eq. (7) by s.f.c., the hourly fuel consumption is obtained, and the overall efficiency at optimum flying speed becomes

$$\eta_{oe_{\text{opt.}}} = \eta_t/14.54\left[k + \frac{1{,}210\ V_{\text{opt.}}}{V(W/P_{pr})w}\right]\text{s.f.c.} \tag{9}$$

where (W/P_{pr}) may be called the profile power loading (lbs. per hp.) and $V_{\text{opt.}}$ is in m.p.h.

For a general discussion it would be more desirable to express $V_{\text{opt.}}$ in terms of design parameters. This can be done by solving Eq. (8) for V. Unfortunately, because this equation is of the fourth degree, no simple exact solution can be obtained. However, an approximate value of $V_{\text{opt.}}$ can be obtained by neglecting the P_{pr} term. Then $V_{\text{opt.}}$ in m.p.h. would be

$$V_{\text{opt.}} = 1.47\sqrt[4]{kww_f/\rho^2} \tag{10}$$

where $w_f = W/f$ (lbs. per sq.ft.) may be called the equivalent flat plate area loading. Substituting Eq. (10) into Eq. (9), the following approximate formula is obtained:

$$\eta_{oe_{\text{opt.}}} = \eta_t/14.54\left[k + \frac{825}{(W/P_{pr})}\sqrt[4]{\frac{kw_f\rho^2}{w}}\right]\text{s.f.c.} \tag{11}$$

For a single-rotored helicopter with the following characteris-

* It should be noticed that quite often for structural and other reasons the disc loading of practical helicopters deviates from its optimum value as given by Eq. (5); hence, η_{oe_h} will be lower than given by Eq. (6).

tics: $w = 5$ lbs. per sq.ft., $W/P_{pr} = 40$ lbs. per hp., $w_f = 800$ lbs. per sq.ft. (very clean machine) and assuming that, in the considered forward flight, $k = 1.1$, $\eta_t = 0.86$, and s.f.c. = 0.45 lb. per hp. per hour, the optimum overall efficiency in horizontal flight would be $\eta_{ov_{opt.}} = 0.043$.*

REFERENCE

1 Stepniewski, W. Z., *Introduction to Helicopter Aerodynamics*, Rotorcraft Publishing Committee, Morton, Pa., 1951.

* The above outline represents only the private opinion of the writer.

On the Stability of Plane Parallel Laminar Flows to Two- and Three-Dimensional Disturbances*

Martin Lessen
The Pennsylvania State College, State College, Pa.
February 27, 1952

THE FLOW EQUATIONS of a viscous compressible fluid may be given as follows:

Continuity:

$$\rho_t + (\rho u_k)_k = 0$$

Force:

$$\rho \dot{u}_i = -p_i + (\mu u_{i,\,k})_{,k} + (\mu U_{k,\,i})_{,k} - (2/3)\,(\mu u_{k,\,k})_i$$

Energy:

$$\rho c_v \dot{T} = (\lambda K T_k)_{,k} - [p + (2/3)\mu u_{k,\,k}]u_{l,\,l} + \mu(u_{k,\,l}u_{k,\,l} + u_{k,\,l}u_{l,\,k}) \qquad (1)$$

State:

$$\rho = \rho(p, T), \quad \mu = \mu(T); \quad K = K(T)$$

where the variables are defined as

x_i = rectangular Cartesian space coordinates
t = time coordinate
u_i = velocity component in i direction
ρ = density of fluid
p = pressure
T = temperature
μ = coefficient of viscosity (absolute)
K = conductivity (thermal)

If a plane parallel steady flow with a small time variable three-dimensional disturbance superimposed on it is assumed, such that

$$\begin{aligned}
u_1 &= U(x_2) + u(x_2)\exp[i(\alpha x_1 + \beta x_3 - \alpha c t)] \\
u_2 &= v(x_2)\exp[i(\alpha x_1 + \beta x_3 - \alpha c t)] \\
u_3 &= w(x_2)\exp[i(\alpha x_1 + \beta x_3 - \alpha c t)] \\
\rho &= \bar{\rho}(x_2) + \rho(x_2)\exp[i(\alpha x_1 + \beta x_3 - \alpha c t)] \\
p &= \bar{p} + p(x_2)\exp[i(\alpha x_1 + \beta x_3 - \alpha c t)] \\
T &= \bar{T}(x_2) + T(x_2)\exp[i(\alpha x_1 + \beta x_3 - \alpha c t)] \\
\mu &= \bar{\mu}(x_2) + \mu(x_2)\exp[i(\alpha x_1 + \beta x_3 - \alpha c t)] \\
K &= \bar{K}(x_2) + K(x_2)\exp[i(\alpha x_1 + \beta x_3 - \alpha c t)]
\end{aligned}$$

the equations for the disturbance may be obtained by elimination of the steady-state terms from Eq. (1) as satisfying themselves and, in addition, dropping the terms nonlinear in the disturbance quantities in the usual manner. It should be noted at this point that, generally, absolutely parallel flows cannot exist.

* This work was carried out under O.N.R. Contract NONR-656(01).

Continuity:

$$i\alpha(U - c)\rho + \bar{\rho}(i\alpha u + v' + i\beta w) + \bar{\rho}'v = 0 \qquad (2a)$$

Force:

$$\bar{\rho}[i\alpha(U - c)u + U'v] = -i\alpha p + \bar{\mu}\left[u'' - \left(\frac{4}{3}\alpha^2 + \beta^2\right)u + \frac{i\alpha}{3}v' - \frac{\alpha\beta}{3}w\right] + \bar{\mu}'(u' + i\alpha v) + U''\mu + U'\mu' \qquad (2b)$$

$$\bar{\rho}[i\alpha(U - c)v] = -p' + \bar{\mu}\left[\frac{4}{3}v'' + (\alpha^2 + \beta^2)v + \frac{i\alpha}{3}u' + \frac{i\beta}{3}w'\right] + \bar{\mu}'\left(\frac{4}{3}v - \frac{2}{3}i\alpha u - \frac{2}{3}i\beta w\right) + i\alpha U'\mu \qquad (2c)$$

$$\bar{\rho}[i\alpha(U - c)w] = -i\beta p + \bar{\mu}\left[w'' - \left(\alpha^2 + \frac{4}{3}\beta^2\right)w - \frac{\alpha\beta}{3}u + \frac{i\beta}{3}v'\right] + \bar{\mu}'(i\beta v + w') \qquad (2d)$$

Energy:

$$\bar{\rho}c_v[i\alpha(U - c)T + \bar{T}'v] = \bar{K}\,[T'' - (\alpha^2 + \beta^2)T] + \bar{K}'T' + K\bar{T}'' + K'\bar{T}' - \bar{p}(i\alpha u + v' + i\beta w) + 2\bar{\mu}U' \times (u' + i\alpha v) + \mu(U')^2 \qquad (2e)$$

The following transformation of dependent variable will now be tried similar to that of Squire[2] after multiplying Eq. (2b) by α, Eq. (2d) by β, and adding:

$$\begin{aligned}
\alpha u + \beta w &= \tilde{\alpha}\tilde{u} \\
v &= \tilde{v} \\
\alpha^2 + \beta^2 &= \tilde{\alpha}^2 \\
(\tilde{\alpha}/\alpha)\bar{p} &= \tilde{\bar{p}} \\
(\tilde{\alpha}/\alpha)\bar{\mu} &= \tilde{\bar{\mu}}
\end{aligned}$$

The continuity and force equations transform directly to two-dimensional form with the exception of the viscosity-disturbance terms. The energy equation also transforms to two-dimensional form except for the terms $2\bar{\mu}U'(u' + i\alpha v)$ and a viscosity disturbance term. It should be noted at this point that, even for a classical incompressible fluid, the aforementioned energy equation terms do not satisfy the Squire transformation.

In the region where U is not approximately equal to c, the solution of the disturbance equations is given primarily by the inviscid terms. These terms obey the Squire transformation. In the "inner friction" region where $U \approx c$, if it is assumed that the temperature (and therefore density) disturbance has an unimportant effect on the eigenvalue problem,[1] the viscosity disturbance and the energy equation can be neglected. Therefore, for this region also, the Squire transformation is applicable.

Thus, if instability occurs for a three-dimensional disturbance, it will occur for a two-dimensional disturbance at a lower Reynolds Number for the same steady-state flow, since $\tilde{\alpha} > \alpha$. It is therefore only necessary to examine the stability of parallel flows to two-dimensional disturbances.

The equations for a two-dimensional disturbance follow.

Continuity:

$$i\alpha(U - c)\rho + \bar{\rho}(i\alpha u + v') + \bar{\rho}'v = 0$$

Force:

$$\bar{\rho}[i\alpha(U - c)u + U'v] = -i\alpha p + \bar{\mu}\left(u'' - \frac{4}{3}\alpha^2 u + \frac{i\alpha}{3}v'\right) + \bar{\mu}'(u' + i\alpha$$

$$\bar{\rho}[i\alpha(U - c)v] = -p' + \bar{\mu}\left(\frac{4}{3}v'' - \alpha^2 v + \frac{i\alpha}{3}u'\right) + \bar{\mu}'\left(\frac{4}{3}v' - \frac{2}{3}i\alpha u\right)$$

(*Continued on page 432*)

Energy:

$$\bar{\rho}c_v[i\alpha(U - c)T + \bar{T}'v] = -\bar{\rho}(i\alpha u + v')$$

If it is assumed that the temperature (and density) disturbances have a higher order effect on the eigenvalue problem throughout the flow régime, the energy equation can be dropped entirely. This is rigorous for the case of an incompressible fluid with temperature-variable viscosity and for the laminar mixing of dissimilar fluids.

REFERENCES

[1] Lees, Lester, and Lin, C. C., *Investigation of the Stability of the Laminar Boundary Layer in a Compressible Fluid*, N.A.C.A. T.N. No. 1115, 1946; Lees, Lester, *The Stability of the Laminar Boundary Layer in a Compressible Fluid*, N.A.C.A. T.N. No. 1360, 1947.

[2] Squire, H. B., Proc. Roy. Soc. of London (A), Vol. 142, pp. 621–628, (1933).

Two-Dimensional Losses in Turbine Blades

(*Continued from page 408*)

[4] Weinig, F., *The Flow Around Turbine and Compressor Blades*, CGD 291, reproduced by Code 337, BuShips, Navy Department, May, 1946.

[5] Katzoff, S., Finn, Robert S., and Laurence, James C., *Interference Method for Obtaining the Potential Flow Past an Arbitrary Cascade of Airfoils*, N.A.C.A. T.N. No. 1252, 1947.

[6] Goldstein, Arthur W., and Jerrison, Meyer, *Isolated and Grid Airfoils with Prescribed Velocity Distribution*, N.A.C.A. T.N. No. 1308, 1947.

[7] Stodola, A., *Steam and Gas Turbines*, Vol. II, p. 992; McGraw-Hill Book Company, Inc., New York, 1927. (Reprint, Peter Smith, New York, 1945.)

[8] MacGregor, Charles A., *Comparison Between Calculated Design Performance and Experimental Performance Measured in a Cascade Tunnel of a Gas Turbine Blade*, Master's Thesis, Case Institute of Technology, Cleveland, 1947.

[9] Huppert, M. C., and MacGregor, Charles A., *Comparison Between Predicted and Observed Performance of Gas Turbine Stator Blade Designed for Free-Vortex Flow*, N.A.C.A. T.N. No. 1810, 1949.

[10] Tetervin, Neal, *A Method for the Rapid Estimation of Turbulent Boundary Layer Thickness for Calculating Profile Drag*, N.A.C.A. A.C.R. No. L4G14, 1944.

[11] Von Doenhoff, Albert E., *A Method of Rapidly Estimating the Position of Laminar Separation Point*, N.A.C.A. T.N. No. 671, 1938.

A High-Speed Schlieren Technique for Investigation of Aerodynamic Transients

(*Continued from page 420*)

flow problems of any description. In particular, it lends itself most admirably to the study of short-period transients. Other cameras are available[2] which permit the investigation of lower frequency effects over a longer period of time. Fig. 8 shows a series of photographs obtained during the starting process of a supercritical supersonic diffuser showing the effect of a normal shock wave propagating through a steady supersonic flow in the shock configuration in that flow. The exposure time of each frame is in the order of 2 to 4 microsec., and the frequency of exposure is about 7,000 thousand frames per sec.

REFERENCES

[1] Loeb, L. B., *Fundamental Processes of Electrical Discharge in Gases*, John Wiley & Sons, Inc., New York, 1939.

[2] University of Minnesota, Institute of Technology, Department of Aeronautical Engineering, Research Report 26, 1948.

[3] Bradfield, W. S., *Experimental Study of the Application of Pressure Transients to the Starting of a Supersonic Wind Tunnel*, University of Minnesota, Institute of Technology, Department of Aeronautical Engineering, Research Report 70, 1950.